Thermodynamic critical field and superconducting fluctuation of vortices for high temperature cuprate superconductor: La-214

by

Yung Moo Huh

A dissertation submitted to the graduate faculty

in partial fulfillment of the requirements for the degree of

DOCTOR OF PHILOSOPHY

Major: Condensed Matter Physics

Major Professor: Douglas K. Finnemore

Iowa State University

Ames, Iowa

2001

Graduate College

Iowa State University

This is to certify that the Doctoral dissertation of

Yung Moo Huh

has met the dissertation requirements of Iowa State University

_____
Committee Member

_____
Committee Member

_____
Committee Member

_____
Committee Member

_____
Major Professor

_____
For the Major Program

_____
For the Graduate College

This dissertation is dedicated

to my wife, Kyusung Kim and son, Richard Kim Huh

and to those who prayed for Richard

with thanks.

TABLE OF CONTENTS

LIST OF TABLES

LIST OF FIGURES

NOMENCLATURE

$H_c(T)$	Thermodynamic critical field at a finite temperature.
$H_c(0)$	Thermodynamic critical field at zero temperature.
H_{c1}	Lower critical field.
H_{c2}	Upper critical field.
H'_{c2}	The temperature derivative of the H_{c2} at the transition temperature.
M_n	Magnetization in the normal state above T_c.
M_t	Total magnetization in the superconducting state below T_c.
M_{sc}	Superconducting state magnetization (= $M_t - M_n$).
$N(0)$	Density of states at the Fermi surface.
s	Spacing between adjacent CuO_2 layers.
T_c	Transition temperature of a superconductor extracted from 10 Oe susceptibility measurements.
T_{c0}	Transition temperature of a superconductor extracted by fitting H_c(T) data derived from the Hao-Clem model to the Two-Fluid model.
$T_c(H)$	Transition temperature of a superconductor in a presence of magnetic field.
T^*	Crossing temperature at the intersection of two successive curves for close magnetic fields in M_{sc} vs. T plot.

t Reduced temperature (= T/T_c).

x Doping contents of Sr atoms substituting La of the La_2CuO_4 compound.

Δ Superconducting order parameter. The energy gap is defined as 2Δ.

φ_0 Quantum of flux (= $hc/2e$).

γ Temperature coefficient of the normal electronic specific heat (= C^{el}/T).

γ_{ani} Anisotropy ratio (= $\lambda_c/\lambda_{ab} = \xi_{ab}/\xi_c = H^c_{c1}/H^{ab}_{c1} = H^{ab}_{c2}/H^c_{c2}$).

κ Ginzburg-Landau parameter (= λ/ξ).

λ Penetration depth. λ_i is denoted for the penetration depth of screening current along i-axis ($\lambda_i = \lambda\sqrt{m_i}$).

ξ Coherence distance. ξ_i is denoted for the spatial variation of order parameter along i-axis ($\xi_i = \xi/\sqrt{m_i}$).

ABSTRACT

Thermodynamics has been studied systematically for the high temperature cuprate superconductor $La_{2-x}Sr_xCuO_{4-\delta}$, La-214, in the entire superconductive region from strongly underdoped to strongly overdoped regimes. Magnetization studies with $H||c$ have been made in order to investigate the changes in free energy of the system as the number of carriers is reduced. Above the superconducting transition temperature, the normal-state magnetization exhibits a two-dimensional Heisenberg antiferromagnetic behavior. Below T_c, magnetization data are thermodynamically reversible over large portions of the H-T plane, so the free energy is well defined in these regions. As the Sr concentration is varied over the wide range from 0.060 (strongly underdoped) to 0.234 (strongly overdoped), the free energy change goes through a maximum at the optimum doped in a manner similar to the T_{c0} vs. x curve. The density of states, $N(0)$, remains nearly constant in the overdoped and optimum doped regimes, taking a broad maximum around x = 0.188, and then drops abruptly towards zero in the underdoped regime.

The $La_{2-x}Sr_xCuO_4$ (La-214) system displays the fluctuating vortex behavior with the characteristic of either 2D or 3D fluctuations as indicated by clearly identifiable crossing points T^* close to T_c. The dimensional character of the

fluctuations depends on both applied magnetic fields and the density of charge carriers. The dimensional crossover from 2D to 3D occurs in the strongly underdoped regime when the *c*-axis coherence distance ξ_c becomes comparable to the spacing between adjacent CuO_2 layers *s* at sufficiently high magnetic fields near H_{c2}.

CHAPTER 1. GENERAL INTRODUCTION

I. Introduction

The ceaseless search for the ultimate "*Resistanceless*" - superconductivity - has been conducted over ninety years since the first discovery in mercury by Heike Kamerling Onnes [1] at the Low Temperature Laboratory in Leiden in 1911. Then just this past year, Akimitsu and co-workers [2] announced the discovery of superconductivity in the long-ignored binary intermetallic compound magnesium diboride (MgB_2) with a T_c close to 40 K. Studies of MgB_2 by the group in Iowa State University demonstrated that the mechanism under the superconductivity might be explained by the BCS theory framework by measuring the compound's isotope effect [3]. This material holds promise for a low cost alternation for industrial applications due to the large critical current density [4] and the possibility of manufacturing wires with small normal state resistivity [5]. This sets the second milestone in the history of metallurgical superconductivity following the remarkable discovery by Bednorz and Muller of superconductivity above 30 K in the *Ba-La-Cu-O* system in 1986 [6], breaking the long hold record of 23.2 K for T_c in Nb_3Ge since 1973 [7].

The past two years have been filled with truly stunning discoveries in the

superconductivity community. These include the discovery of superconductivity in MgB_2, and ingenious devices based on the Field Effect Transistor (FET) to add charge carriers (organic materials [8] are transformed to superconductors and the C_{60} molecule [9] is found to be a superconductor with a T_c as high as 52 K).

II. Brief History of Superconductivity

After the first discovery of the abrupt disappearance of resistivity [1] at 4.2 K, it took twenty two more years to realize there is another intrinsic property in a superconductor, called the Meissner effect [10] - a complete magnetic field expulsion from the interior of the superconductor. It is now considered that a superconductor exhibits both perfect conductivity and perfect diamagnetism simultaneously.

Many elemental superconductors show the perfect diamagnetic behavior up to the field (critical field, H_c) above which the normal state is restored. By contrast, experiments made on superconducting alloys show complicated magnetic behavior. They expel magnetic field completely only up to a certain value of the applied field (lower critical field, H_{c1}) and upon increasing the field the flux starts to penetrate into the sample while the sample is still in superconducting state. The transition to normal state is realized as soon as the applied field reaches the upper critical field, H_{c2}. These materials were named type-II superconductors and were first reported by Schubnikow and co-workers

[11].

The application of superconductivity in high-field magnets had to wait till the breakthrough of Kunzler's [12] discovery, in 1961, of the possibilities of using Nb_3Sn, for it can sustain a large supercurrent density (~10^5 A/cm^2) at a field as high as 8.8 T, which was found to be superconducting at T = 18 K by Matthias and co-workers [13] in 1954. Matthias's empirical approach [14] and monumental contribution led to discovering the record T_c of 23.2 K in Nb_3Ge by Gavaler [7] in 1973.

Theoretical attempts to explain superconductivity apparently started with the two-fluid model proposed by Gorter and Casimir [15] in 1934 in analogy to quantum fluids of liquid helium. The Londons [16] considered superconductivity as a macroscopic quantum state and derived the electrodynamic equations (London equations) and the penetration depth λ. The λ gives a characteristic length over which the supercurrent, induced by the magnetic field, reduces by a factor e^{-1} from its surface value. Taking non-local effects into consideration, Pippard in 1950 [17] introduced the coherence length ξ, which specifies the range to which order will extend in the bulk material. In their phenomenological approach in 1950, Ginzburg and Landau [18] derived equations allowing for a spatially varying order parameter using their general theory of phase transitions. The dimensionless Ginzburg-Landau parameter κ (= λ/ξ) was introduced and it was shown that if $\kappa << 1$, then the surface energy becomes positive and stabilizes a domain pattern in the intermediate state. It was

Abrikosov [19] in 1957 who distinguished superconductors into type-I ($\kappa < 1/\sqrt{2}$) and type-II ($\kappa > 1/\sqrt{2}$) and defined a vortex by solving the Ginzburg-Landau equations in the presence of magnetic field. The vortex is an excitation of the superconducting current consisting of a core of normal metal around which the phase angle of the electron-pair wavefunction changes by 2π. Magnetic field lines can penetrate the superconductor through the vortices, each carrying exactly quantum of flux φ_0 (= $hc/2e$) in the vortex state.

Early evidence that the ionic lattice waves (or phonons) play a role in superconductivity came with the observations of the isotope effects [20] ($\sqrt{M}T_c$ = constant). Frohlich [21] and Bardeen [22] showed, simultaneously and independently, that the electron-phonon interaction provides an attractive potential energy, which might be larger than the screened Coulomb repulsive energy. Soon after, Cooper [23] discovered that the "normal" Fermi sea is unstable (known as the *Cooper instability*) under the formation of correlated pairs for arbitrarily weak coupling so long as the potential is attractive near the Fermi surface. Two electrons can be bound together in a state of zero total momentum with opposite spin, known as a Cooper pair.

In 1957, Bardeen, Cooper, and Schrieffer [24] published the paper "Theory of Superconductivity" – the BCS theory. Convincing experimental evidence soon followed confirming the theory. The existence and the magnitude of the superconducting gap energy predicted by the theory were directly measured in Superconductor-Insulator-Normal metal (SIN) junctions by Giaever [25]. The

flux quantum with 2*e*, determined experimentally by Doll and Nabauer [26] and by Deaver and Fairbank [27], indicates the formation of a pair of electrons - the cornerstone of the theory. Josephson [28] subsequently showed that the Cooper pairs could tunnel through a thin insulating layer between two superconductors (SIS junction) and that this tunneling would generate a dc current with zero bias voltage, or an ac current when a dc bias voltage is applied. The experimental evidence confirming the basic pairing theory is very strong.

In 1986 there was another revolutionary discovery of superconductivity in the copper oxide system above 30 K made by Bednorz and Muller [6]. The dream of superconductivity above the boiling temperature of liquid nitrogen (77 K) came true for the first time in history with the discovery of the $YBa_2Cu_3O_{7-\delta}$ in 1987 [29]. The current record high critical transition temperature in cuprate superconductors is 164 K in $HgBa_2Ca_2Cu_3O_{8+\delta}$ at 31 GPa [30]. The mechanism of superconductivity behind the high temperature cuprate superconductors is still under intensive investigation and remains an unsolved problem.

III. Dissertation Organization

The cuprate superconductors are very special because they are doped insulators in which the density of charge carriers can be varied systematically. The purpose of this study is to investigate the generic thermodynamic properties that occur over the entire range of the superconductive region as the charge

carrier concentration is varied. The focus is on magnetization experiments in the high temperature cuprate superconductor: $La_{2-x}Sr_xCuO_{4+\delta}$ - La-214 system.

Theory and models employed throughout the dissertation are discussed in Chapter 2. Sample preparation and characterization are explained in Chapter 3. Main ideas and data are presented in Chapter 4, Chapter 5, and Chapter 6, each of which is a complete and separate paper published or submitted to journals. Chapter 4 consists of the analysis of the normal state magnetization and the extended study of superconducting properties on a high quality $La_{1.90}Sr_{0.10}CuO_4$ single crystal. Chapter 5 and Chapter 6 are thorough studies on the thermodynamic critical field and superconducting fluctuation of vortices, respectively, as the charge carrier concentration changes. A complete mapping of the thermodynamic critical field curve is conducted in the entire range ($0.06 < x < 0.234$) of the superconductive regime for $La_{2-x}Sr_xCuO_4$. In Chapter 7 are general conclusions.

References

1. H. Kamerling Onnes, Leiden Comm. **120b**, **122b**, **124c** (1911).
2. J. Akimitsu, in Proceedings of the Symposium on Transition Metal Oxides, Sendai, 10 January 2001; J. Nagamatsu, N. Nakagawa, T. Muranaka, Y. Zenitani, and J. Akimitsu, Nature (London) **410**, 63 (2001).

3. S. L. Budʹko, G. Lapertot, C. Petrovic, C. Cunningham, N. Anderson, and P. C. Canfield, Phys. Rev. Lett. **86**, 1877 (2001).

4. D. K. Finnemore, J. E. Ostenson, S. L. Budʹko, G. Lapertot, and P. C. Canfield, Phys. Rev. Lett. **86**, 2420 (2001).

5. P. C. Canfield, D. K. Finnemore, S. L. Budʹko, J. E. Ostenson, G. Lapertot, C. E. Cunningham, and C. Petrovic, Phys. Rev. Lett. **86**, 2423 (2001).

6. J. D. Bednorz and K. A. Muller, Z. Phys. B **64,** 189 (1986).

7. J. R. Gavaler, Appl. Phys. Lett. **23**, 480 (1973).

8. J. H. Schon, Ch. Kloc, and B. Batlogg, Nature **406**, 702 (2000).

9. J. H. Schon, Ch. Kloc, and B. Batlogg, Nature **408**, 549 (2000).

10. W. Meissner and R. Ochsenfeld, *Naturwissenschaften*, **21**, 787 (1933).

11. L. W. Schubnikow, W. I. Chotkewitsch, J. D. Schepelew, and J. N. Rjabinin, Phys. Z. Sowjetunion, **10**, 165 (1936).

12. J. E. Kunzler, E. Beuhler, F. S. L. Hsu, and J. H. Wernick, Phys. Rev. Lett. **6**, 89 (1961).

13. B. T. Matthias, T. H. Geballe, S. Geller, and E. Corenzwit, Phys. Rev. **87**, 884 (1953).

14. B. T. Matthias, Phys. Rev. **97**, 74 (1955); Prog. Low Temp. Phys. **2**, 138 (1957), edited by C. J. Gorter, North Holland, Amsterdam (1957); J. K. Hulm and B. T. Matthias, Science, **208**, 881 (1980).

15. C. J. Gorter and H. B. G. Casimir, Phys. Z. **35**, 963 (1934); Physica **1**, 306 (1934).

16. F. London and H. London, Proc. Roy. Soc. (London) A **149**, 71 (1935); F. London, *Superfluids*, Vol. I. Wiley, New York, (1950).

17. A. B. Pippard, Proc. Roy. Soc. (London), Ser. A **203**, 210 (1950).

18. V. L. Ginzburg and L. D. Landau, *Zh. Eksperim. i Teor. Fiz.* **20**, 1064 (1950).

19. A. A. Abrikosov, *Zh. Eksperim. i Teor. Fiz.* **32**, 1442 (1957); Sov. Phys. JETP **5**, 1174 (1957).

20. H. Kamerling Onnes and W. Tuyn, Leiden Comm. **160b** (1922); E. Justi, Phys. Z. **42**, 325 (1941); E. Maxwell, Phys. Rev. **78**, 477 (1950); C. A. Reynolds, B. Serin, W. H. Wright, and L. B. Nesbitt, Phys. Rev. **78**, 487 (1950).

21. H. Frohlich, Phys. Rev. **79**, 845 (1950).

22. J. Bardeen, Phys. Rev. **80**, 567 (1950).

23. L. N. Cooper, Phys. Rev. **104**, 1189 (1956).

24. J. Bardeen, L. N. Cooper, and J. R. Schrieffer, Phys. Rev. **108**, 1175 (1957).

25. I. Giaever, Phys. Rev. Lett. **5**, 464 (1960); I. Giaever and K. Megerle, Phys. Rev. **122**, 1101 (1961).

26. R. Doll and M. Nabauer, Phys. Rev. Lett. **7**, 51 (1961).

27. B. S. Deaver Jr. and W. M. Fairbank, Phys. Rev. Lett. **7**, 43 (1961).

28. B. D. Josephson, Phys. Rev. Lett. **1**, 251 (1962).

29. M. K. Wu, J. R. Ashburn, C. J. Torng, P. H. Hor, R. L. Meng, L. Gao, Z. J. Huang, Y. Q. Wang, and C. W. Chu, Phys. Rev. Lett. **58**, 908 (1987).

30. L. Gao, Y. Y. Xue, F. Chen, Q. Xiong, R. L. Meng, D. Ramirez, C. W. Chu, J. H. Eggert and H. K. Mao, Phys. Rev. B **50**, 4260 (1994).

CHAPTER 2. THEORY AND MODELS

I. Thermodynamic Critical Field

When a superconductor is cooled below a critical temperature there is not only an abrupt loss of electrical resistance but there are also abrupt changes in many of the other properties of the material such as magnetization, specific heat, thermoelectric effect, and thermal conductivity. All these changes, including the loss of resistance, take place at the same temperature known as the (critical) transition temperature T_c due to the essential microscopic change in the electron system in the material. The transition temperature between the superconducting state ($T < T_c$) and the normal state ($T > T_c$) is, in the absence of an applied magnetic field, independent of the shape or size of the sample. This is a well defined thermodynamic phase transition and a new condensed state is present below T_c. The electrons condense into singlet - spin zero - momentum and these pairs of electrons are strongly correlated. An energy gap opens between the correlated ground state condensed superfluid and single particle excitations out of the ground state.

The existence of the reversible Meissner effect, which is characterized by perfect diamagnetism, makes it possible to apply thermodynamics to

superconductivity. Hence the free energy becomes the important variable to describe the transition between normal and superconducting states. The difference in free energy between two states defines the overall energy change as the superconducting transition occurs. Experimentally the free energy change during the transition can be obtained by integrating the area under the magnetization curve from zero up to a certain field where superconductivity is destroyed. Since the free energy difference between the superconducting and normal states varies as

$$-\int MdH = \mathrm{G_n} - \mathrm{G_s} = H_c^2/8\pi\,, \tag{1}$$

where G_n and G_s are the Gibbs free energies per unit volume in the respective phases, it becomes possible to discuss free energy changes in terms of the thermodynamic critical field H_c.

From early experiments on elemental superconductors, it was found empirically that $H_c(T)$ is quite well approximated by a quadratic temperature dependence [1]

$$H_c(T) = H_c(0)\,(1 - t^2) \tag{2}$$

where t is the reduced temperature T/T_c. For a few elemental superconductors [2], $H_c(T)$ data are plotted in the Figure 2.1 (a) and (b). In Figure 2.1 (a), they are for s-p band metal group and in Figure 2.1 (b) for d-band metal group. They show quite similar shapes in $H_c(T)$ in each band metal group. It is worth while to note that d-band elements has larger values in the ratio $H_c(T)/T_c$ than s-p band superconductors. This is predicted by the BCS theory [1], where the $H_c(T)/T_c$ is

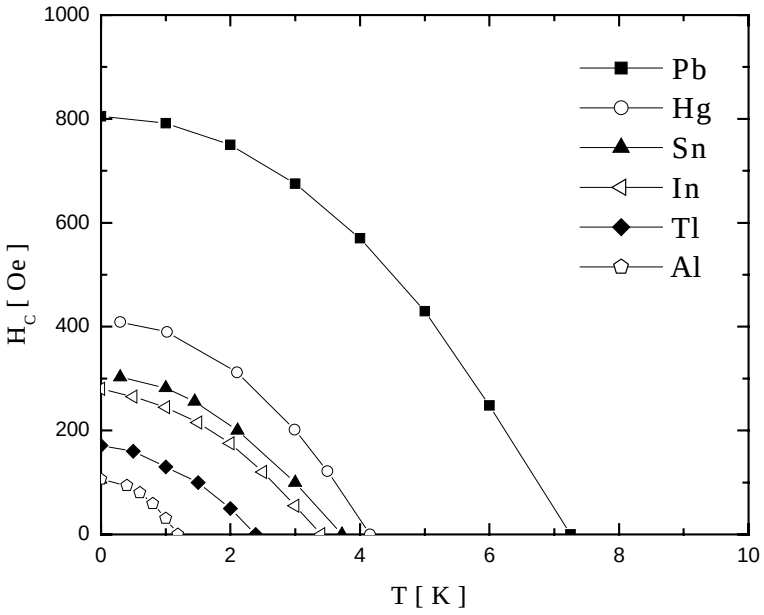

Figure 2.1 (a) $H_c(T)$ for the s-p band metal superconductors.

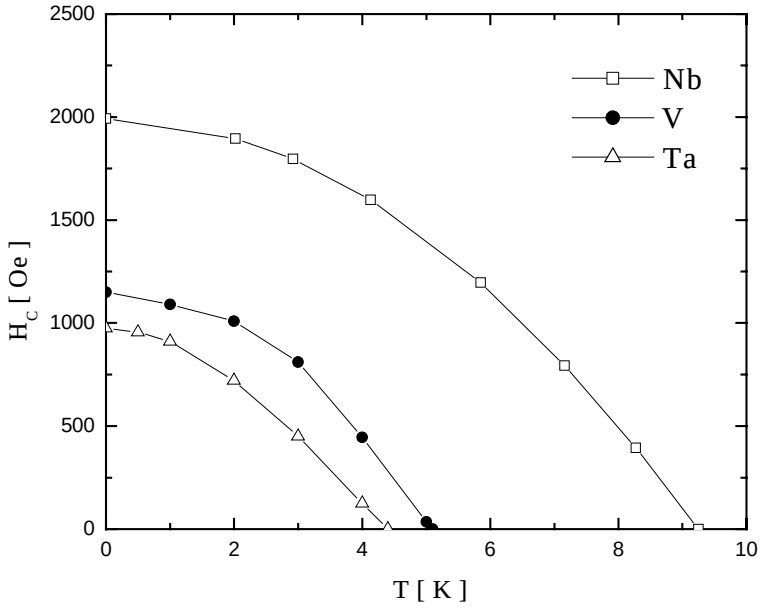

Figure 2.1 (b) $H_c(T)$ for the d band metal superconductors.

proportional to the square root of density of states $N(0)$.

What makes the thermodynamic critical field interesting is that it provides a measure of the energy change averaged over all participating electrons and can be directly related to microscopic variables predicted in the BCS theory. The H_c at zero temperature relates energy gap $\Delta(0)$ by

$$H_c(0) = [4\pi N(0)]^{1/2} \Delta(0) = [4\pi N(0)]^{1/2} (\Delta(0)/k_B T_c)\, k_B T_c, \quad (3)$$

where $N(0)$ is the electronic density of states taken for a system of unit volume. By rewriting Eq. (3) we obtain

$$H_c(0)/T_c = [4\pi N(0)]^{1/2} (\Delta(0)/k_B T_c) k_B \quad (4)$$

or equivalently

$$H_c(0)/T_c = (6/\pi)^{1/2} (\Delta(0)/k_B T_c)\, \gamma^{1/2}, \quad (5)$$

where γ (= 2/3 π^2 $N(0)$ k_B^2) is the electronic specific heat coefficient in the normal state and the gap ratio $\Delta(0)/k_B T_c$ at zero temperature is given as a universal constant 1.76 in the BCS theory. Therefore, within the BCS theory, the ratio of $H_c(0)$ to T_c is solely governed by the density of states in a given system.

The successful agreement of the BCS theory with the empirical results are represented in Figure 2.2 in which $H_c(0)/T_c$ and the square root of the experimentally measured γ [numerical values are taken from Ref. 2] are plotted, along with the BCS theoretical prediction as a solid line. The series of electron tunneling measurements on elemental superconductors have shown that $\Delta(0)/k_B T_c$ is not exactly 1.76 but has a value ranging from 1.65 to about 2.30 depending on the ratio of T_c/θ_D, the so called weak (strong) coupling effect. For

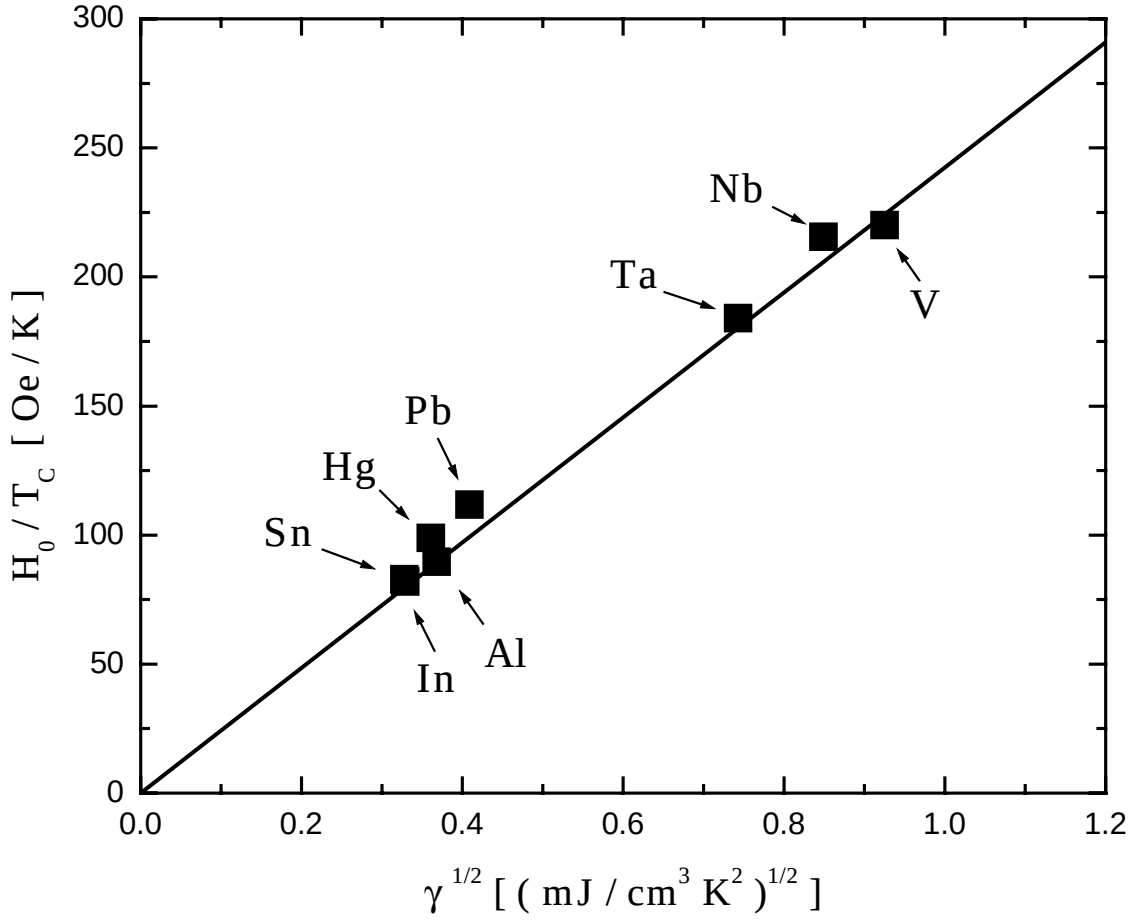

Figure 2.2 The BCS theory prediction (solid line) and empirical results for the elemental superconductors.

these elements, however, $\Delta(T)/\Delta(0)$ vs. t still has the BCS shape and the BCS equations correctly predict $H_c(T)$ and other thermodynamic variables. For Sn, In, Hg, the BCS theory correctly describes the H_c vs. T curves providing two adjustable variables, $\Delta(T)/k_BT_c$, and γ, are used (see Appendix in Chapter 5).

II. Reversible Magnetization

Both the Hao-Clem model and the Kogan variation on the London model have been used successfully to describe high temperature superconductors in their appropriate regimes of application. We wish to describe these models here.

The magnetic properties of high temperature cuprate superconductors exhibit extreme type-II superconductivity, characterized by a large value of the Ginzburg-Landau (GL) parameter $\kappa = \lambda/\xi$ (>>1), where λ is the penetration depth and ξ is the coherence length. Abrikosov predicted the high-field (near H_{c2}) expression of magnetization [3] to be

$$-4\pi M(H, T) = [\beta_A(2\kappa^2 - 1)]^{-1}(H_{c2}(T) - H), \tag{6}$$

and the magnetization vanishes linearly with a constant slope

$$d(-4\pi M)/dH = -[\beta_A(2\kappa^2 - 1)]^{-1}, \tag{7}$$

where β_A is a geometric constant independent of κ and H. For increasing H, Abrikosov theory gives again a constant slope independent of H

$$d(-4\pi M)/dT = [\beta_A(2\kappa^2 - 1)]^{-1}[dH_{c2}/dT] \tag{8}$$

since the dH_{c2}/dT stays constant near T_c. For the intermediate field region (H_{c1}

$<< H << H_{c2}$, where H is the applied magnetic field and H_{c1} and H_{c2} are the lower and upper critical fields, respectively), the London model introduced by Abrikosov [4] approximates the reversible magnetization

$$-4\pi M(H, T) = H - B \approx (\varphi_0/8\pi\lambda^2) \ln(\eta H_{c2}/H), \quad (9)$$

where η is a constant of order of unity [5]. This expression gives a temperature-dependent but field-independent slope

$$d(-4\pi M)/dlnH = -(\varphi_0/8\pi\lambda^2). \quad (10)$$

Because $d(-4\pi M)/dlnH \propto 1/\lambda^2$, the Ginzburg-Landau theory yields $d(-4\pi M)/dlnH \propto (1 - T/T_c)$ near T_c [6]. Hence Eq. (10) can be used to obtain the temperature variation of λ.

In high temperature cuprate superconductors, measurements of magnetization reveal different properties from the prediction of both high-field Abrikosov expression and the London model. For example, (i) an M vs. T plot at fixed H with decreasing T shows a quick deviation from the linear regime and a rounding of M vs. T increases as H increases, (ii) $H_{c2}(T)$ vs. T curves extrapolated to zero magnetization give a positive, rather than negative slope, (iii) there exists a unique crossing point T^* in M vs. T near T_c, (iv) the strong H dependence is found in $d(-4\pi M)/dT$ as well as in $d(-4\pi M)/dlnH$; above T^*, the $-M$ value increases logarithmically with field while below T^* it decreases logarithmically with field, (v) diamagnetism persists even above T_c.

To attack these puzzling behavior and extract thermodynamic quantities from the reversible magnetization, a variational model was developed by Hao

and Clem [4] including the free energy from vortex cores and allowing for the interaction between vortices. Hao and Clem pointed out limitations of the London model (Eq. (6)) due to its lack of the effect of the depression of the order parameter to zero at the vortex centers resulting in the unphysical divergence of both the magnetic flux density and the supercurrent density of an isolated vortex on the axis of the vortex. In this model, they constructed a model for the wave function involving two variables, ξ_v and f_∞, for the effective core radius of a vortex and the depression in the order parameter due to overlapping of vortices, respectively. They then work out the free energy and minimizing it with respect to variables. This gives an internal field in the form of

$$H = \frac{\kappa f_\infty^2 \xi_v^2}{2}\left[\frac{1-f_\infty^2}{2}\ln\left[\frac{2}{B\kappa\xi_v^2}+1\right]-\frac{1-f_\infty^2}{2+B\kappa\xi_v^2}+\frac{f_\infty^2}{\left(2+B\kappa\xi_v^2\right)^2}\right]+\frac{f_\infty^2\left(2+3B\kappa\xi_v^2\right)}{2\kappa\left(2+B\kappa\xi_v^2\right)^3}$$
$$+B+\frac{f_\infty^2}{2\kappa\xi_v K_1\left(f_\infty\xi_v\right)}\left[K_0\left(\xi_v\left(f_\infty^2+2B\kappa\right)^{1/2}\right)-\frac{B\kappa\xi_v K_1\left(\xi_v\left(f_\infty^2+2B\kappa\right)^{1/2}\right)}{\left(f_\infty^2+2B\kappa\right)^{1/2}}\right], \tag{11}$$

where $f_\infty(\kappa,B)$ and $\xi_v(\kappa,B)$ are variational parameters that minimize the total free energy and, for the case of $\kappa > 10$, are approximately given by:

$$f_\infty^2 = 1-\left[\frac{B}{\kappa}\right]^4, \tag{12}$$

$$\left[\frac{\xi_v}{\xi_{v0}}\right]^2 = \left[1-2\left[1-\frac{B}{\kappa}\right]^2\frac{B}{\kappa}\right]\left[1+\left[\frac{B}{\kappa}\right]^4\right], \tag{13}$$

where ξ_{v0} is the value of ξ_v at $B = 0$, which minimizes the free energy of a single vortex and satisfies

$$\kappa\xi_{v0} = \sqrt{2}\left[1 - \frac{K_0^2(\xi_{v0})}{K_1^2(\xi_{v0})}\right]^{1/2}. \qquad (14)$$

For $\kappa >> 1$, ξ_{v0} becomes $\sqrt{2}/\kappa$. The magnetization M is related to H by

$$-4\pi M = H - B. \qquad (15)$$

When the magnitude of the magnetization is small compared with the applied field, the demagnetization effect can be neglected and then the internal field H becomes equal to the applied field. For smaller κ (for example, $\kappa \approx 5$), $\xi_v(\kappa, B)$ is better approximated by

$$\left[\frac{\xi_v}{\xi_{v0}}\right]^2 = 1 + \left[\frac{B}{\kappa}\right]^4. \qquad (16)$$

These equations (from Eq. (11) to (16)) are written in dimensionless units, in which the magnetization and the applied field are given in units of $\sqrt{2}\,H_c$. Hao-Clem model successfully analyzed the experimental reversible magnetization data for a $YBa_2Cu_3O_7$ single crystal [7] and obtained both the values of κ and the temperature dependence of $H_c(T)$.

The next improvement took into account the thermal fluctuations of the order parameter and entropy associated with vortex fluctuation. Bulaevskii and co-workers [8] showed that for $H \| c$, the thermal distortions of the pancake vortices out of the straight stacks (forms 3D vortex lines at $T = 0$) result in an extra contribution to the entropy in the total free energy. Subsequently, Kogan and co-workers [9] modified the London model, after taking entropy terms into account. The magnetization obtained from the total free energy is

$$-4\pi M = \frac{\varphi_0}{8\pi\lambda_{ab}^2(T)}\ln\frac{\eta H_{c2}}{H} - \frac{4\pi k_B T}{\varphi_0 s}\ln\frac{16\pi k_B T\kappa^2}{\alpha\varphi_0 sH\sqrt{e}}, \tag{17}$$

where the λ_{ab} is the in-plane penetration depth, and η and α are constants of order unity. The first term on the right of Eq. (17) is the usual London result as in Eq. (6) for the dense undistorted system, while the second term is from the entropy of thermally fluctuating pancake vortices. The two terms compete with each other as T varies. The slope $d(-4\pi M)/dlnH$ depends on T and becomes zero, therefore giving rise to a crossing point in the M vs. T plot, at a temperature T^* at which M becomes field-independent:

$$-4\pi M(T^*) = \frac{4\pi k_B T}{\varphi_0 s}\ln\eta\alpha\sqrt{e}\,. \tag{18}$$

The temperature T^* is defined by

$$k_B T^* = \frac{\varphi_0^2 s}{32\pi^2\lambda_{ab}^2(T^*)}, \tag{19}$$

i.e. thermal energy ($k_B T^*$) becomes equal to twice the core energy of a pancake vortex, $2\times(H_c^2/8\pi)\times(\pi\xi_{ab}^2)\times s$. This is the energy required to generate a vortex-antivortex pair and corresponds to the Kosterlitz-Thouless transition in two-dimensional superconductors. The existence of the unique crossing point was reported by Kes and co-workers in $Bi_2Sr_2CaCu_2O_8$ [10] and Bulaevskii and co-workers showed that their properties are in good agreement with theory [8]. In Figure 2.3 (a), (b), and (c), three magnetization models are sketched for Abrikosov high field model, Hao-Clem model, and Kogan's modified London model, respectively.

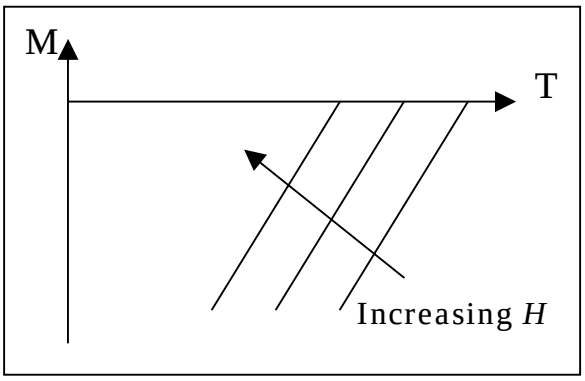

Figure 2.3 (a) Sketch of the Abrikosoc high field approximation. Magnetization has the constant slope near H_{c2} with increasing field.

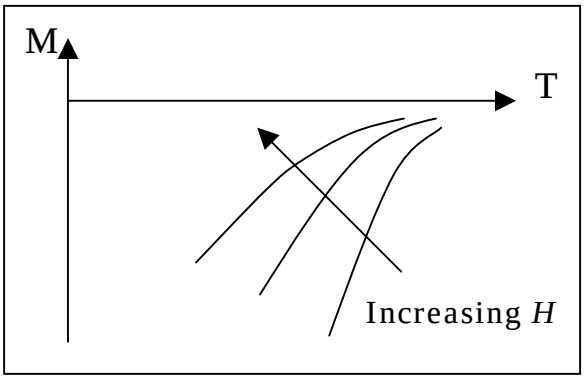

Figure 2.3 (b) Sketch of the Hao-Clem model. Field-dependent slopes are seen.

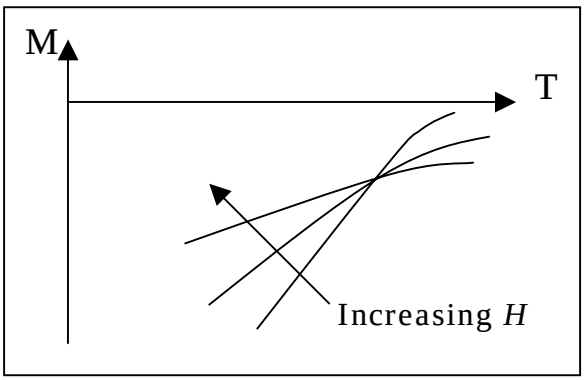

Figure 2.3 (c) Sketch of the modified London model. There exists a unique crossing point.

III. Scaling Theory of Fluctuation of Vortices

In addition to the idea of fluctuating vortices, the models have to be improved to include the dimensionality of the fluctuations. In some materials the coupling of vortices along the *c*-axis is strong and the vortex behaves as a 3D structure. In other materials, the *c*-axis coupling is weak and the vortex behaves as a stack of pancakes where the pancakes in any one layer have a 2D fluctuation. High temperature cuprate superconductors exhibit large anisotropies due to the layered structure in nature. With extremely short coherence length and high transition temperature, they are more likely to give rise to fluctuations of vortices than conventional superconductors. The fluctuating quantity is either the fluctuation of vortex position (the phase of the order parameter) in low magnetic fields or the amplitude of order parameter of fluctuating vortices in high fields near H_{c2}.

Determining the dimensionality of the fluctuations drew large attention and Ullah and Dorsey [11] obtained expressions for the scaling functions of various thermodynamic and transport quantities. The scaling function for the magnetization can be written in the variable $[T - T_c(H)]/(TH)^n$, where n is 1/2 for a 2D system and 2/3 for a 3D system. If we plot magnetization data in $M/(TH)^n$ vs. $[T - T_c(H)]/(TH)^n$, the data collapse onto a single curve depending on the dimensionality of the system. The scaling functions are valid only in either the two- or three- dimensional limits. Even though they are obtained from

the case of the lowest Landau level (high fields), the scaling forms are not restricted to the high-field case and do not change their functional form when we include higher Landau levels.

In the critical fluctuation region near H_{c2}, Tesanovic and co-workers [12] derived explicit closed form expressions for the magnetization of the 2D type-II superconductors. The magnetization in the magnetic field parallel to the *c*-axis is given by

$$-4\pi M = -2\pi M^* \left[1 - \tau - h + \sqrt{(1 - \tau - h)^2 + 4h} \right], \qquad (20)$$

where $\tau = (T - T^*)/(T_{c0} - T^*)$ and $h = H/H'_{c2}(T_{c0} - T^*)$. H'_{c2} is the slope of the H_{c2} line at T_{c0} and $M^*(T^*)$ is the value of magnetization determined directly from the crossing point. This expression is valid at $h \geq |1 - \tau|/3$. The two parameters T_{c0} and H'_{c2} can be found by fitting data to Eq. (20).

References

1. J. Bardeen, L. N. Cooper, and J. R. Schrieffer, Phys. Rev. **108**, 1175 (1957).
2. M. W. Zemansky, Heat and Thermodynamics, (1957), McGraw-Hill, fourth Ed. York, PA.
3. A. L. Fetter and P. C. Hohenberg, in Superconductivity, edited by R. D. Parks (Dekker, New York, 1969), p. 817.

4. A. A. Abrikosov, *Zh. Eksperim. i Teor. Fiz.* **32**, 1442 (1957); Sov. Phys. JETP **5**, 1174 (1957).

5. Z. Hao and J. R. Clem, Phys. Rev. Lett. **67**, 2371 (1991).

6. V. G. Kogan, M. M. Fang and S. Mitra, Phys. Rev. B **38**, 11958 (1988).

7. Z. Hao, J. R. Clem, M. W. McElfresh, L. Civale, A. P. Malozemoff and F. Holtzberg, Phys. Rev. B **43**, 2844 (1991).

8. L. N. Bulaevskii, M. Ledvij and V. G. Kogan, Phys. Rev. Lett. **68**, 3773 (1992).

9. V. G. Kogan, M. Ledvij, A. Yu. Simonov, J. H. Cho, and D. C. Johnston, Phys. Rev. Lett. **70**, 1870 (1993).

10. P. H. Kes, C. J. van der Beek, M. P. Maley, M. E. McHenry, D. A. Huse, M. J. Menken, and A. A. Minovsky, Phys. Rev. Lett. **67**, 2383 (1991).

11. S. Ullah and A. T. Dorsey, Phys. Rev. Lett. **65**, 2066 (1990); Phys. Rev. B **44**, 262 (1991).

12. Z. Tesanovic, L. Xing, L. Bulaevskii, Q. Li and M. Suenaga, Phys. Rev. Lett. **69**, 3563 (1992).

CHAPTER 3. EXPERIMENTS

I. Introduction

$La_{2-x}Sr_xCuO_{4-\delta}$, La-214, may be the simplest structure among the high temperature cuprate superconductor systems (Figure 3.1). It has the body-centered-tetragonal structure and consists of single planar CuO_2 sheets formed from Cu-centered O_4 squares that are corner shared. Two additional O atoms are located above and below each Cu atom to form an axially elongated CuO_6 octahedron [1]. In Figure 3.1, O atoms are located at the edge of the each octahedron and the closed circles are for Cu atoms. The open circles are the La atom sites and also where the Sr atom sits when replacing La upon doping. Each unit cell contains two formula units (therefore two Cu atoms) per unit cell of size ~ 0.38 × 0.38 × 1.33 nm^3. At high temperatures (depending on the doping concentration) there is a structural phase transition to an orthorhombic phase, arising from the oxygen octahedra tilting about the tetragonal [1 1 0] direction, resulting in slight difference in the lattice parameter by small amounts from those in the tetragonal phase.

The parent material La_2CuO_4 is an antiferromagnetic Mott insulator with a Neel temperature of about 300 K. It is insulating because of the strong repulsive

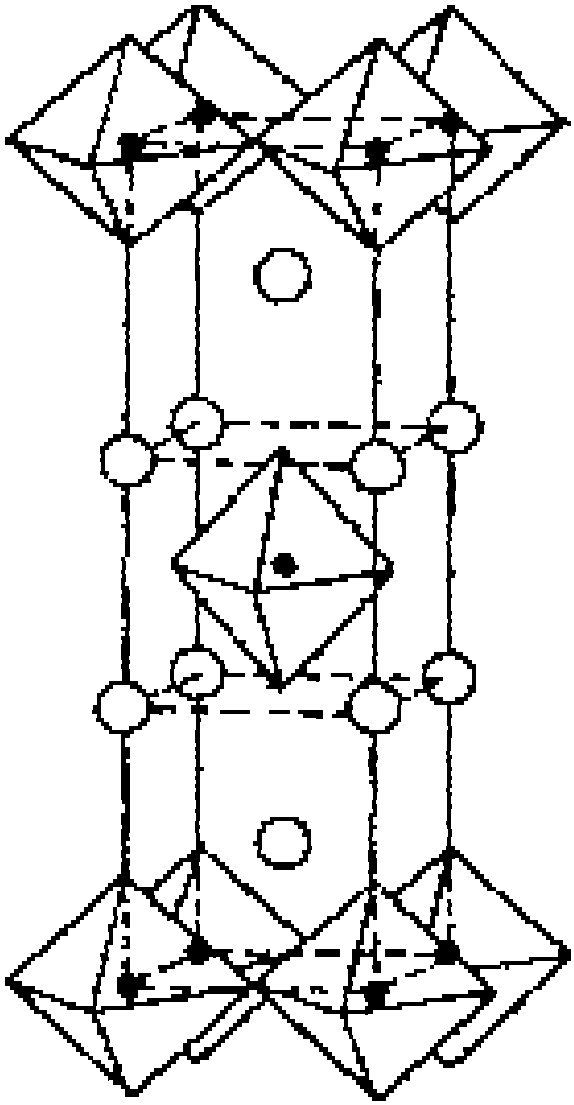

Figure 3.1 The crystal structure of $La_{2-x}Sr_xCuO_4$ [from Ref. 2].

force between electrons occupying the same crystal lattice sites, unlike usual insulators in which all the Brillouin zones that contain any electrons at all are full. The oxidation states of the La and O ions are assumed to be 3+ and 2-, respectively, leaving Cu in an oxidation state of 2+ carrying a local magnetic moment with spin S = 1/2. Thus the Cu ion would have a $3d^9$ electron configuration with one hole in the d shell and the O configuration is $2p^6$, a complete p shell. It becomes a metal, however, when sufficiently doped with Sr. If we substitute a Sr^{2+} ion for one of the La^{3+}, then we remove one positive charge from the *LaO* layer and an electron is removed from the CuO_2 layer to compensate it. Therefore, each Sr acts as an acceptor and creates one hole in the uppermost band of the CuO_2 layer (it is possible to have holes in *LaO* layers, but holes in CuO_2 layers have lower energy). The positive sign of the Hall coefficient measurements indeed indicates that the carriers are holes. The Hall coefficient decreases rapidly with doping and changes sign near $x = 0.35$ [3].

The structural and magnetic phase diagram is shown in Figure 3.2. As the hole concentration is increased by doping with Sr, the Neel temperature falls quickly and the bulk antiferromagnetism disappears around $x = 0.02$. Increasing x first leads to a spin-glass region from $x = 0.02$ to $x = 0.05$ and then to superconductivity near $x = 0.05$. Coexistence of the antiferromagnetic-cluster nature of the spin glass and superconducting phases is found near $x = 0.06$ [5]. The transition temperature T_c increases with further doping until a maximum value of about 40 K is reached at optimum doping $x = 0.15$, beyond which T_c

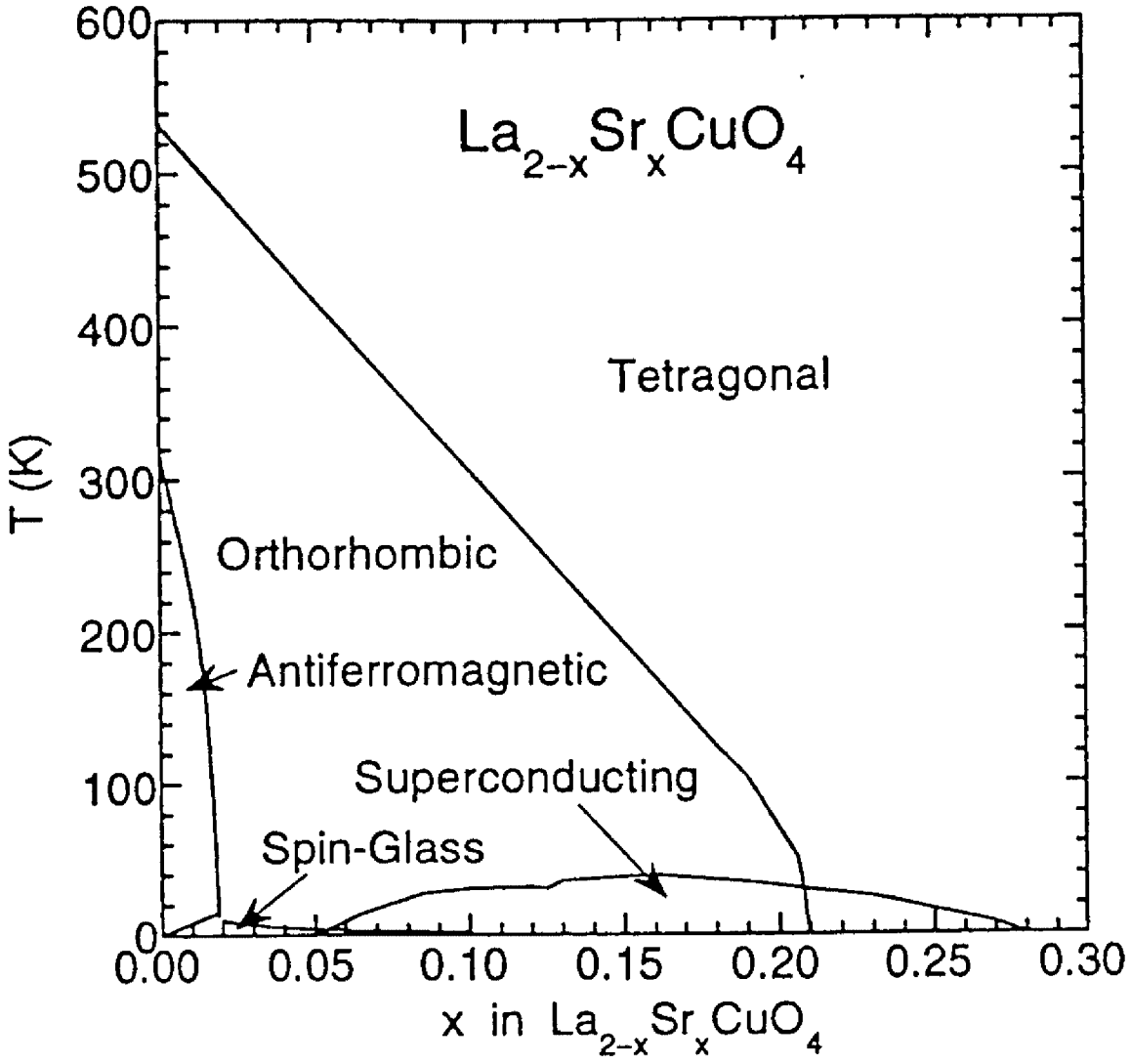

Figure 3.2 Structural and magnetic phase diagram of $La_{2-x}Sr_xCuO_4$ [from Ref. 4].

decreases, until about x = 0.26, above which superconductivity is no longer observed [6]. Further doping yields a normal-metal behavior (0.26< x < 0.6) and then semiconducting properties (x > 0.6) [2].

II. Sample Preparation

The three single crystals used through this work were prepared by a solution method for x = 0.06 [7] and a floating zone method in an image furnace for x = 0.10 [8] and x = 0.13 [9]. The x = 0.06 sample is the one used to study "Charge Segregation, Cluster Spin Glass, and Superconductivity" [5] and the x = 0.10 sample is for the study of "Glassy spin freezing and NMR wipeout effect" [10].

The x-ray photographs were taken at several places on the surface of the crystal to establish that it was a single crystal and the c axis was found to be perpendicular to one of the cleavage planes for x = 0.10 sample as shown in Figure 3.3 and Figure 3.4. In Figure 3.3 (a) and (b), the images are from the opposite sides of sample in the c-axis direction. In Figure 3.4 (a) and (b), the images are from two randomly chosen points perpendicular to the c-axis.

Magnetically aligned samples of $La_{2-x}Sr_xCuO_4$ were prepared by grinding appropriate amounts of Lanthanum oxide (La_2O_3), strontium carbonate ($SrCO_3$), and copper oxide (CuO) (>99.99% purity) in an agate mortar and pestle. Mixed and ground powders were pressed in hydraulic pressure to pellets of size ~ 0.75

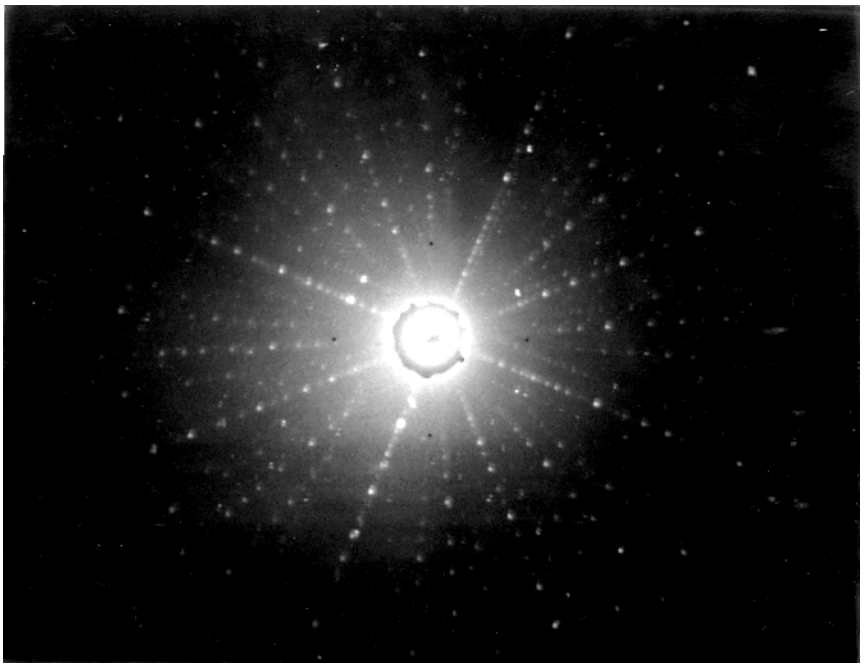

Figure 3.3 (a) The x-ray image in *c*-direction for $La_{1.90}Sr_{0.10}CuO_4$.

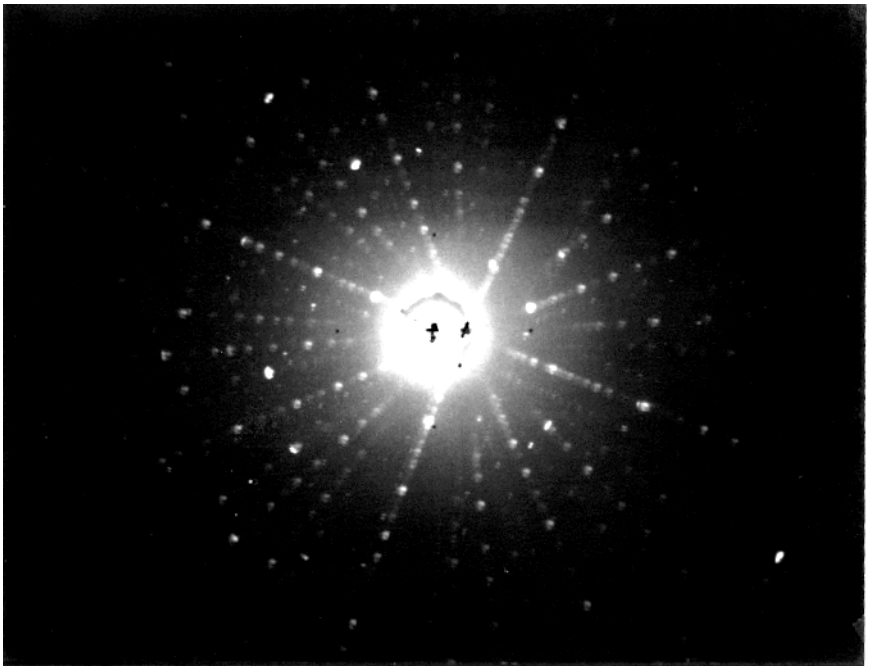

Figure 3.3 (b) The x-ray image in *c*-direction for $La_{1.90}Sr_{0.10}CuO_4$.

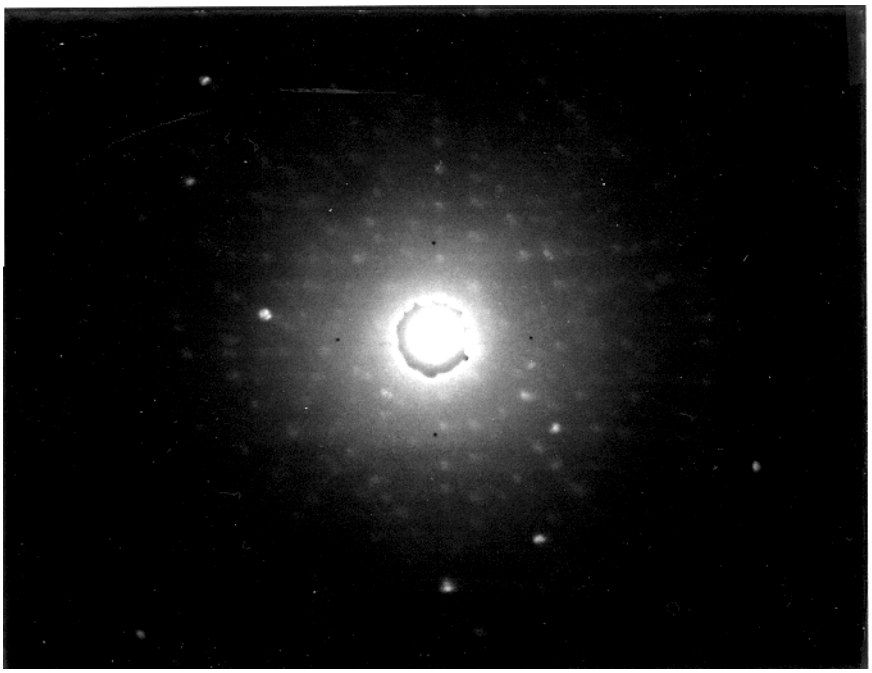

Figure 3.4 (a) The x-ray image perpendicular to *c*-axis for $La_{1.90}Sr_{0.10}CuO_4$.

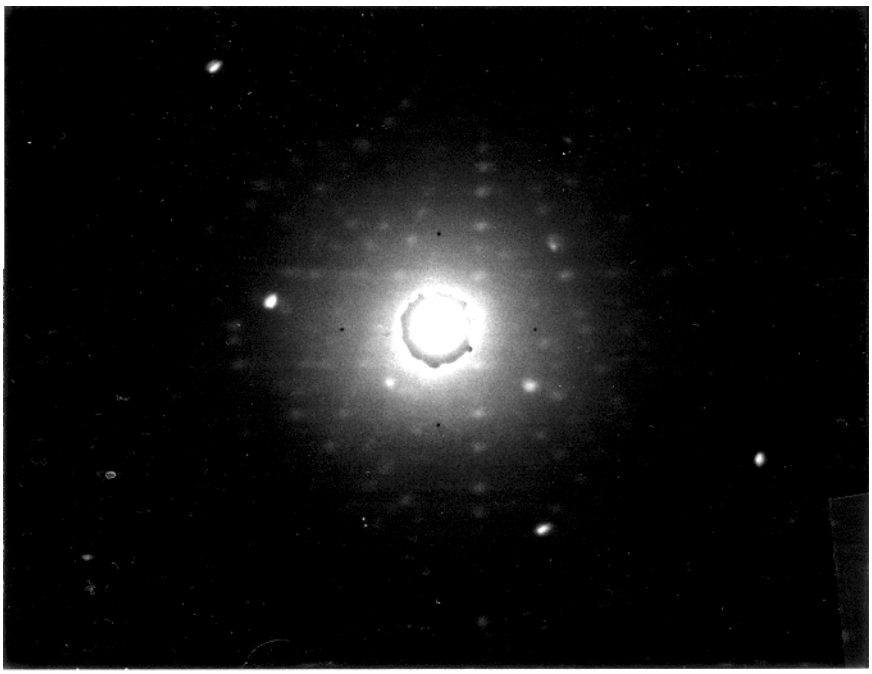

Figure 3.4 (b) The x-ray image perpendicular to *c*-axis for $La_{1.90}Sr_{0.10}CuO_4$.

$\times$ 0.25 $\times$ 0.125 in^3. Pellets were placed in an alumina boat and initially fired for 24 hours at 750 °C, and then at temperatures ranging from 850 °C to 970 °C in air for 48 and 72 hours, respectively, with intermediate pulverizing, grinding and pelletizing. Each time samples were quenched down to room temperature by quickly exposing to air. After repeated pulverizing, grinding, pelletizing and sintering at successively higher temperatures (1000 °C, 1050 °C and 1100 °C) in a tube with a flow of pure oxygen (flow rate of 2.5 cubic centimeters per minute) for 24 hours each time, measurements of the transition temperature and Meissner shielding fraction were made in a field of 1.0 mT as the first diagnostic of sample quality. The final pellet was ground to a particle size of about 20 μm. This powder was mixed and suspended in a low viscosity and low magnetic susceptibility liquid epoxy (Epotek 301), oriented in a magnetic field of 8.0 T, and then the epoxy was allowed to harden in the field. X-ray diffraction patterns [11] from θ-2θ scans for the samples which we have chosen for the present experiments exhibit only the (0 0 1) peaks, which indicate nice alignment of the grains in the *c*-direction, and the lattice parameter extracted was about 1.3 nm comparing well with the accepted value of 1.33 nm. The FWHM for the (0 0 8) peak shows a rather broad peak about 5° wide. All metal elements were analyzed by employing an inductively coupled plasma (ICP) technique from which the Sr content *x* was determined.

Magnetization data were taken with $H \| c$ in a Quantum Design superconducting quantum interference device magnetometer over the full range

of temperatures from 2.0 K to 300 K and magnetic fields up to 7.0 T. The measurements were performed with 6-cm scan length except x = 0.13 single crystal sample for which 3-cm scan length was used. Reversible magnetization data are obtained by averaging zero-field-cooled and field-cooled data above irreversible temperature for each field within one percent of differences.

For any given x–value, the best indication of sample quality seems to be the transition temperature and Meissner shielding fractions. Samples are carefully selected by comparing with the accepted values of transition temperatures for the given hole concentrations published in the literatures [12] to avoid complications due to the possible oxygen deficiency. The transition temperatures in Figure 3.5 are plotted along with the empirical parabolic expression (solid line) [13]. The triangles indicate that they are single crystals. As x increases, T_c shows broadening in the neighborhood of x ~ 1/8 which is known as "1/8–anomaly" in the La-214 system.

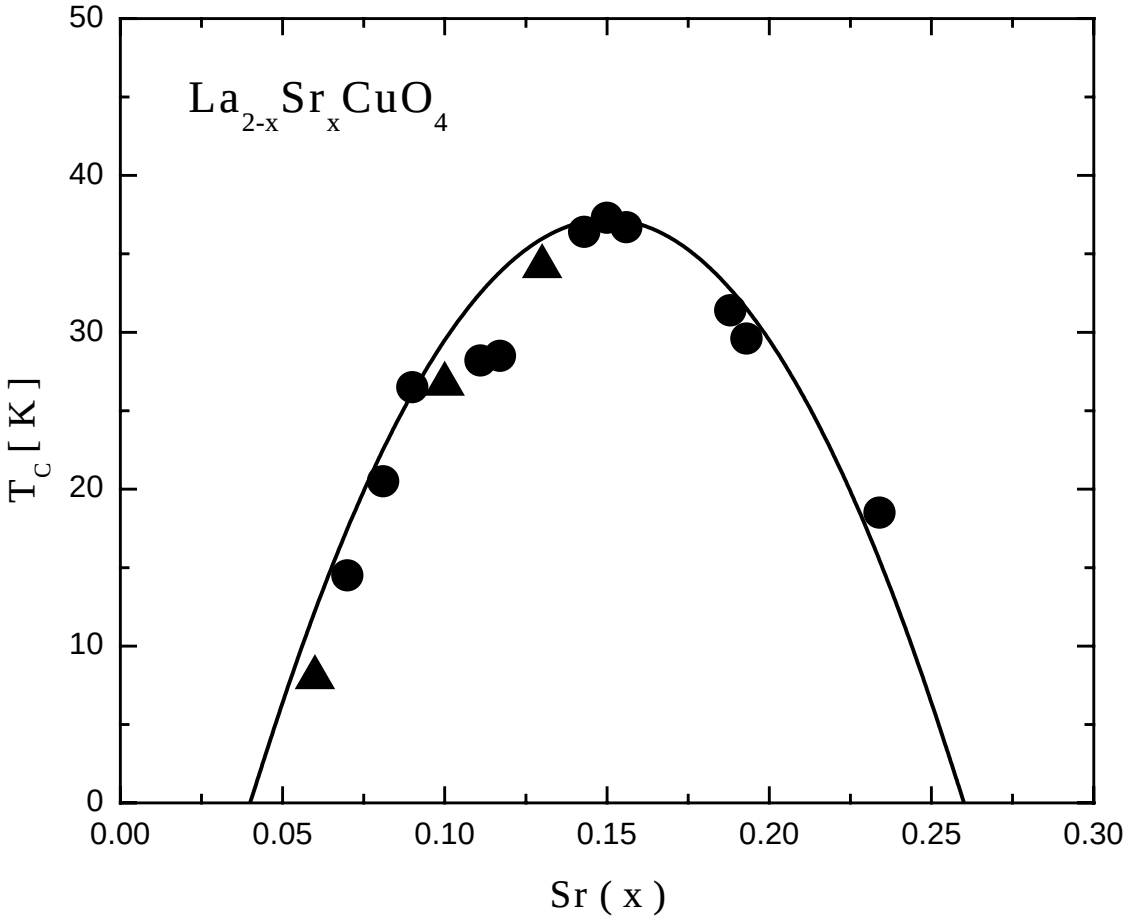

Figure 3.5 Transition temperatures of $La_{2-x}Sr_xCuO_4$. The triangles are for single crystals and the circles are for aligned powder samples.

References

1. D. C. Johnston, in *Handbook of Magnetic Materials, Normal-state magnetic properties of single-layer cuprate high-temeprature superconductors and related materials*, edited by K. H. J. Buschow, Vol. 10, (North-Holland, Amsterdam, The Netherlands, 1997), p. 1.

2. K. Sreedhar and P. Ganguly, Phys. Rev. B **41**, 371 (1990)

3. H. Y. Hwang, B. Batlogg, H. Takagi, H. L. Kao, J. Kwo, R. J. Cava, J. J. Krajewski, and W. F. Peck, Jr, Phys. Rev. Lett. **72**, 2636 (1994).

4. D. C. Johnston, F. Borsa, P. Carretta, J. H. Cho, F. C. Chou, M. Corti, R. J. Gooding, E. Lai, A. Lascialfari, L. L. Miller, N. M. Salem, B. J. Suh, D. R. Torgeson, D. Vaknin, K. J. E. Vos, and J. L. Zarestky, in *High-T_c Superconductivity 1996: Ten Years after the Discovery*, edited by E. Kaldis, E. Liarokapis, and K. A. Müller (Kluwer, Dordrecht, 1997), p. 311.

5. M.-H. Julien, F. Borsa, P. Carretta, M. Horvatić, C. Berthier, and C. T. Lin, Phys. Rev. Lett. **83**, 604 (1999).

6. J. B. Torrance, T. Yokura, A. I. Nazzal, A. Bezinge, T. C. Huang, and S. S. P. Parkin, Phys. Rev. Lett. **61**, 1127 (1988).

7. C. T. Lin, E. Schönherr and K. Peters, Physica C (Amsterdam) **282C–287C**, 491 (1997).

8. A. Revcolevschi and J. Jegoudez, Prog. Mater. Sci. **42**, 321 (1997); S. Petit, A. H. Moudden, B. Hennion, A. Vietkin, and A. Revcolevschi, Eur. Phys. J. B **3**, 163 (1998).

9. This sample was provided by Dr. Q. Li at Brookhaven National Laboratory

10. M.-H. Julien, A. Campana, A. Rigamonti, P. Carretta, F. Borsa, P. Kuhns, A. P. Reyes, W. G. Moulton, M. Horvatić, C. Berthier, A. Vietkin and A. Revcolevschi, Phys. Rev. B **63**, 144508 (2001).

11. For powder diffraction pattern, λ = 0.07093 nm was used.

12. P. G. Radaelli, D. G. Hinks and A. W. Mitchell, B. A. Hunter and J. L. Wagner, B. Dabrowski, K. G. Vandervoort, H. K. Viswanathan, and J. D. Jorgensen, Phys. Rev. B **49**, 4163–4175 (1994); J. B. Torrance, A. Bezinge, A. I. Nazzal, T. C. Huang, S. S. Parkin, D. T. Keane, S. J. LaPlaca, P. M. Horn and G. A. Held, Phys. Rev. B **40**, 8872 (1989); J. B. Torrance, Y. Tokura, A. I. Nazzal, A. Bezinge, T. C. Huang and S. S. Parkin, Phys. Rev. Lett. **61**, 1127 (1988); H. Takagi, R. J. Cava, M. Marezio, B. Battlog, J. J. Krajewski and W. F. Peck, Jr., Phys. Rev. Lett. **68**, 3777 (1992);

13. T. Nagano, Y. Tomioka, Y. Nakayama, K. Kishio and K. Kitazawa, Phys. Rev. B **48**, 9689 (1993).

14. J. L. Tallon, C. Bernhard, H. Shaked, R. L. Hitterman and J. D. Jorgensen, Phys. Rev. B **51**, 12911–12914 (1995); M. R. Presland, J. L. Tallon, R. G. Bukley, R. S. Liu, and N. E. Flower, Physica C **176**, 95 (1991).

CHAPTER 4. REVERSIBLE MAGNETIZATION AND SUPERCONDUCTING STATE THERMODYNAMIC PARAMETERS FOR UNDERDOPED $La_{1.90}Sr_{0.10}CuO_4$

A paper published in Phys. Rev. B. Volume **63**, 064512 (2001)

Yung M. Huh, J. E. Ostenson, F. Borsa, V. G. Kogan, and D. K. Finnemore
Ames Laboratory, U.S. Department of Energy and
Department of Physics and Astronomy, Iowa State University, Ames, Iowa 50011

A.Vietkin and A. Revcolevschi
Laboratorie de Physico-Chimie des Solides, Universite Paris-sud,
Orsay, France

M.-H. Julien
Laboratoire de Spectrometrie Physique, Universite J. Fourier,
BP 87, 38402 Saint Martin d'Heres, France

Abstract

Magnetization studies have been made of single-crystal $La_{1.90}Sr_{0.10}CuO_4$ with $H \| c$ in order to determine the magnitude of the flux expulsion and free energy in a material that has substantially less than optimal doping. Well above the superconducting transition temperature, the normal-state magnetization exhibits a two-dimensional Heisenberg antiferromagnetic behavior. Below T_c, there is a large portion of the H-T plane where the sample shows reversible behavior so that thermodynamic variables such as the free energy and the shape of the magnetization curves can be determined. At low temperature, the vortices

have a well-defined Abrikosov regime that transforms to two-dimensional fluctuation behavior at higher temperatures. The magnetization vs. temperature curves show a unique crossing point at 22 K where the magnetization is independent of magnetic field. From this value of the crossing point, the effective layer spacing *s* is derived to be 1.6 nm compared to the CuO_2 lattice spacing of 0.66 nm. The fluctuations are found to obey two-dimensional scaling in that $M/(TH)^{1/2}$ is a universal function of $[T - T_c(H)]/(TH)^{1/2}$. Below 12 K, the data fit the Hao-Clem theory rather well and give κ_c values of about 175 and thermodynamic critical fields ranging from 112 mT at 12 K to 133 mT at 6 K.

I. Introduction

Many of the high-temperature superconductors now can be prepared in single-crystal form with sufficiently high purity that there is a wide range of thermodynamic reversibility in the magnetization curves. From these measurements of reversible magnetization, the change in free energy with magnetic field can be determined from $G_n - G_s(H) = -\int_0^H M_{sc}\,dH$. There is a very direct connection between reversible magnetization and free energy changes.

The underdoped high-temperature superconductor $La_{1.90}Sr_{0.10}CuO_4$ is a rather special material for the study of reversible magnetization and fluctuation diamagnetism because it still retains a relatively high transition temperature,

and yet it also shows a substantial range of pseudogap behavior well above T_c [1]. As the sample is cooled, the pseudogap begins to open at about 600 °C and the material goes superconducting at T_c ~ 30 K. Optimum doping for this material occurs for a Sr content of about 0.15, so the single crystal under study here has about 2/3 the optimum number of charge carriers. There is a rich phase diagram in the *H*-*T* plane [2, 3] with several different changes in the vortex lattice. With the onset of superconductivity on cooling, quantized vortices first form in a liquid state, and then, with further cooling, this transforms to a variety of glasslike structures or regular lattice structures often depending on impurities and precipitates in the material. Important variables are the superfluid density, the anisotropy of the effective mass, $\gamma_{\text{ani}}^{\ 2} = m_c/m_{ab}$, the entropy associated with the flux-line lattice, and the nature of defects in the material. Changes in the flux-line lattice such as the melting transition are usually measured with transport properties [2], but some of these changes may also be reflected in the free energy and in the shape of the reversible magnetization curves.

Some time ago, Kes and co-workers [4] showed that the reversible magnetization curves, *M* vs. *H*, of $Bi_2Sr_2CaCu_2O_{8+\delta}$, Bi-2212, have two rather different types of behavior depending on *T*. At low temperature, a plot of *M* vs. *H* followed the classical Abrikosov [5] rigid-lattice behavior with |*M*| falling monotonically toward zero for fields larger than the lower critical field H_{c1} and smaller than the upper critical field H_{c2}. As the temperature rises, however,

there are entropy terms [4, 6] in the free energy related to fluctuations in the flux-line lattice, and the reversible magnetization curves have been shown to have a crossover from Abrikosov-like [5] behavior at low temperature to fluctuation-like behavior [4, 6] as the temperature approaches the transition temperature, T_c. There is, in fact, a unique crossing point on the M vs. T plot where M is independent of H. For Bi-2212, where the anisotropic ratio, $\gamma_{\text{ani}} = [m_c/m_{ab}]^{1/2}$, is about 200, this crossover occurs at a reduced temperature of about $T/T_c = 0.95$ [4]. The data show magnetization vs. temperature (M vs. T) curves for various magnetic fields that cross at a single temperature, $T^* = 88.3$ K where M is independent of H. If these same data can be cast as M vs. H curves, the curves show Abrikosov-like behavior well below 86 K, and fluctuation-like behavior above 86 K. In the fluctuation regime, Li *et al.* [7] have shown two-dimensional (2D) scaling behavior for $Bi_2Sr_2Ca_2Cu_3O_{10+\delta}$, Bi-2223, in that a plot of $M/(TH)^{1/2}$ is a universal function of $[T - T_c(H)]/(TH)^{1/2}$. In addition, Welp and co-workers [8] have shown three-dimensional, 3D, scaling behavior for $YBa_2Cu_3O_{7-\delta}$, Y-123, in that $M/(TH)^{2/3}$ is a universal function of a $[T - T_c(H)]/(TH)^{2/3}$. Theoretical work by Tesanovic and Andreev [9] has worked out these closed form relation for the scaling in both 2D and 3D.

Oxygen depletion is a standard way to alter the superfluid density and thus possibly increasing the 2D behavior in these high-temperature superconductors. This is illustrated by the work of Janossy *et al.* [10] who have shown that the effective mass ratio, $\gamma_{\text{ani}} = [m_c/m_{ab}]^{1/2}$, can be raised in $YBa_2Cu_3O_{7-\delta}$ from about 5

to 25 by depleting the oxygen content from ~7.0 to ~6.5. Depleting oxygen, or underdoping, then may be a method to transform a superconductor from 3D to 2D behavior. In addition to the work with Y-123, this group also has shown that optimally doped $La_{1.85}Sr_{0.15}CuO_4$ has an anisotropy ratio of about γ_{ani} ~ 10 to 20, and Willemin et al, have shown that $La_{1.90}Sr_{0.10}CuO_4$, has γ_{ani} = 43 [11]. Hence $La_{1.90}Sr_{0.10}CuO_4$, might be expected to show a crossover from Abrikosov-like magnetization curves to fluctuation-like magnetization curves at a relatively low reduced temperature.

Two other cases where the magnetization curves resemble the fluctuation-like behavior are the stripe phase superconductor, $La_{1.45}Nd_{0.40}Sr_{0.15}CuO_4$ [12, 13], and Bi-2212 with a dense array of columnar defects [14]. For the $La_{1.45}Nd_{0.40}Sr_{0.15}CuO_4$ sample, M vs. H curves show fluctuation-like curves at reduced temperatures as low as T/T_c = 0.5. For the Bi-2212 sample with columnar defects [14], the crossover point disappears. In addition, many of the vortex cores reside on the columnar defects thus altering the field dependence of the magnetization.

The purpose of this work is to study the shape of the magnetization, M vs. H, curves for underdoped La-214 in order to determine the free energy of the vortex lattice and the temperature range over which fluctuation behavior is observe. To do this, it is necessary to determine the normal-state magnetization [15] above T_c to confirm that the Cu spins follow a 2D Heisenberg antiferromagnetic behavior [16] and to obtain analytical fits to subtract

background. Several different spin configurations and models can give a susceptibility that slowly decreases as the temperature decreases [17] as is seen here. If one assumes that the superconducting transition does not change the configuration of the background spin susceptibility, then the superconducting flux expulsion can be obtained from the measured total magnetization by subtracting the normal-state background. This procedure, of course, only makes sense if the magnetization is thermodynamically reversible, so it is also important to establish the irreversibility line, H_{irr} vs. T and verifies that there is a large reversible region in the H vs. T plane. Reversible magnetization data are then fit to a theoretical model to estimate the thermodynamic critical field curve. A secondary goal of the work is to look for diamagnetic fluctuations at the temperatures well above T_c in the regime normally called the pseudogap regime. This is difficult because the signal becomes progressively smaller as T increases and the signal gradually disappears into the background magnetization.

II. Experiment

The single crystal used in these measurements was prepared by a floating zone method in an image furnace [18], and it is the same crystal used for NMR spin-lattice relaxation studies [19]. X-ray photographs were taken at several places on the surface of the crystal to establish that it was a single crystal and the c axis was found to be perpendicular to one of the cleavage planes.

Magnetization data were taken with $H \| c$ in a Quantum Design superconducting quantum interference device magnetometer over the full range of temperatures from 4.5 K to 200 K and magnetic fields up to 7.0 T.

III. Results and Discussion

From 55 to 200 K, where the sample is normal, the magnetization is of the form

$$M = CH + M_s \tanh(\beta H) \quad (1)$$

as shown in Figure 4.1. The inset shows the behavior at low field and the solid lines are the fits to Eq. (1).

Results show that $4\pi M_s = 0.060 \pm 0.001$ G and $\beta = (8.15 \pm 1.54) \times 10^{-4}$ G^{-1} over the whole temperature range so the second term in Eq. (1) is independent of temperature. Over most of the *H-T* plane, this whole term is small compared to both *CH* and the superconducting magnetization. This means that there is a small "ferromagnetic" moment parallel to the *c* axis that saturates at a few tenth of a Tesla and remains constant over the entire temperature range.

Values of *C*, which is the dimensionless volume susceptibility, range from 1.32×10^{-6} at 200 K to 8.76×10^{-7} at 55 K and are close to those measured by Nakano *et al.* [20] and Johnston [15] in this range of doping. Hence the normal-state magnetization follows 2D Heisenberg antiferromagnetic behavior rather well.

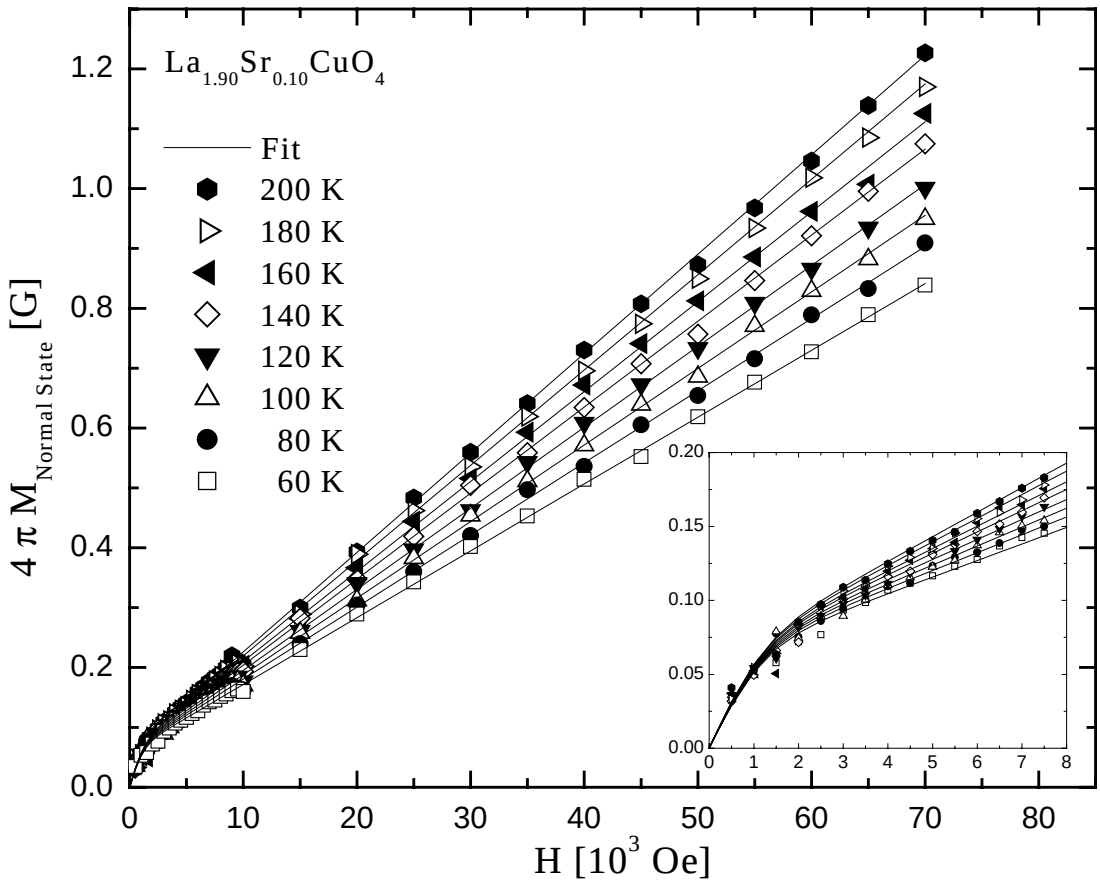

Figure 4.1 Normal state magnetization every 20 K from 60 to 200 K. The solid lines are fits of the data to Eq. (1). The inset expands the low-field portion.

To subtract the background magnetization at lower temperatures, we follow the lead of de Jongh [16] and assume that magnetization from the Cu spins continues to follow 2D antiferromagnetic behavior at temperatures below 40 K. Values of $C(T)$ are obtained by linearly extrapolating the C vs. T curve between 200 and 55 K to lower temperature. To investigate worst cases for background subtraction, two other assumptions about the temperature dependence of C have been made: (i) C falls linearly to zero as T goes to zero, (ii) C rises about 20% above the 40 K value as T goes to zero as happens for some antiferromagnets [16]. The normal-state background is small enough that the basic conclusions about the thermodynamic critical line are not changed within ±1 mT.

With the assumption that the onset of superconductivity does not alter the magnetization of the Cu spins, and the superconducting magnetization M_{sc} is derived from $M_{sc} = M_t - M_b$, where M_t is the total magnetization and M_b is the background magnetization. At 16 K and 5 T, the background is about 20 % of the total magnetization. A study of the irreversibility shows that H_{irr} rises from zero at 28 K to 0.5 T at 15 K, 1.0 T at 10 K, and 2.5 T at 6 K. Hence there is a wide range of thermodynamic reversibility in the H-T plane.

Superconducting magnetization curves are shown for every 2 K from 8 K to 30 K in Figure 4.2. All of these data are in the region of thermodynamic reversibility. Below 18 K, the M vs. H curves monotonically approach zero from the negative side in a fashion similar to an Abrikosov type-II superconductor [5]. Above 22 K, the magnetization rises from zero at $H = 0$ similar to fluctuation

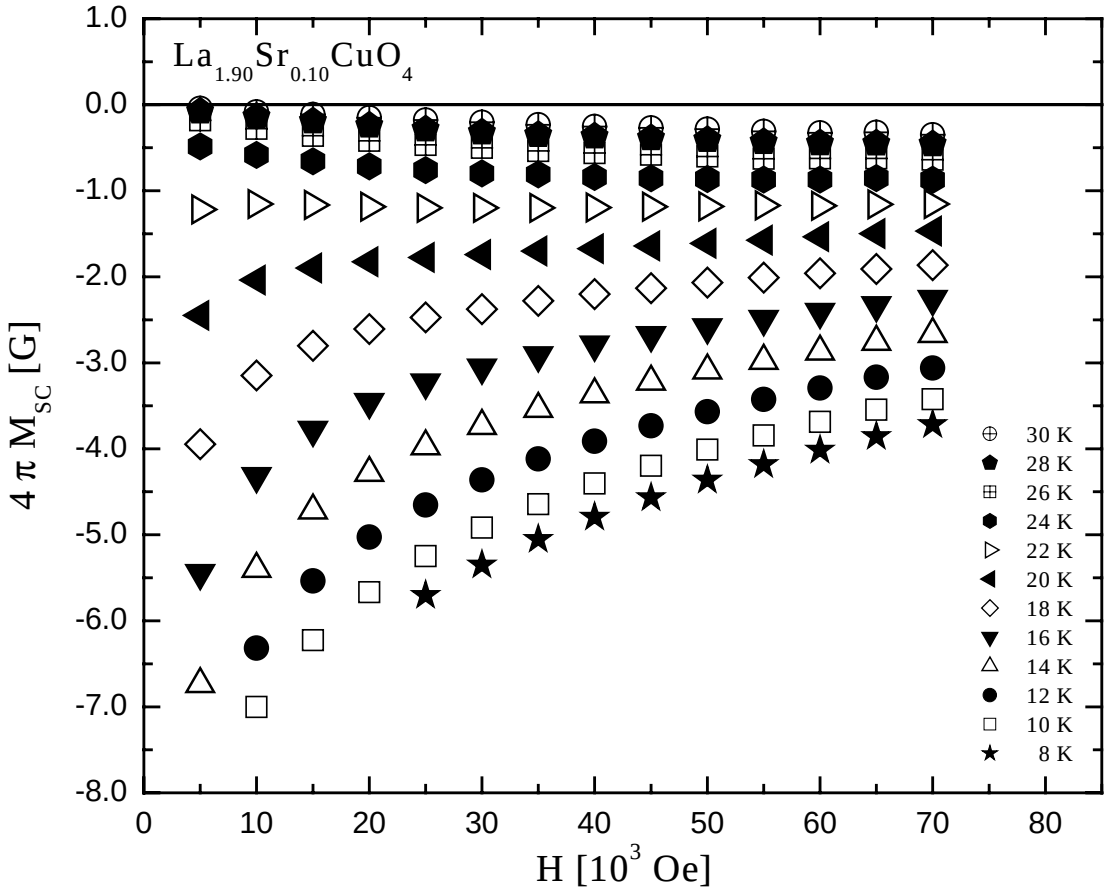

Figure 4.2 Superconducting magnetization curves every 2 K from 8 to 30 K showing Abrikosov-like behavior below 18 K and fluctuation-like behavior above 22 K.

behavior [4]. If these same data are cast as M vs. T, as shown in Figure 4.3, there is a crossing point just above 22 K where the curves cross and the magnetization is independent of H [4, 6]. At the crossover temperature T^* the magnetization is given by $M^* = -k_B T^*/\phi_0 s$ [6]. Using $T^* = 22.0$ K and $4\pi M^* = -1.13$ G gives an effective layer spacing, $s = 1.6$ nm compared with the CuO_2 plane spacing of 0.66 nm. It is possible that the $s = 1.6$ nm value from these measurements arises because only part of the sample is superconducting thus giving rise to smaller M^* value as described by Kogan *et al.* [21]. With this interpretation, the ratio of 0.66 nm/1.6 nm gives 41% of this underdoped $La_{1.90}Sr_{0.10}CuO_4$ sample being superconducting. In a closely related measurement, Iwasaki *et al.* found a value of $s = 1.49$ nm for $La_{1.92}Sr_{0.08}CuO_4$ [22]. In addition, Mosqueira *et al.* [23] have studied the crossover in $La_{1.90}Sr_{0.10}CuO_4$ for grain-aligned powders. They find $T_c = 28$ K, $T^* = 25$ K, and essentially the same M^* as seen here.

The crossover feature that is well obeyed from 0.5 to 7.0 T is not obeyed in the low flux density limit of 0.001 T or 1mT. As shown by the solid line in Figure 4.3, an M vs. T curve taken at 1.0 mT deviates from zero somewhere in the 26 ~ 27 K range. The curve shown for 0.1 T also misses the crossing point. A 1.0 mT magnetization run is often used to define a T_{c0}, the mean-field transition temperature, and for this sample, a temperature more like 26.5 K. This would imply that for this sample, T_{c0} is about 5 K above T^*.

There is a substantial amount of fluctuation diamagnetism all the way up

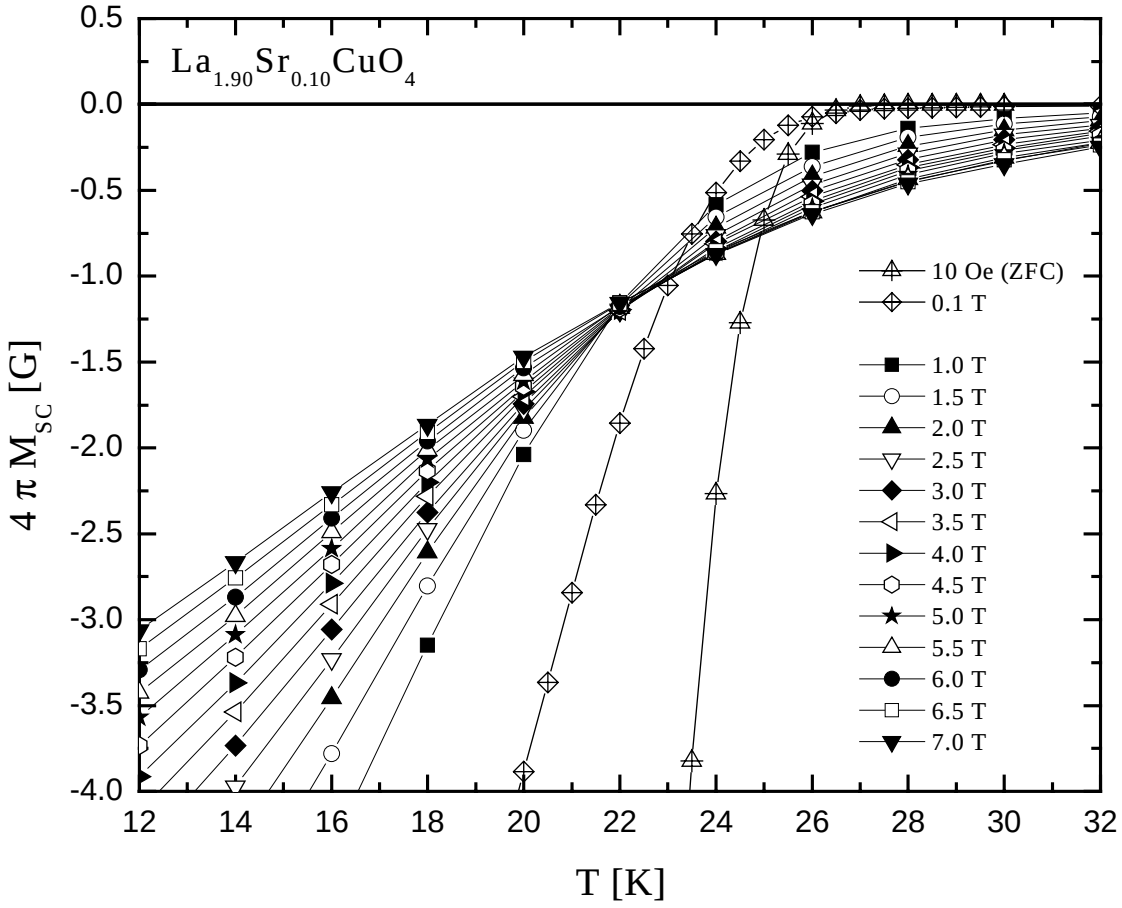

Figure 4.3 Magnetization vs. temperature showing the crossover at 22 K. Data are plotted every half Tesla from 1.0 to 7.0 T.

to 30 K, as shown in Figure 4.3, that might be fit to fluctuation theories [8]. Even at 30 K, the magnetization is still increasing with increasing field all the way up to 7.0 T, as shown in Figure 4.2. If the data are plotted as $M/(TH)^{1/2}$ vs. $[T - T_c(H)]/(TH)^{1/2}$, the data lie on a common curve as shown in Figure 4.4. In this analysis, $T_c(H)$ is determined by taking T_{c0} = 26.8 K from the Hao-Clem fits to these data and by taking the slope of dH_{c2}/dT = –3.20 T/K from Eq. (13) of Tesanovic *et al.* [9]. Attempts to fit to 3D scaling gave less good fits.

In an attempt to make a reasonable estimate of the thermodynamic critical field, each of the magnetization curves in Figure 4.2 were fit to theoretical models for the magnetization in three different ways. The Hao-Clem model [24] is a variational calculation that includes the energy of the core of the vortices and uses H_c and κ_c as adjustable variables. All of the data reported in these measurements are far from H_{c2} so the fit gives an uncertainty of about 10% in κ_c. Selecting the average value of κ_c = 175 for all temperatures, the data have been fit to the universal Hao-Clem curve with just H_c as the adjustable parameter with the results shown in Figure 4.5. If both k_c and H_c are taken as variables, the fits can be improved slightly, but the data are not close enough to H_{c2} to realistically evaluate κ_c better than this average value. As shown in the inset of Figure 4.5 where the dimensionless variables $M' = M_{sc}/\sqrt{2}\,H_c$ and $H' = H/\sqrt{2}\,H_c$ are plotted, the data fit the Hao-Clem [24] model rather well with the H_c values ranging from H_c = 133 mT at 6 K to H_c = 112 mT at 12 K. These H_c values are plotted as solid squares in Figure 4.5. If these are fit to a parabolic critical field

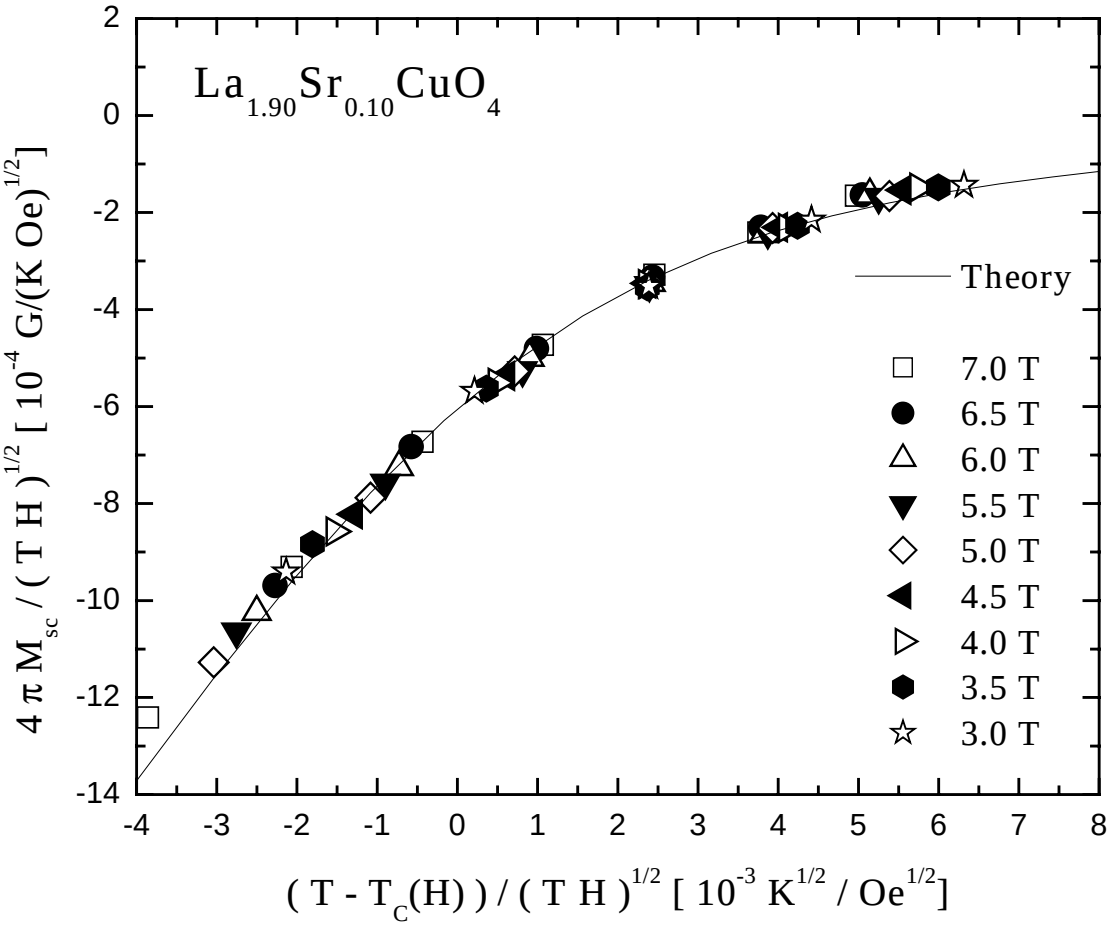

Figure 4.4 2D scaling behavior of the magnetization every half Tesla from 3.0 to 7.0 T.

curve, $H_c = H_c(0)[1-(T/T_c)^2]$, one finds $H_c(0)$ = 140 mT and T_{c0} = 26.8 K. The slope dH_{c2}/dT at T_{c0} from these fits gives −2.6 T/K at T_c in reasonable agreement with the value derived from Tesanovic [9] of −3.2 T/K. These data also are to be compared with a previous study by Li *et al.* [25] who found $H_c(0)$ = 143 mT and T_c = 28.23 K for an x = 0.092. They also found $H_c(0)$ = 251 mT and T_c = 34.39 K for an x = 0.154 sample at essentially optimum doping. If a straight line is drawn on an $H_c(0)$ vs. x plot from the optimum doped sample through the datum for this sample, H_0 would extrapolate to zero at x ~ 0.03. The current H_c vs. T results then are in good agreement with these previous data [25].

An alternative way to determine H_c is to use the theory of Kogan *et al.* [21] that is based on London theory and takes more full account of the entropy associated with the fluctuations. In the first method, we determine s from the crossing measurements by, $s = -k_B T^*/\phi_0 M^*$ = 1.66 nm, assuming that $ln[\eta\alpha\sqrt{e}]$ = 1. Then we fit the M vs. H data to Eq. (1) in Kogan *et al.* [21] to give the best values of κ_c and λ_{ab}. From these, we calculate the H_c values shown by the open squares of Figure 4.5.

In the second method that uses the Kogan *et al.* [21] approach, we assume that s = 0.66 nm given by the CuO_2 plane spacing and determine $ln[\eta\alpha\sqrt{e}]$ from $M^* = -[k_B T^*/\phi_0 s] ln[\eta\alpha\sqrt{e}]$. Inserting these values into Eq. (1) of Kogan *et al.* and fitting the data gives $H_{c2}(T)$ that can be converted to the H_c values shown by the open circles of Figure 4.5.

The central result of these various methods to determining H_c from the M

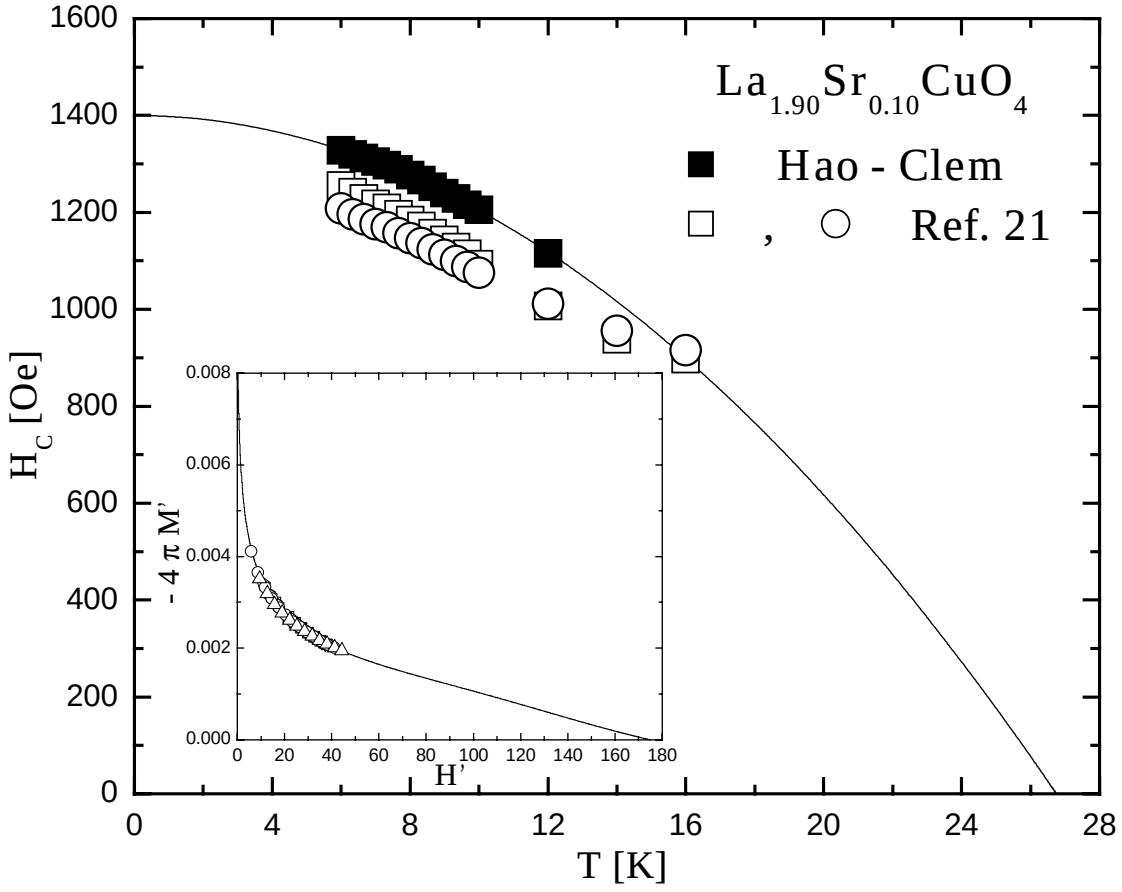

Figure 4.5 Thermodynamic critical field H_c vs. T determined from three different ways. The inset shows a fit of the data from 6 to 12 K to the universal Hao-Clem curve for $\kappa_c = 175$.

vs. H data is that all the methods give roughly the same result. An extrapolation of the Hao-Clem H_c vs. T data (solid squares of Figure 4.5) gives T_{c0} = 26.8 K in reasonable agreement with the temperature where the 1.0 mT M vs. T curve breaks away from zero. Extrapolating the second Kogan method (open circles of Figure 4.5) gives about 27.4 K. All of the H_c data of Figure 4.5 indicate a ratio of $H_c(0)/T_{c0}$ = 5.4 mT/K.

Magnetization curves were measured as a function of the polar angle away from $H \| c$ to determine how sensitive the magnetization was to orientation. Tipping the crystal by ±10° reduced the magnetization at 10 K and 2.0 T by about 5% and tipping by 30° reduced the magnetization by about 25%. When the field was in the a-b plane, the magnetization was rather noisy and highly irreversible so no extensive data are reported here. We assume that the noise arose from bundles of flux jumping from place to place in the crystal.

IV. Conclusion

$La_{1.90}Sr_{0.10}CuO_4$ is a bulk superconductor that expels flux over the entire H-T plane in a manner similar to the optimally doped cuprate superconductors and the classical type-II superconductors. Normal-state magnetization data in the temperature range from 55 to 200 K obeys 2D Heisenberg antiferromagnetic behavior rather well. This gives a relatively small background to subtract in the study of the superconducting magnetization. The background also contains a

small saturating ferromagnetic term parallel to the *c* axis that is the same for all temperatures. It saturates at about 0.2 T. There is a large portion of the *H*-*T* plane where the magnetization is thermodynamically reversible giving a large region where the free-energy change with magnetic field can be measured. Superconducting magnetization curves are Abrikosov-like for temperatures below 18 K and they show fluctuation behavior above 22 K. The crossover on the *M* vs. *T* plot shows $4\pi M^* = -1.13$ G and $T^* = 22.0$ K to give $s = 1.6$ nm compared with the CuO2 plane spacing of 0.66 nm. The fit of the *M* vs. *T* data to the model of fluctuating pancake vortices is rather good and gives a crossing point for all fields above 0.5 T. The fit of the reversible magnetization curves to the Hao-Clem model gives a κ_c value of about 175 and a zero temperature thermodynamic critical field of $H_c(0) = 140$ mT. For a T_{c0} of 26.8 K, a classical superconductor like tin would have an $H_c(0)$ closer to 300 mT. Hence this underdoped high-T_c material with about 2/3 the optimal carrier density excludes about half the flux expected for a classical superconductor. For classical superconductors, BCS (Ref. 26) predicts the ratio of $H_c(0)/T_{c0}$ to be governed by the density of states, $N(0)$, by $H_c(0)/T_{c0} = 1.75\,[4\pi N(0)]^{1/2} k_B$. It is not known whether BCS applies here but if it does, one might expect $H_c(0)/T_{c0}$ to be reduced as carriers are reduced below optimal doping. For most classical superconductors, the ratio of $H_c(0)/T_{c0}$ is about 10 mT/K. For this underdoped high-T_c material the ratio is about 5.4 mT/K which may reflect a relatively small value of $N(0)$ compared to that found for classical superconductors.

The attempt to study fluctuation diamagnetism above T_c was only a partial success. As shown by the magnetization data in Figure 4.3, there is a substantial diamagnetic magnetization at 32 K, well above T_c. Indeed the magnetization is diamagnetic all the way up to 40 K. Above 40 K, however, the signal is small compared to the background magnetization of the Cu spins. There is sufficient uncertainty in analyzing the background magnetization, that fluctuating diamagnetism in the 40-100 K pseudogap range cannot be determined from these data.

Acknowledgement

We thank C. Song for the x-ray study which showed that the sample was a single crystal and determined the direction of the major axes. Ames Laboratory is operated for the U.S. Department of Energy by Iowa State University under Contract No. W-7405-ENG-82 and supported by the DOE, the Office of Basic Energy Sciences.

References

1. T. Timusk and B. Statt, Rep. Prog. Phys. **62**, 61 (1999).
2. G. W. Crabtree, W. K. Kwok, L. M. Paulius, A. M. Petrean, R. J. Olsson, G. Karapetrov, V. Tobos, and W. G. Moulton, Physica C **332**, 71 (2000).

3. G. Blatter, M. V. Feigel'man, V. B. Geshkenbein, A. I. Larkin, and V. M. Vinokur, Rev. Mod. Phys. **66**, 1125 (1994).

4. P. H. Kes, C. J. van der Beek, M. P. Maley, M. E. McHenry, D. A. Huse, M. J. Menken, and A. A. Minovsky, Phys. Rev. Lett. **67**, 2383 (1991).

5. Abrikosov, Zh. Éksp. Teor. Fiz. **32**, 1442 (1957) [Sov. Phys. JETP **5**, 1174 (1957)].

6. L. N. Bulaevskii, M. Ledvij, and V. G. Kogan, Phys. Rev. Lett. **68**, 3773 (1992).

7. Q. Li, M. Suenaga, L. N. Bulaevskii, T. Hikata, and K. Sato, Phys. Rev. B **48**, 13 865 (1993).

8. U. Welp, W. K. Kwok, R. A. Klemm, V. M. Vinokur, J. Downey, and G. W. Crabtree, Physica C **185-189**, 1785 (1991).

9. Z. Tesanovic, L. Xing, L. Bulaevskii, Qiang Li, and M. Suenaga, Phys. Rev. Lett. **69**, 3563 (1992); Z. Tesanovic and A. V. Andreev, Phys. Rev. B **49**, 4064 (1994).

10. B. Janossy, D. Prost, S. Pekker, and L. Fruchter, Physica C **181**, 51 (1991).

11. B. Janossy, H. Kojima, I. Tanaka, and L. Fruchter, Physica C **176**, 517 (1991); M. Willemin, C. Rossel, J. Hofer, H. Keller, and A. Revcolevschi, Phys. Rev. B **59**, R717 (1999).

12. J. E. Ostenson, S. Bud'ko, M. Breitwisch, and D. K. Finnemore, Phys. Rev. B **56**, 2820 (1997).

13. J. E. Ostenson and D. K. Finnemore, Chin. J. Phys. (Taipei) **36**, 297 (1998).

14. C. J. van der Beek, M. Konczykowski, T. W. Li, P. H. Kes, and W. Benoit, Phys. Rev. B **54**, R792 (1996).

15. D. C. Johnston, Phys. Rev. Lett. **62**, 957 (1989).

16. L. J. de Jongh, Magnetism and Magnetic Materials, edited by C. D. Graham and J. Rhyne, AIP Conf. Proc. No. 10 (AIP, New York, 1973), p. 561.

17. E. Dagotto, Rep. Prog. Phys. **62**, 1525 (1999); S. Bacci, E. Gagliano, and E. Dagotto, Phys. Rev. B **44**, 285 (1991).

18. Revcolevschi and J. Jegoudez, Prog. Mater. Sci. **42**, 321 (1997); S. Petit, A. H. Moudden, B. Hennion, A. Vietkin, and A. Revcolevschi, Eur. Phys. J. B **3**, 163 (1998).

19. M.-H. Julien, A. Campana, A. Rigamonti, P. Carretta, F. Borsa, P. Kuhns, A. P. Reyes, W. G. Moulton, M. Horvatić, C. Berthier, A. Vietkin and A. Revcolevschi, Phys. Rev. B **63**, 144508 (2001).

20. T. Nakano, M. Oda, C. Manabe, N. Momono, Y. Miura, and M. Ido, Phys. Rev. B **49**, 16 000 (1994).

21. G. Kogan, M. Ledvij, A. Yu. Simonov, J. H. Cho, and D. C. Johnston, Phys. Rev. Lett. **70**, 1870 (1993).

22. H. Iwasaki, F. Matsuoka, and K. Tanigawa, Phys. Rev. B **59**, 14 624 (1999).

23. J. Mosqueira, M. V. Ramallo, A. Revcolecschi, C. Torron, and F. Vidal, Phys. Rev. B **59**, 4394 (1999).

24. Z. Hao and J. R. Clem, Phys. Rev. Lett. **67**, 2371 (1991).

25. Qiang Li, M. Suenaga, T. Kimura, and K. Kishio, Phys. Rev. B **47**, 11 384 (1993).

26. J. Bardeen, L. N. Cooper, and J. R. Schrieffer, Phys. Rev. **108**, 1175 (1957).

CHAPTER 5. THERMODYNAMIC CRITICAL FIELD FOR $La_{2-x}Sr_xCuO_4$

A paper to be published in Phys. Rev. B.

Yung M. Huh and D. K. Finnemore
Ames Laboratory, U.S. Department of Energy and
Department of Physics and Astronomy, Iowa State University, Ames, Iowa 50011

Abstract

Thermodynamic critical fields, H_c, have been measured for the high temperature cuprate superconductor $La_{2-x}Sr_xCuO_{4-\delta}$, La-214, family in order to investigate the changes in free energy of the system as the number of carriers is reduced. Magnetization data are thermodynamically reversible over large portions of the *H-T* plane, so the free energy is well defined in these regions. M_{sc} *vs. H* data are then fit to theoretical models to determine the thermodynamic critical fields. As the Sr content is varied over wide range from 0.060 (strongly underdoped) to 0.234 (strongly overdoped), the values of thermodynamic critical fields at zero temperature, $H_c(0)$, go through a maximum at optimum doping in a manner similar to the transition temperature vs. Sr content, T_{c0} vs. x, curve. The ratio of $H_c(0)$ to T_{c0} also peaks in the region of somewhat larger than optimum doping. The free energy changes between superconducting state and normal state are correlated strongly with transition temperatures and show rather

small dependence on Meissner shielding fraction measured at 10 Oe. By using energy gap ratio $\Delta(0)/k_B T_{c0}$ and the specific heat coefficient γ as two adjustable parameters, the BCS relations in conjunction with the $H_c(T)$ vs. T measurements give $\Delta(0)/k_B T_{c0}$ = 2.01±0.11 throughout the entire superconductive range in La-214 system. The temperature coefficient of the normal electronic specific heat γ tends to remain nearly constant in optimum and overdoped regimes taking a broad maximum around x = 0.188 and then drops abruptly towards zero in the underdoped regime.

I. Introduction

Free energy is a key variable in the understanding of the superconducting to normal state phase change because it provides an overall energy scale for the transition and it can be obtained by integrating the area under the magnetization curve from zero up to upper critical field. Because the free energy difference between the superconducting and normal state varies as $G_n - G_s = H_c^2/8\pi$, it becomes possible to discuss free energy changes in terms of this thermodynamic critical field. It is a macroscopic variable that averages over the elementary excitations of the system and thus does not give an atom by atom picture of events in the material. It does, however, give the energy scale as a fundamental variable in the problem as the carrier concentration is systematically changed in the La-214 system.

In the high temperature cuprate superconductors, the free energy seems to be a difficult variable to measure at first sight because the upper critical field H_{c2} is so high, and because thermal fluctuations are extended well above T_c introducing new physics close to H_{c2} and T_c. In addition, the range of thermodynamic reversibility is limited at low magnetic field by substantial flux pinning easily found in a material with weak linked grain boundaries.

Recently, however, the progress in sample preparation have provided a single crystal of $La_{1.90}Sr_{0.10}CuO_4$ [1] with an irreversibility line, H_{irr} *vs.* T that rises from zero for 28 K to 0.5 T at 15 K, 1.0 T at 10 K, and to 2.5 T at 6 K. At all fields above this line, the magnetization is thermodynamically reversible to better than one percent. This provides a very large region of the H-T plane where the experiment can be performed. For this particular sample [1], magnetization curves show an Abrikosov-like vortex behavior (decreasing in magnitude of magnetization with increasing magnetic field) below 20 K and the M_{sc} *vs.* H curves obey the Hao-Clem model [2] rather well. At 22 K the M_{sc} *vs.* H curves show a crossing point where the magnetization is independent of magnetic field similar to that seen by Kes and co-workers in Bi-2212 [3]. Then, above 22 K, the sample shows strong fluctuation effects (decreasing in magnitude of magnetization with increasing magnetic field) and theories of Tesanovic and co-workers [4] and Kogan and co-workers [5] become applicable. In this region, the entropy associated with the motion of the vortices becomes important and must be included in the free energy. Using these reversible

magnetization curves, this underdoped $La_{1.90}Sr_{0.10}CuO_4$ sample shows a thermodynamic critical field, H_c, ranging from 113 mT at 12 K to 133 mT at 6 K. Typically, classical superconductors such as Sn and Pb show a ratio of $H_c(0)/T_{c0}$ in the range from 8.0 mT/K to 10 mT/K, whereas this underdoped $La_{1.90}Sr_{0.10}CuO_4$ sample has 5.2 mT/K.

The purpose of the work reported here is to measure the thermodynamic critical field, H_c, as well as the ratio of $H_c(0)/T_{c0}$ as a function of carrier concentration for the $La_{2-x}Sr_xCuO_4$ system as the Sr content is varied over a full superconductive range from strongly underdoped to strongly overdoped regimes. Moreover, by using the BCS theory, the energy gap and the variation of specific heat coefficient as a function of the Sr contents are deduced. To do this experiment, there are several difficulties that must be overcome. It is necessary to have samples with very few flux pinning sites so that there are thermodynamically reversible magnetization curves available over a large region of the *H*-*T* plane. The oxygen content must be held fixed so that the change of Sr content controls the carrier concentration. In addition, the normal state magnetization from the copper spins must be well behaved so that this background can be subtracted to give the change in magnetization caused exclusively by the onset of superconductivity.

The samples used in this work were composed of three single crystals and fifteen magnetically aligned powders. It was thought that it would be easier to control the uniformity of the oxygen content with powders [6]. Standard

diagnostics for good sample quality include measurement of the Meissner shielding fraction at low field, 1.0 mT, and sharpness of transition temperature. A study was then made of the normal state magnetization from just above transition temperature to 200 K arising from the *Cu* spins and compared with published measurement [7]. A substantial sudden deviation of the behavior of the normal-state susceptibility near the transition temperature from the high temperature is assumed to arise due to the onset of superconductivity. By assuming this normal-state magnetization persists even in the superconducting state we obtained superconducting magnetization, M_{sc}, in the consistent manner as we reported in the previous work [1]. To check the sensitivity of the results to this background subtraction, a series of samples with different Meissner shielding fraction were measured to look for changes in the results as this fraction increases.

This work is to study systematically the changes in normal state and superconducting properties as the carrier concentration changes in the entire range of the superconductive region of La-214 system. In the normal state, it is determined how the *Cu* spin susceptibility changes. In the superconducting state, we obtained the variation of the thermodynamic critical field $H_c(T)$and the ratio $H_c(0)/T_{c0}$ as the carrier concentration changes. Using the energy gap ratio $\Delta(0)/k_B T_{c0}$ and the temperature coefficient of normal electronic specific heat γ as two adjustable parameters, the $H_c(T)$ vs. T data are then fit to the BCS theory [8] to deduce both $\Delta(0)/k_B T_{c0}$ and γ for each x-values.

II. Experiment

Magnetically aligned samples of $La_{2-x}Sr_xCuO_4$ were prepared by grinding appropriate amounts of lanthanum oxide (La_2O_3), strontium carbonate ($SrCO_3$), and copper oxide (CuO). Pellets were pressed and fired in flowing oxygen. After repeated grinding and firing at successively higher temperatures, measurements of the transition temperature and Meissner shielding fraction were made with a measurements in a field of 1.0 mT as the first diagnostic of sample quality. The final pellet was ground to a particle size of about 20 μm. This powder was mixed and suspended in a low viscosity and low magnetic susceptibility liquid epoxy (Epotek 301), oriented in a magnetic field of 8.0 T, and then the epoxy was allowed to harden in the field. All metal elements were analyzed by employing an inductively coupled plasma (ICP) technique from which Sr contents x were determined.

The effective doping concentration for $La_{2-x}Sr_xCuO_{4-\delta}$ is defined as $x - 2\delta$ by assuming that one oxygen ion provides two holes in the CuO_2 planes. We will treat our samples contain no oxygen vacancies and we shall characterize them by their Sr content x. For this matter, we selected samples carefully by comparing transition temperatures with the accepted values for given hole concentrations [9].

In addition to the results for these grain aligned samples, single crystals of x = 0.060 SC and 0.13 SC, were prepared by a solution method [10] and a

floating zone method in an image furnace, respectively [11]. The results from a previously reported single crystal of $La_{1.90}Sr_{0.10}CuO_4$ [1] are given together in all of the summary plots.

Magnetization measurements were made with field applied in the *c* direction in a Quantum Design SQUID magnetometer over the full range of temperatures from 2.0 K to 300 K and magnetic fields from zero to 7.0 T. The measurements were performed with 6-cm scan length except x = 0.13 single crystal sample for which 3-cm scan length was used. Reversible magnetization data are obtained by averaging zero-field-cooled and field-cooled data above the irreversibility temperature for each field within one percent of differences. The Meissner shielding fractions listed in Table 5.1 are determined from zero-field-cooled magnetization by the value of the 4πM/H in a field of 1.0 mT without considering demagnetization factor. For spherical particles, a Meissner screening fraction of about 150 percent of full expulsion is expected. A linear extrapolation of data to the zero magnetization line defines the transition temperature T_c.

III. Results and Discussion

Samples studied in this work are listed in the Table 5.1 where SC in the sample label indicates they are single crystals and T_{c0} is derived by fitting the Hao-Clem model, and we will use these values as the mean-field-transition

Table 5.1 Transition temperatures and Meissner shielding fractions of single crystals and magnetically aligned powder samples of $La_{2-x}Sr_xCuO_4$.

Sr (x)	T_c [K]	T_{c0} [K]	Meissner [%]
0.06 SC	8.0	N/A	33
0.070	14.5	14.94	13
0.081	20.5	21.72	50
0.090	26.5	26.94	47
0.10 SC	26.7	26.80	150
0.111	28.2	27.99	49
0.117	28.5	28.24	68
0.13 SC	34.2	34.52	140
0.143	36.4	36.52	170
0.150	37.3	37.21	101
0.156	36.7	36.53	117
0.188	31.4	31.54	102
0.193	29.6	29.15	120
0.234	18.5	18.38	98

temperature throughout this work. The differences between transition temperatures obtained from the 1.0 mT experiment and the Hao-Clem fitting are about ±0.5 K. It is not possible to tell with this work whether the small values of Meissner shielding fractions for some samples (most of them are of underdoped regime) either are intrinsic for a sample with a given hole concentration or are due to the size of the particles being smaller than magnetic penetration depth. Rather, we prepared samples to have the largest values of fraction for the given doping concentrations without altering transition temperature, and they can be changed depending on the preparation conditions. Figure 5.1 (a) and (b) shows the magnetization measurements at 1.0 mT and Meissner shielding effects and transition temperatures are compared.

A. Normal-State Properties

In the temperature range from 60 to 200 K, the normal state magnetization of both single crystals and aligned powders is similar to the single crystal data reported earlier [1]. To illustrate these data, the magnetization data at 80 K are presented in Figure 5.2 for five different Sr contents. Single crystal samples with Sr content of 0.10 and 0.13 are shown along with powder samples of 0.156, 0.188, and 0.234. Data in the inset emphasize magnetization below 1.0 T. The solid lines are fit results to the following Eq. 1.

The normal state magnetization obeys the form,

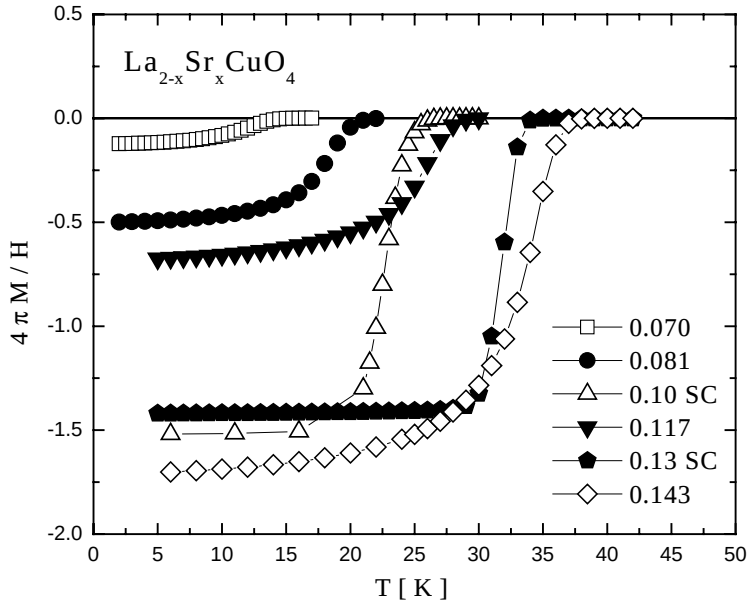

Figure 5.1 (a) The low field susceptibilities of underdoped $La_{2-x}Sr_xCuO_4$.

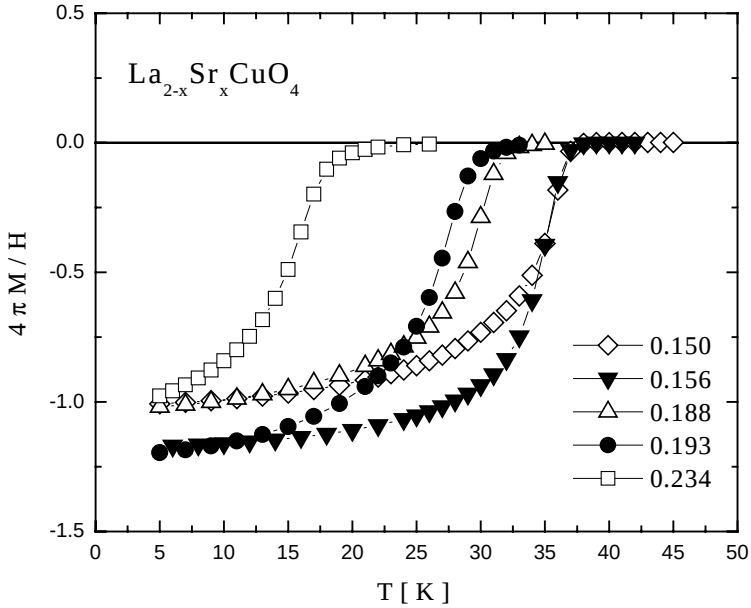

Figure 5.1 (b) The low field susceptibilities of overdoped $La_{2-x}Sr_xCuO_4$.

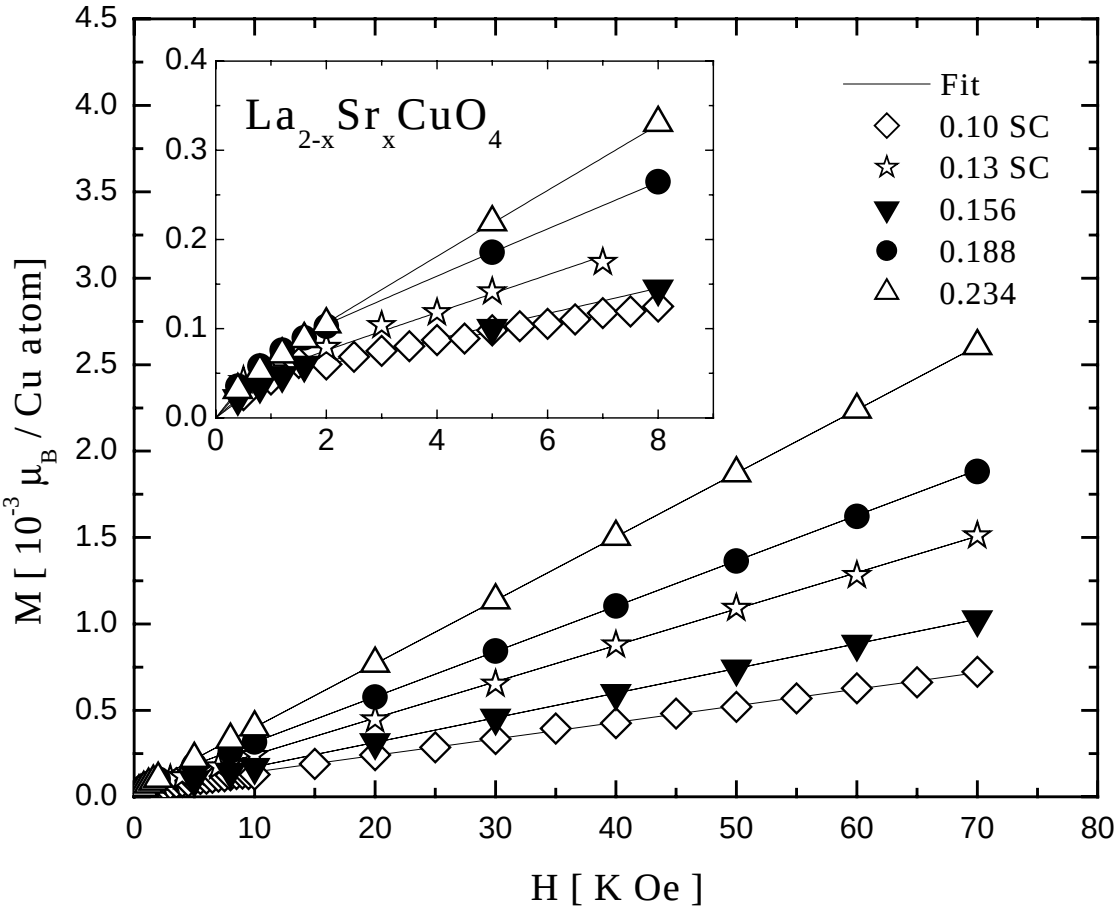

Figure 5.2 Normal state magnetization at 80 K for different Sr contents of $La_{2-x}Sr_xCuO_4$.

$$M_n = CH + M_s \tanh(\beta H), \quad (1)$$

where the CH term dominates over most of the H-T plane and both M_s and β are constants. For any given sample, both M_s and β are independent of temperature within the uncertainty of the measurement while C is the only temperature dependent variable and it is the dimensionless volume susceptibility. As the hole concentration changes over the entire superconductive region, M_s remains in the neighborhood of 5×10^{-5} μ_B/Cu-atom and β of 1×10^{-3} Oe^{-1} so that the second term in Eq. (1) saturates at about 0.1 T. The values of M_s and β are listed in the Table 5.2 and we assume that magnetic moments arise only from *Cu* spins. In Figure 5.3, the values of C are plotted for seven samples ranging from x = 0.10 (closed squares) to 0.23 (closed stars) in the temperature up to 200 K. For comparison, data from Nakano *et al.* [7] are also shown as solid lines for samples with x of 0.10, 0.14, 0.16, 0.20, and 0.26 starting x = 0.10 from the bottom.

B. Superconducting State Magnetization

The superconducting transition temperatures were first determined from measurements of the zero-field cooled Meissner shielding magnetization in an applied magnetic field of 1.0 mT. By linearly extrapolating 4πM/H to zero line, we obtained values of T_c from Figure 5.1 and they are listed in Table 5.1. They are close to those accepted in the literatures [9] with a maximum of 37.3 K at an x of about 0.150. Irreversibility curves for all of these samples, H_{irr} vs. t, are

Table 5.2 Normal state fitting parameters in $M_n = CH + M_s \tanh(\beta H)$.

Sr (x)	M_s [$10^{-5}\mu_B$/Cu atom]	β [10^{-3} Oe^{-1}]
0.060 SC	N/A	N/A
0.070	5.07	1.07
0.081	3.51	0.846
0.090	6.20	1.27
0.100 SC	4.80	0.815
0.111	3.87	0.904
0.117	3.19	0.961
0.130 SC	3.39	1.66
0.143	4.33	1.28
0.150	6.13	1.37
0.156	3.05	1.53
0.188	5.45	1.05
0.193	27.5	0.910
0.234	3.40	1.02

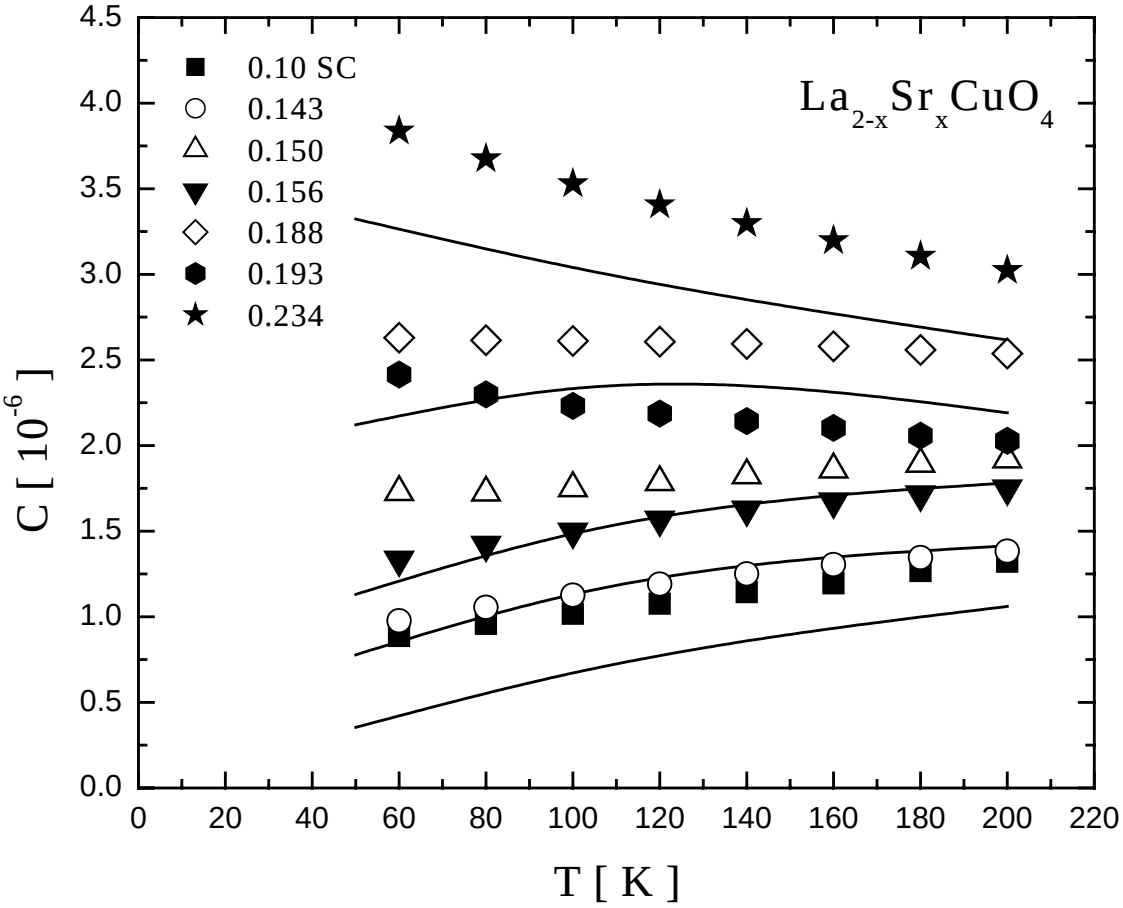

Figure 5.3 Temperature dependence of *C*. Solid lines are normal state susceptibilities from Ref. 7 for $La_{2-x}Sr_xCuO_4$.

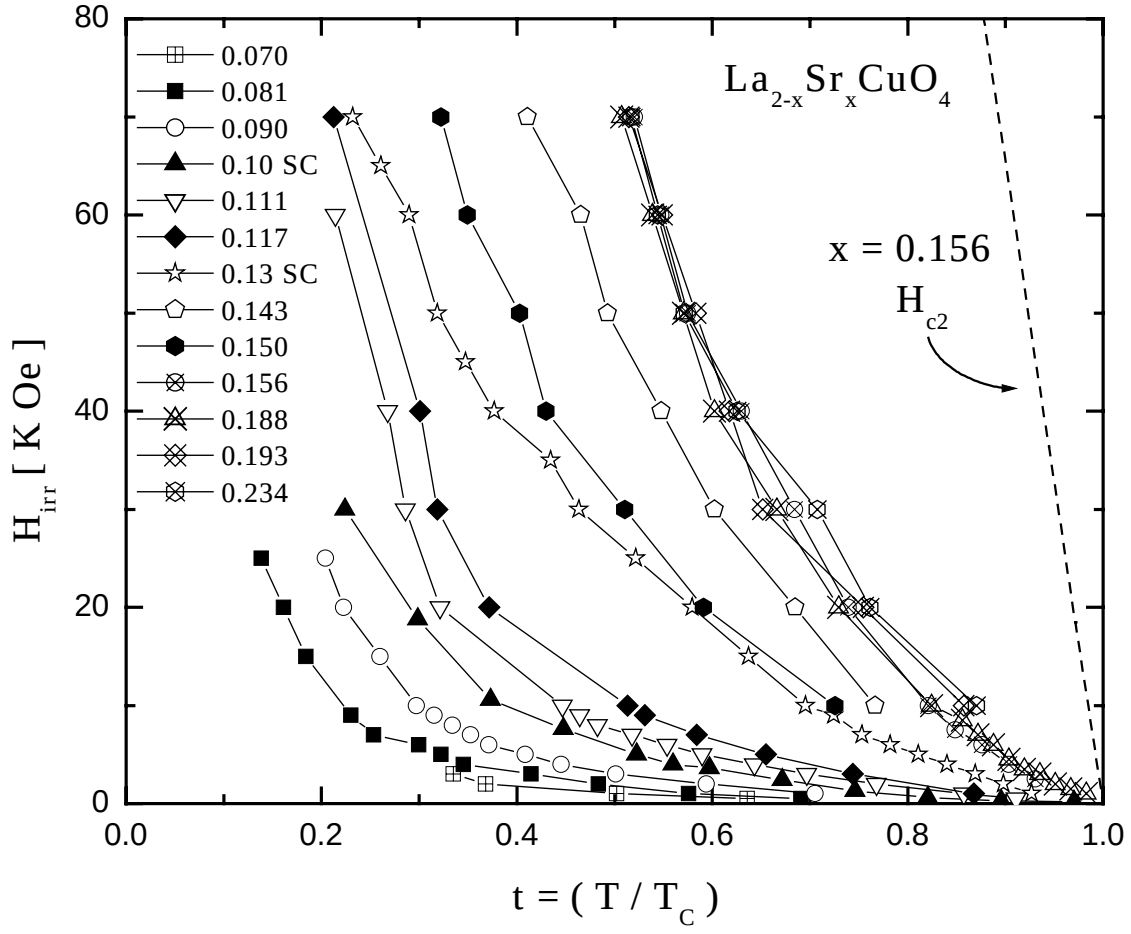

Figure 5.4 Irreversibility field lines of $La_{2-x}Sr_xCuO_4$.

plotted in Figure 5.4. Apparently increasing doping concentration tends to increase flux pinning so that irreversible fields increase at a certain reduced temperature until it reaches $x = 0.156$ and do not show noticeable change up to $x = 0.234$ in a reduced temperature scale.

The superconducting magnetization is given by $M_{sc} = M_t - M_n$, where M_t is the total measured reversible magnetization and M_n is the normal state magnetization below transition temperature. Values of M_n are determined at temperatures below 60 K, from Eq. (1) and C is taken to be a linear extension of the data above 60 K to lower temperatures in a form $C = \chi_0 + AT$ where A is a constant slope in C *vs.* T plot, which is considered as the characteristic of 2D antiferromagnetic Heisenberg behavior [12]. Note also that the sign of the slope changes from positive to negative near $x = 0.188$. Samples showing background signals other than linearly decreasing susceptibility, it is regarded contaminated with magnetic impurities arising from the sample preparation condition and then they are fitted by including terms of Curie-Weiss law resulting in the final form of $C = \chi_0 + AT + B/(T + \Theta)$. Both B and Θ are constants found at high temperatures of each sample. Numerical values for these parameters for all the samples are given in Table 5.2 and Table 5.3. The background signal and onset of irreversible field are illustrated in Figure 5.5 along with total magnetization at 18 K of $La_{1.90}Sr_{0.10}CuO_4$.

Plotted in Figure 5.6 are examples of superconducting magnetization, M_{sc}, for samples of five different Sr contents at 23 K. This M_{sc} data for each sample is

Table 5.3 Normal state fitting parameters in $C = \chi_0 + AT + B/(T + \Theta)$.

Sr (x)	χ_0 [10^{-6}]	A [10^{-9} K^{-1}]	B [10^{-5} K]	Θ [K]
0.06 SC	N/A	N/A	N/A	N/A
0.070	0.2696	2.781	9.092	11.497
0.081	0.3882	2.887	13.16	17.278
0.090	-1.714	14.47	32.45	45.2355
0.10 SC	0.7075	3.083	0	0
0.111	0.5221	3.399	13.13	14.8798
0.117	1.048	2.169	7.732	2.98677
0.13 SC	1.778	4.095	0	0
0.143	0.8251	2.916	0	0
0.150	1.614	1.512	0	0
0.156	1.188	2.956	0	0
0.188	2.671	-0.6138	0	0
0.193	2.081	-0.8592	1.94	-3.1286
0.234	3.293	-2.703	6.438	29.9181

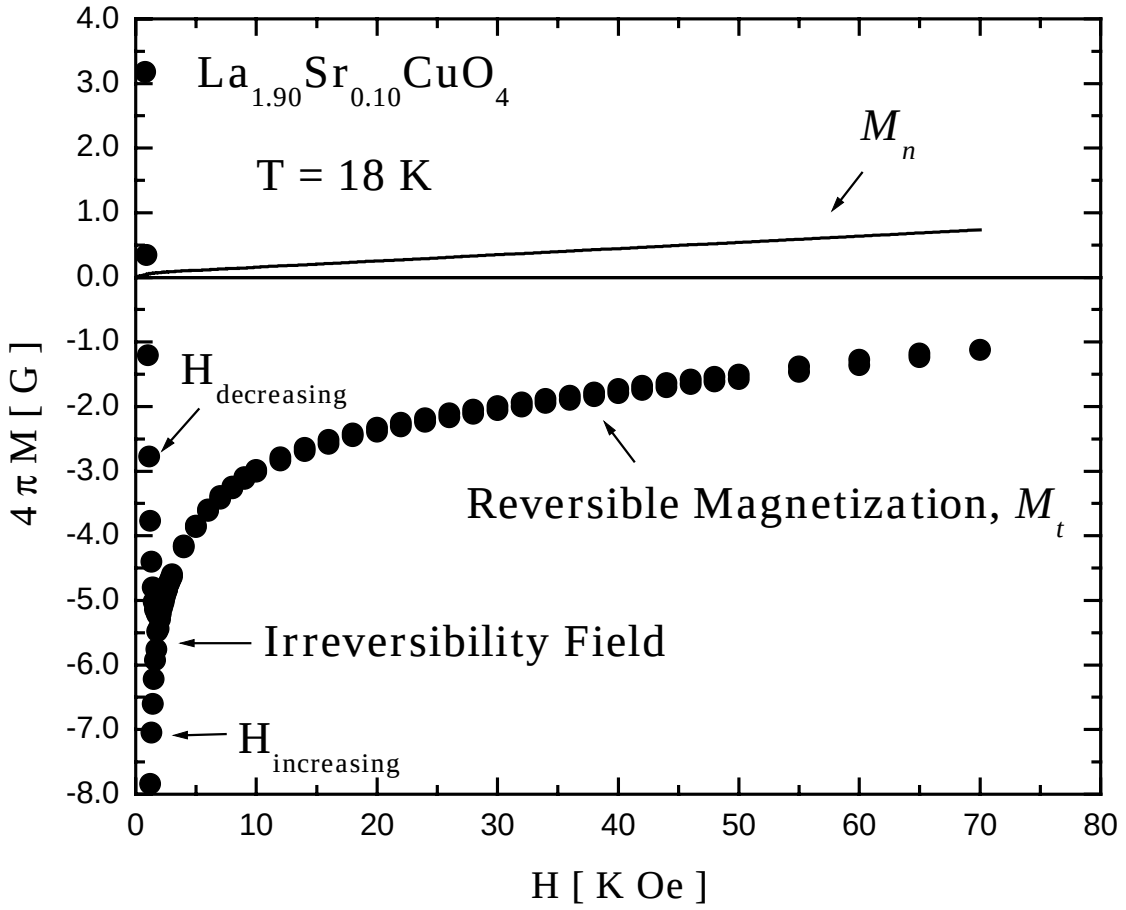

Figure 5.5 The background signal M_n and total reversible magnetization M_t at 18 K (< T_c) of $La_{1.90}Sr_{0.10}CuO_4$.

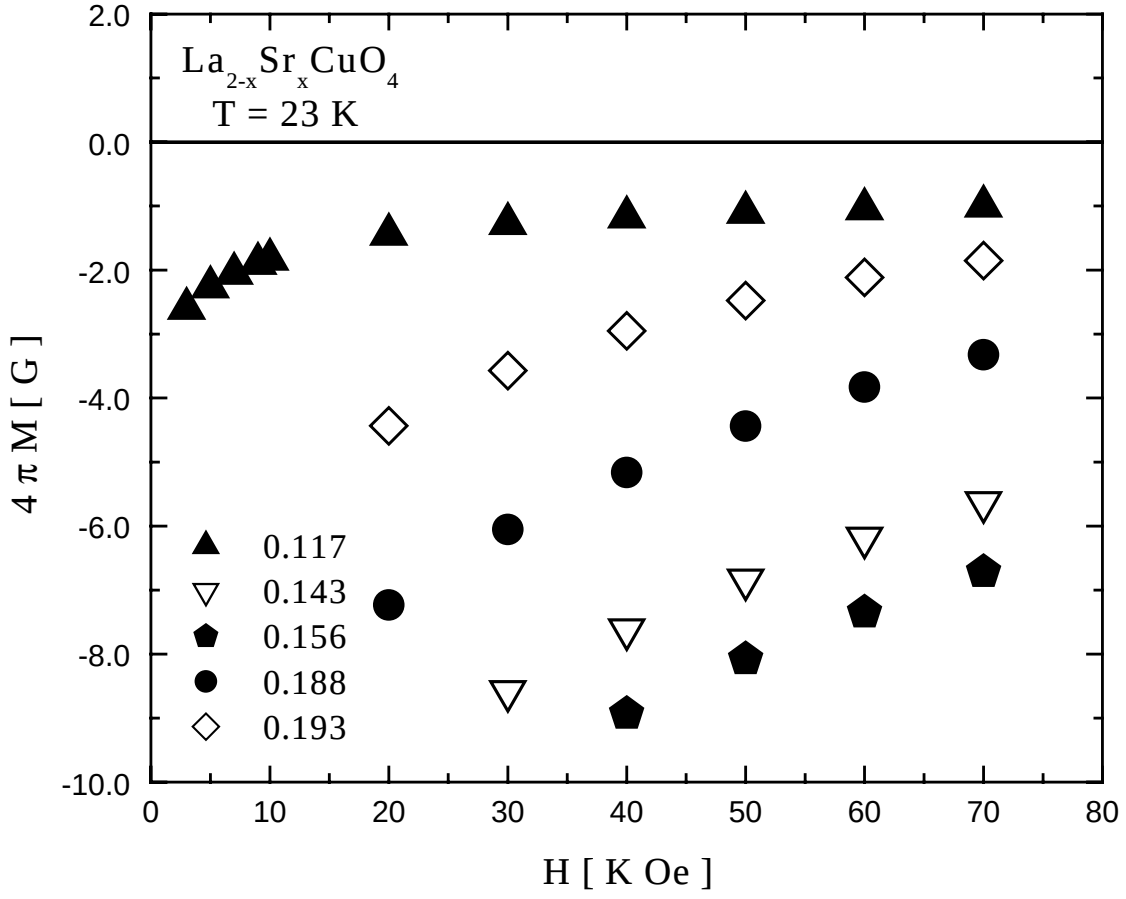

Figure 5.6 The superconducting magnetization, $M_{sc} = M_t - M_n$, at 23 K of $La_{2-x}Sr_xCuO_4$.

then fitted to the Hao-Clem model [2] at each temperature to determine thermodynamic critical field, H_c, and Ginzburg-Landau parameter, κ_c, in the *c*-axis direction. Two typical fitting results are presented in Figure 5.7 (a) and (b) for 0.13 SC and 0.156 samples respectively. The thermodynamic critical field $H_c(T)$ for the underdoped and optimum doped $La_{2-x}Sr_xCuO_4$ are plotted in Figure 5.8 (a) and overdoped $La_{2-x}Sr_xCuO_4$ are in Figure 5.8 (b). For any given temperature, values of H_c shown as data points in Figure 5.8 (a) and (b) go through a maximum near optimum doping, x = 0.156. Solid lines represent the temperature dependence of H_c assuming the Two-Fluid model [8], $H_c(T) = H_c(0)(1 - t^2)$, where t is a reduced temperature, T/T_{c0}. These curves are then extrapolated to zero temperature and zero field to obtain $H_c(0)$ and T_{c0}.

Sample quality is a central factor in making these measurements so it is important to see if these variables change with different Meissner shielding fraction. We prepared five samples from the same initial batch with different preparation conditions (x = 0.150, 0.15 K, 0.15 L, 0.15 M, and 0.15 N) such as final sintering temperature, duration time in furnace, and the amount of oxygen flowing starting. They show different Meissner shielding fraction from 112% to 50%. However, at the same time their transition temperatures were changed in x = 0.15 series against our intention, possibly resulting from the oxygen deficiency and therefore hole concentration might be changed. The zero-field magnetization at 10 Oe and their H_c derived from Hao-Clem model are plotted in Figure 5.9 (a) and (b) respectively. We found that the H_c depends strongly on the

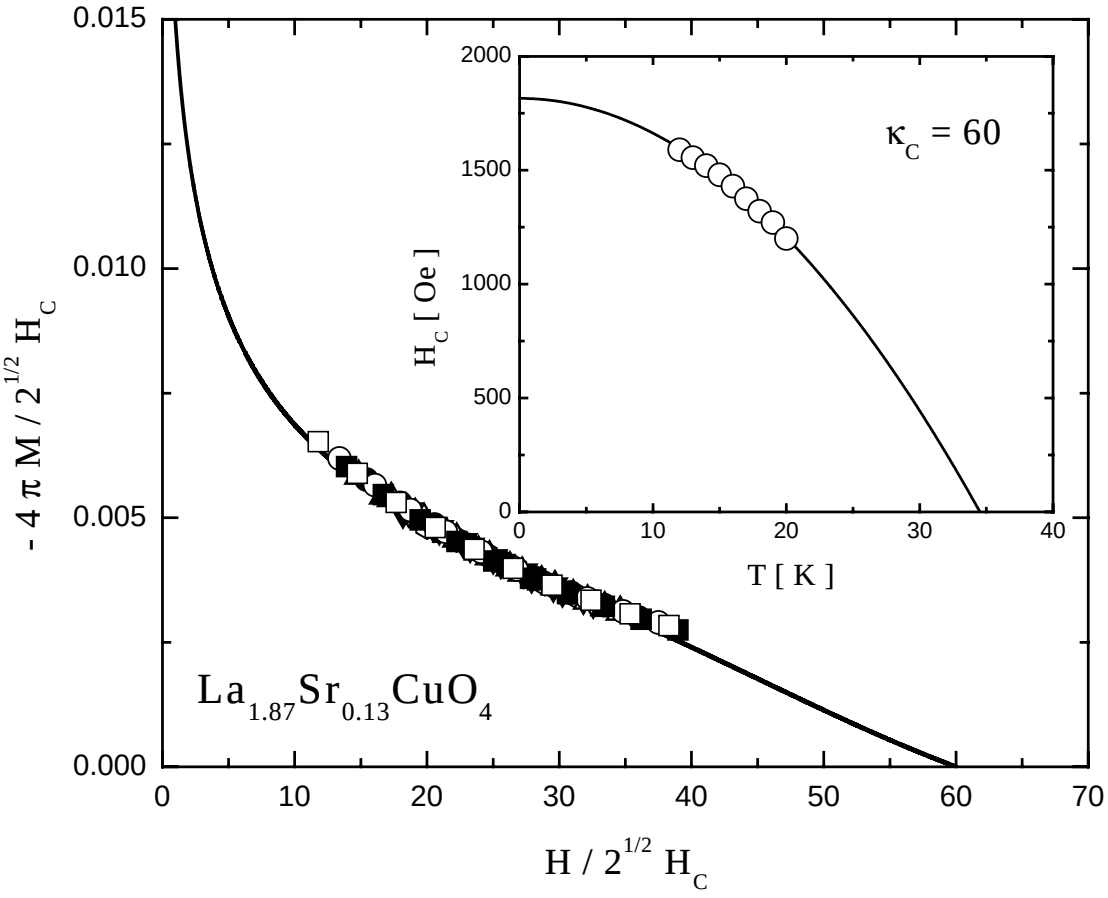

Figure 5.7 (a) The Hao-Clem curve for $\kappa_c = 60$ from 12 to 20 K. The inset shows the H_c(T) with the Two-Fluid model curve for $La_{1.87}Sr_{0.13}CuO_4$.

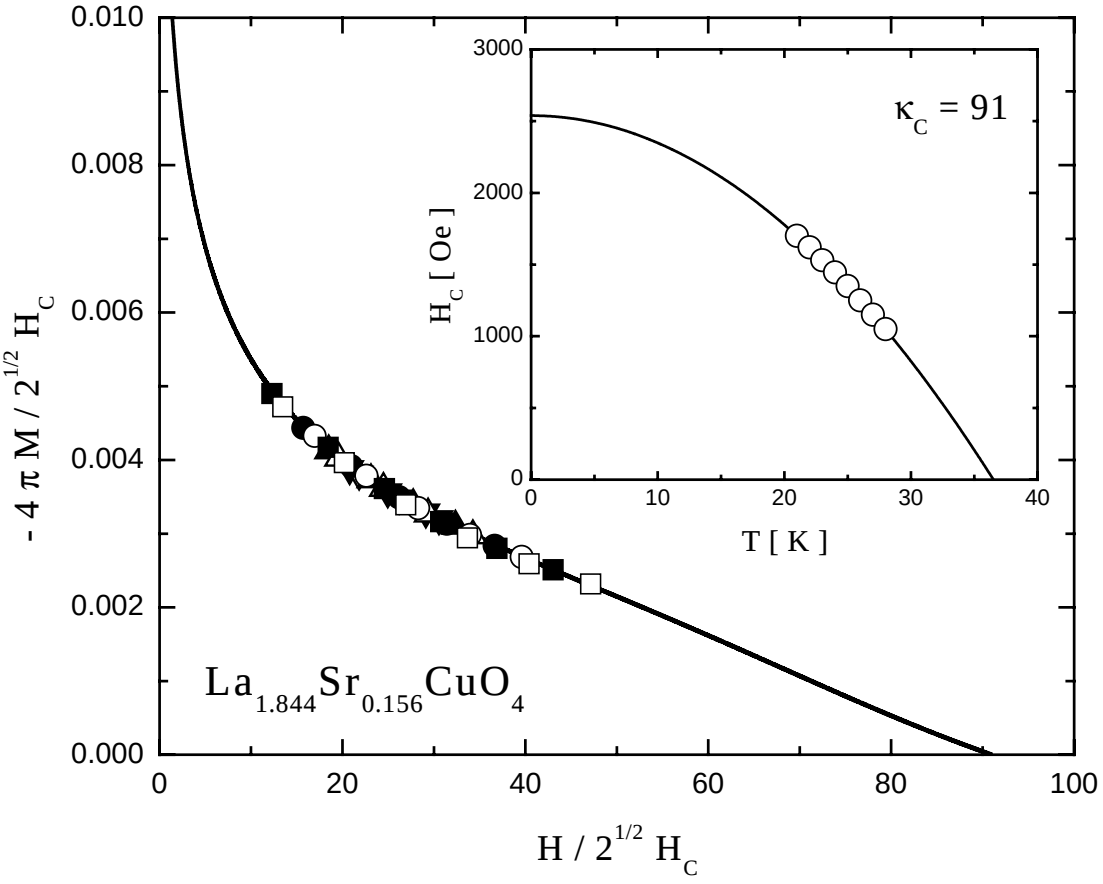

Figure 5.7 (b) The Hao-Clem curve for κ_c = 91 from 21 to 28 K. The inset shows the H_c(T) with the Two-Fluid model curve for $La_{1.844}Sr_{0.156}CuO_4$.

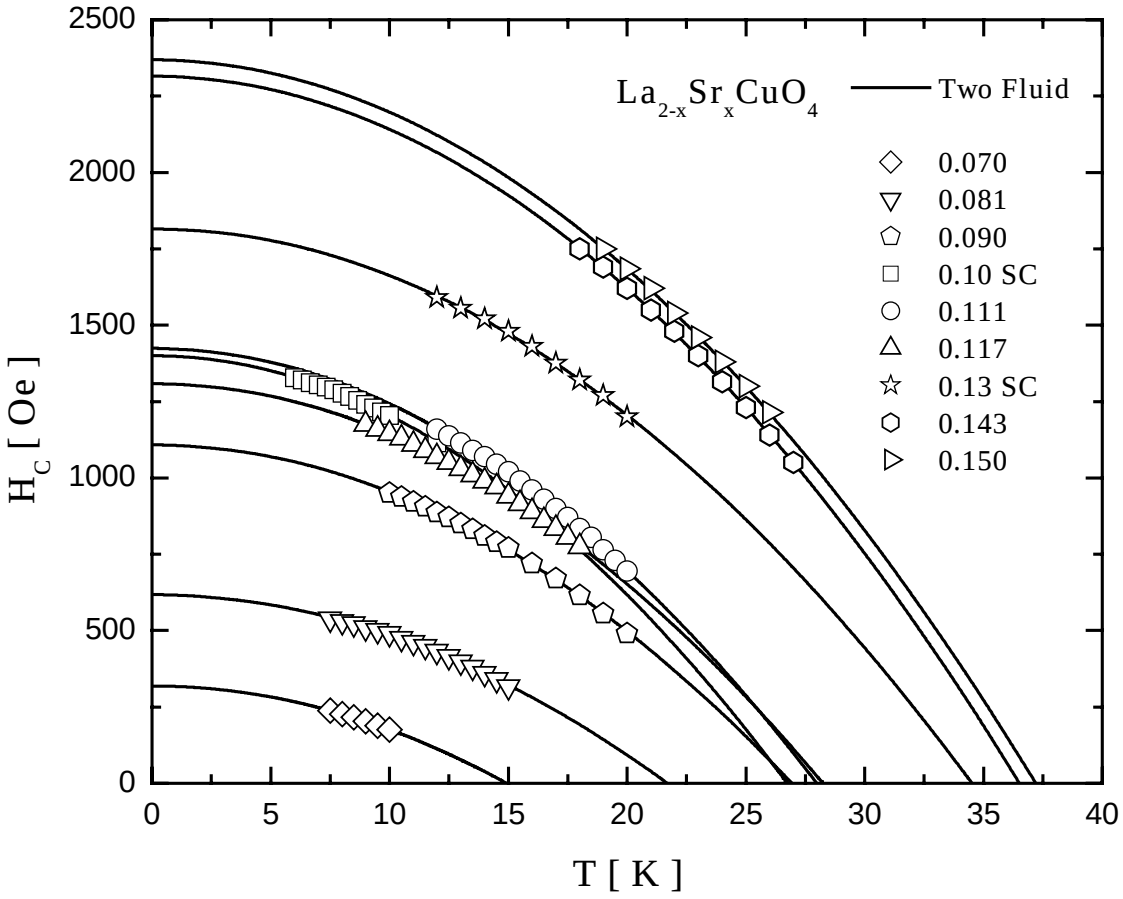

Figure 5.8 (a) The H_c(T) with the Two-Fluid model curves for the underdoped and optimum doped $La_{2-x}Sr_xCuO_4$.

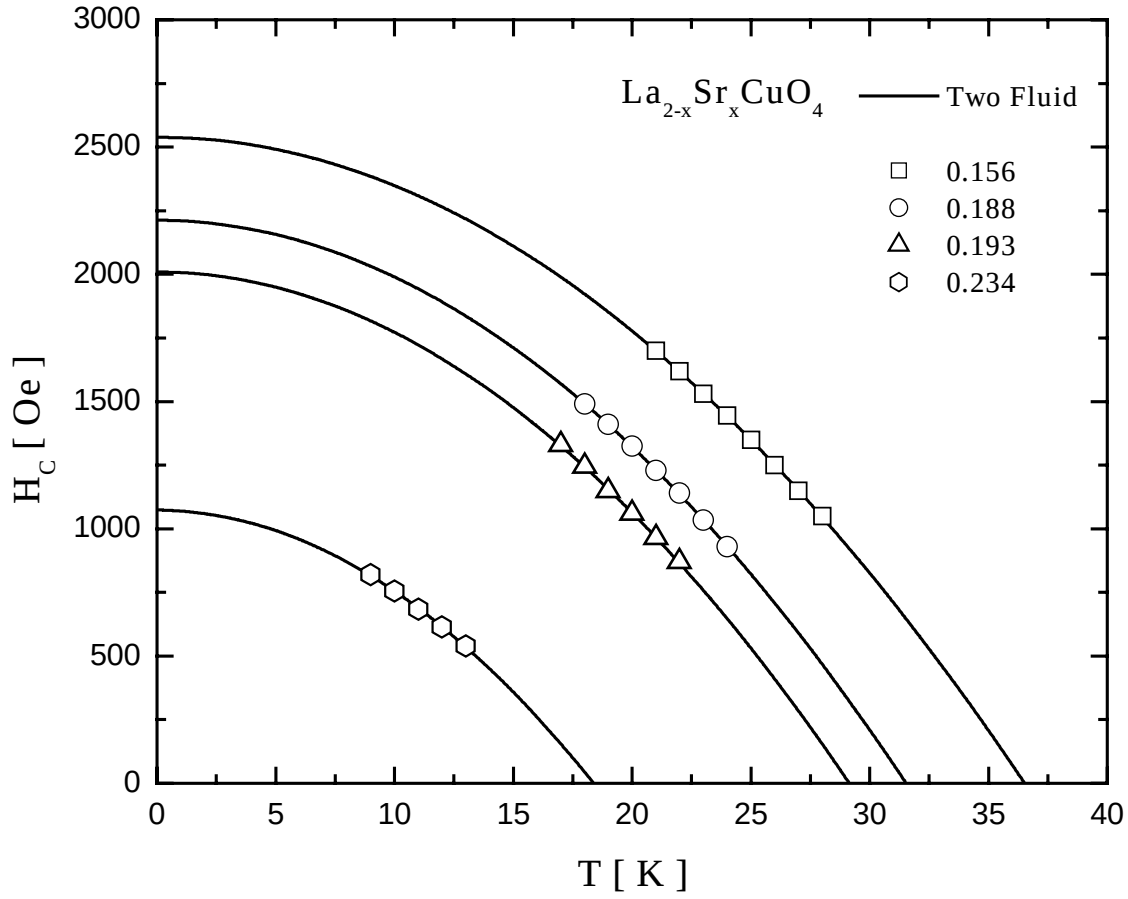

Figure 5.8 (b) The H_c(T) with the Two-Fluid model curves for the overdoped $La_{2-x}Sr_xCuO_4$.

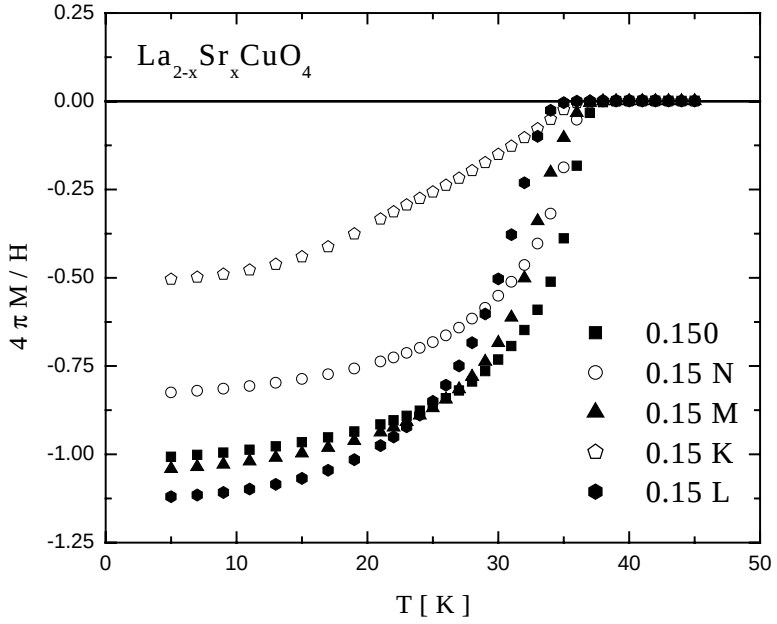

Figure 5.9 (a) The low field susceptibilities of 0.15 series of $La_{2-x}Sr_xCuO_4$.

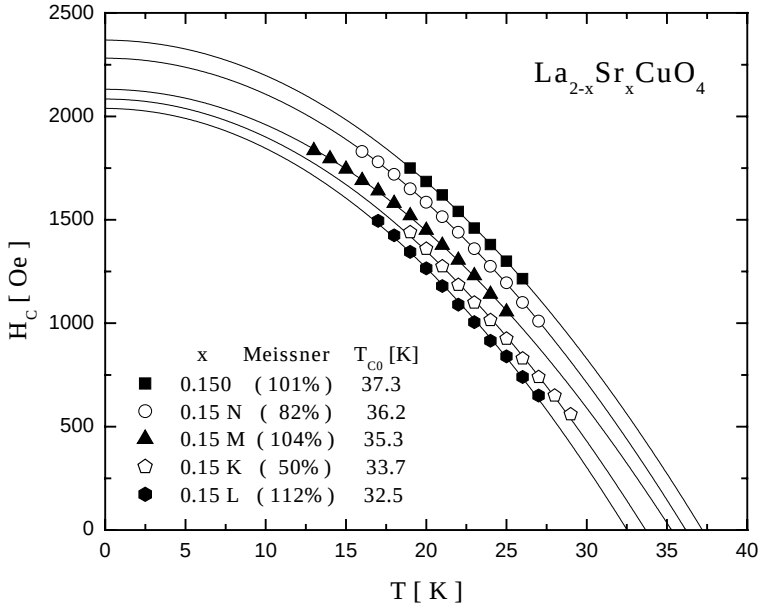

Figure 5.9 (b) The H_c(T), Meissner shielding fraction, and T_{c0} of 0.15 series.

transition temperature rather than Meissner shielding fraction. Although 0.15 K (50 %) shows substantially smaller Meissner fraction than 0.15 L (112 %), they display the similar values of T_{c0} (33.7 K and 32.5 K respectively). The sample 0.15 K has larger values of $H_c(T)$ than 0.15 L for all of the available temperature range. This conclusion justifies the validity of H_c of samples with small values of Meissner shielding fraction so long as they have the acceptable transition temperatures for hole concentrations. However it really needs to measure samples with the same amount of oxygen as well as Sr content showing different Meissner shielding fraction to confirm this conclusion.

To see the correlation of H_c with T_{c0}, if any, we plot T_{c0} vs. $H_c(0)$ in Figure 5.10 of all the samples studied. It is of interest if we draw the rough straight line from the data points to extrapolate T_{c0} at which a sample may have zero $H_c(0)$, then we have about 10 K of transition temperature. This may explain the apparently no reversible diamagnetic signal in the sample x = 0.06 SC for which the transition temperature is 8 K [13]. Magnetization measurements of x = 0.06 SC below transition temperature are shown in Figure 5.11 and zero-field and field cooled measurements at 10 Oe are included as inset to show it is truly a bulk superconductor.

The main results are plotted in Figure 5.12, 5.13, 5.14, and 5.15. Each shows, respectively, a plot of the variation of the $H_c(0)$, $H_c(0)/T_{c0}$, the free energy change, and density of states as a function of carrier concentration throughout the entire superconductive range of La-214 system. In Table 5.4 are listed their

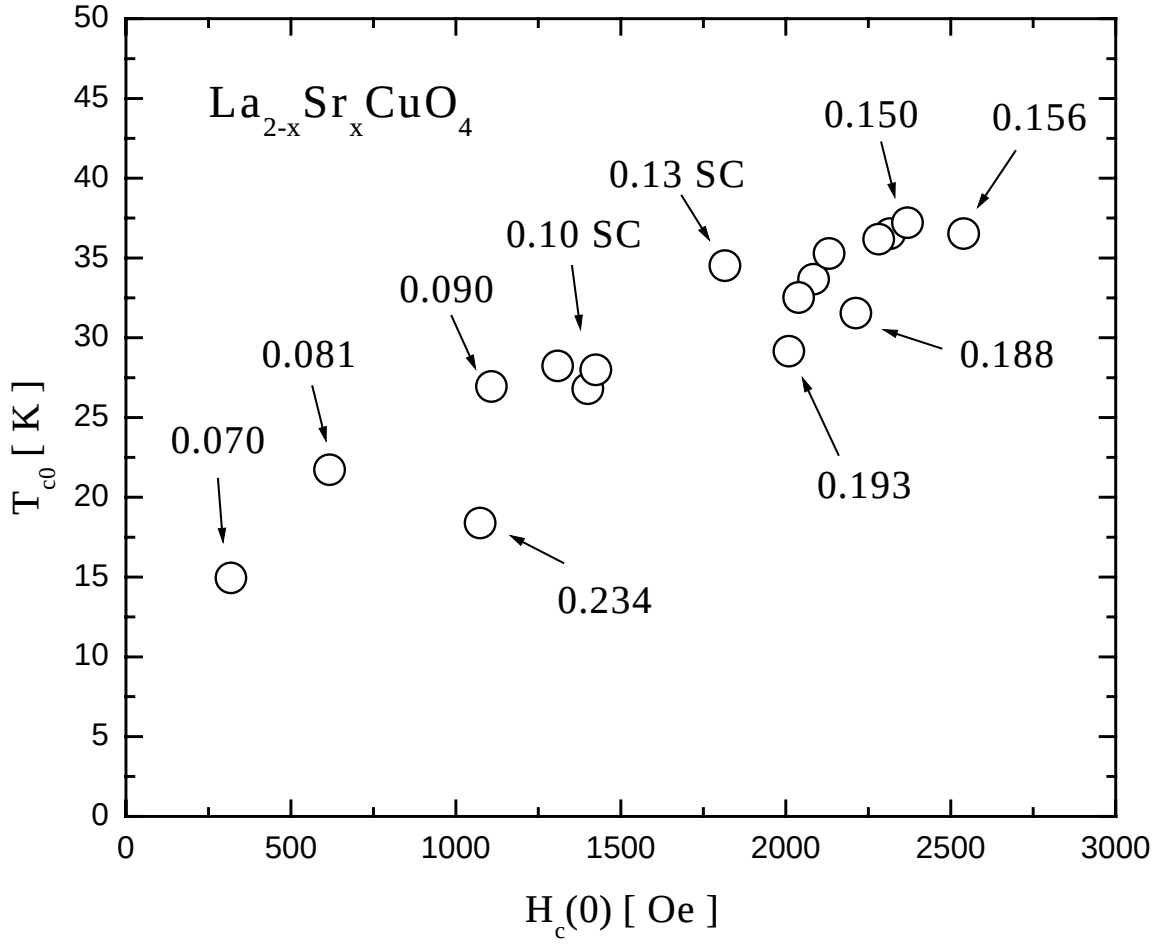

Figure 5.10 The T_{c0} vs. $H_c(0)$ plot of $La_{2-x}Sr_xCuO_4$. Refer to Table 5.4 for unmarked data.

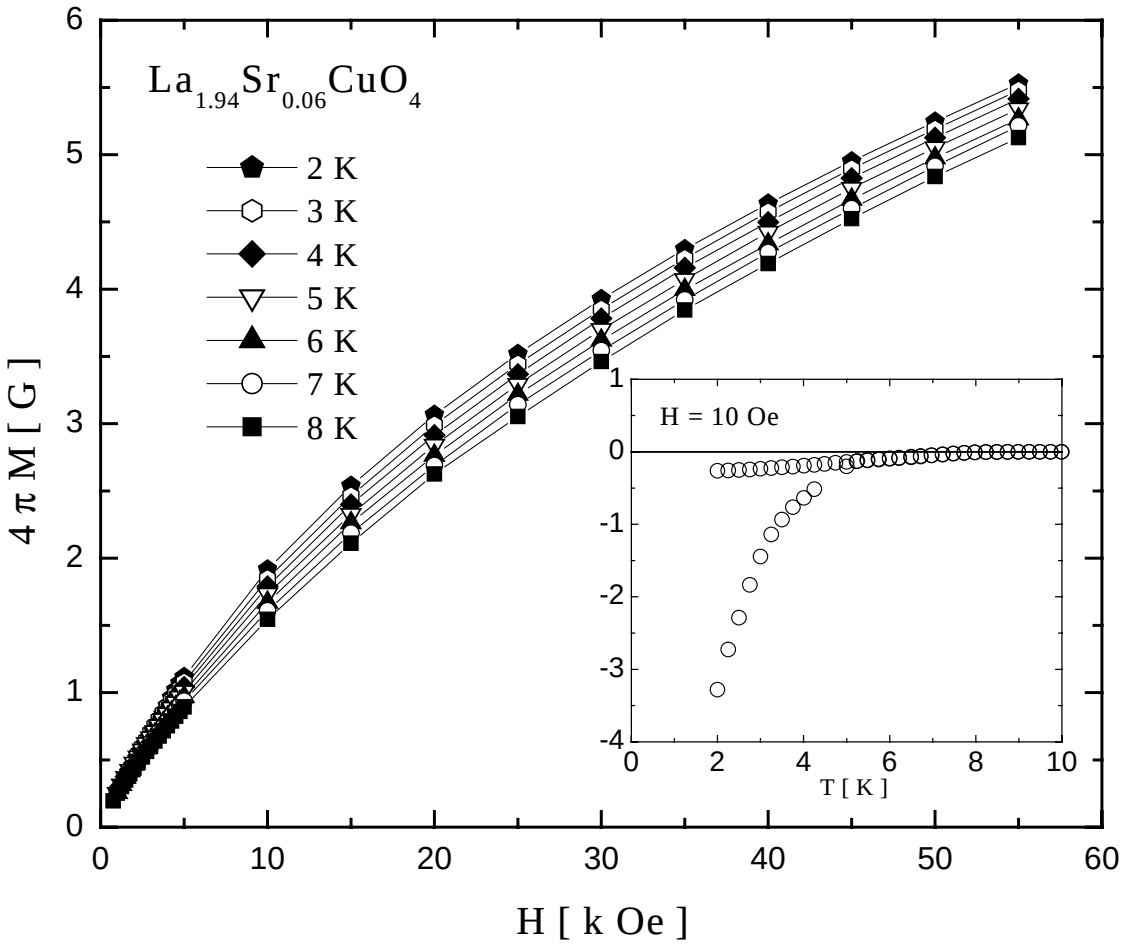

Figure 5.11 Magnetization below T_{c0} (= 8 K) of $La_{1.94}Sr_{0.06}CuO_4$. The inset shows the Meissner effect at 10 Oe.

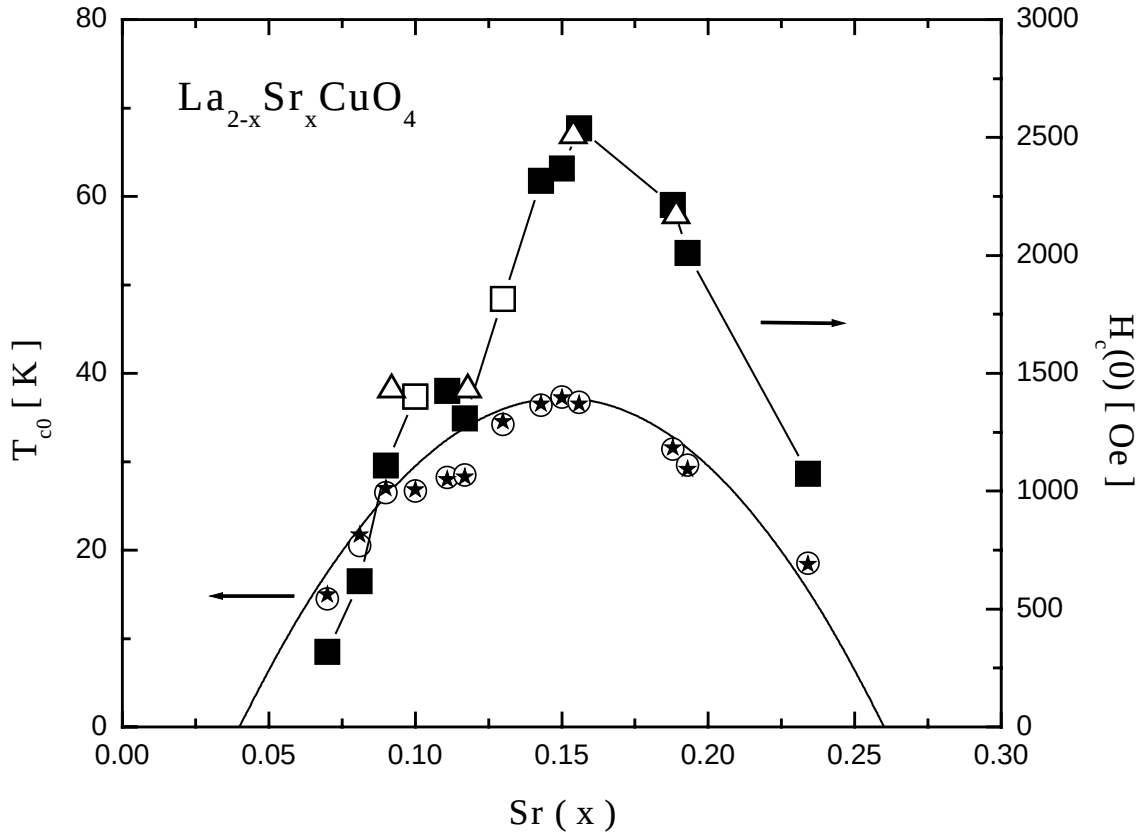

Figure 5.12 Thermodynamic critical field at zero temperature $H_c(0)$ and T_{c0} of $La_{2-x}Sr_xCuO_4$. Open squares and triangles (from Ref. 14) are of single crystals and closed squares are of aligned powder samples. Open circles and closed star are transition temperatures obtained from low field susceptibility measurements and the Hao-Clem fit results with Two-Fluid model, respectively. Closed line is a guide for the eye.

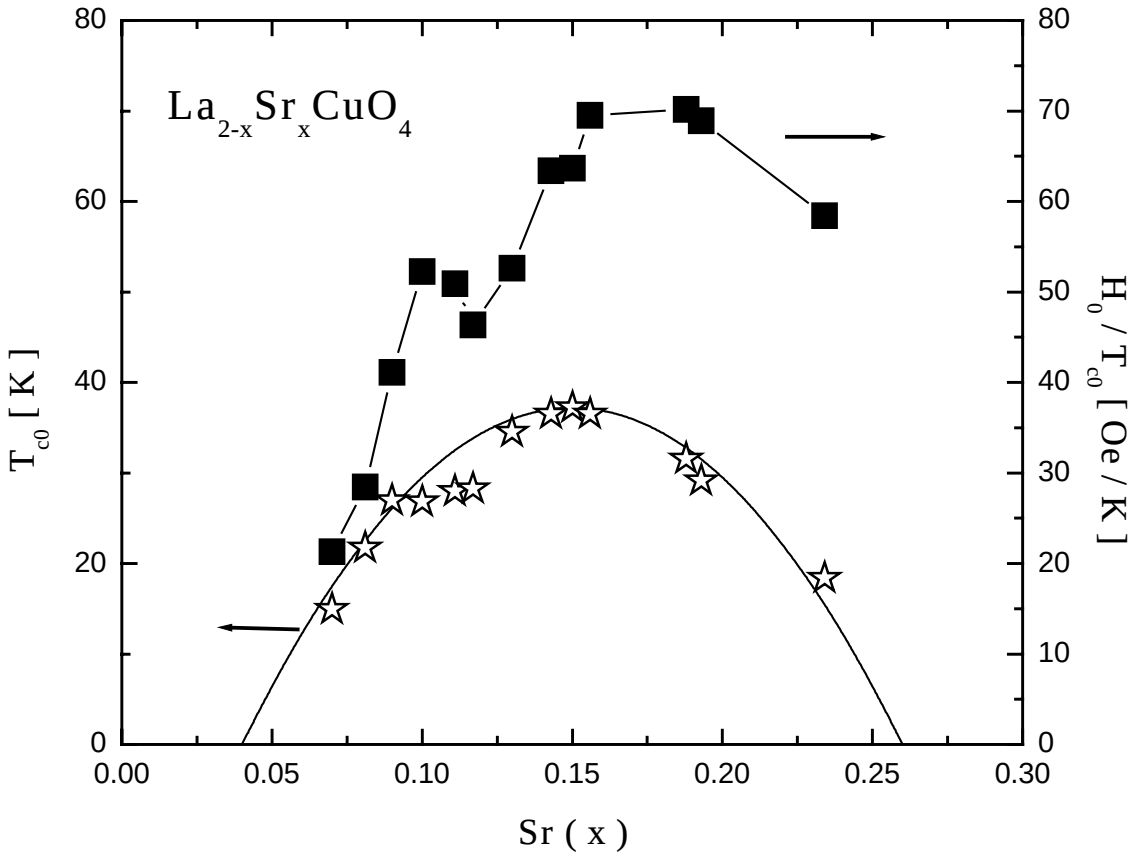

Figure 5.13 The T_{c0} and ratio $H_c(0)/T_{c0}$ of $La_{2-x}Sr_xCuO_4$. The $H_c(0)/T_{c0}$ remains nearly constant in the optimum and overdoped regimes and drops abruptly towards zero in the underdoped regime.

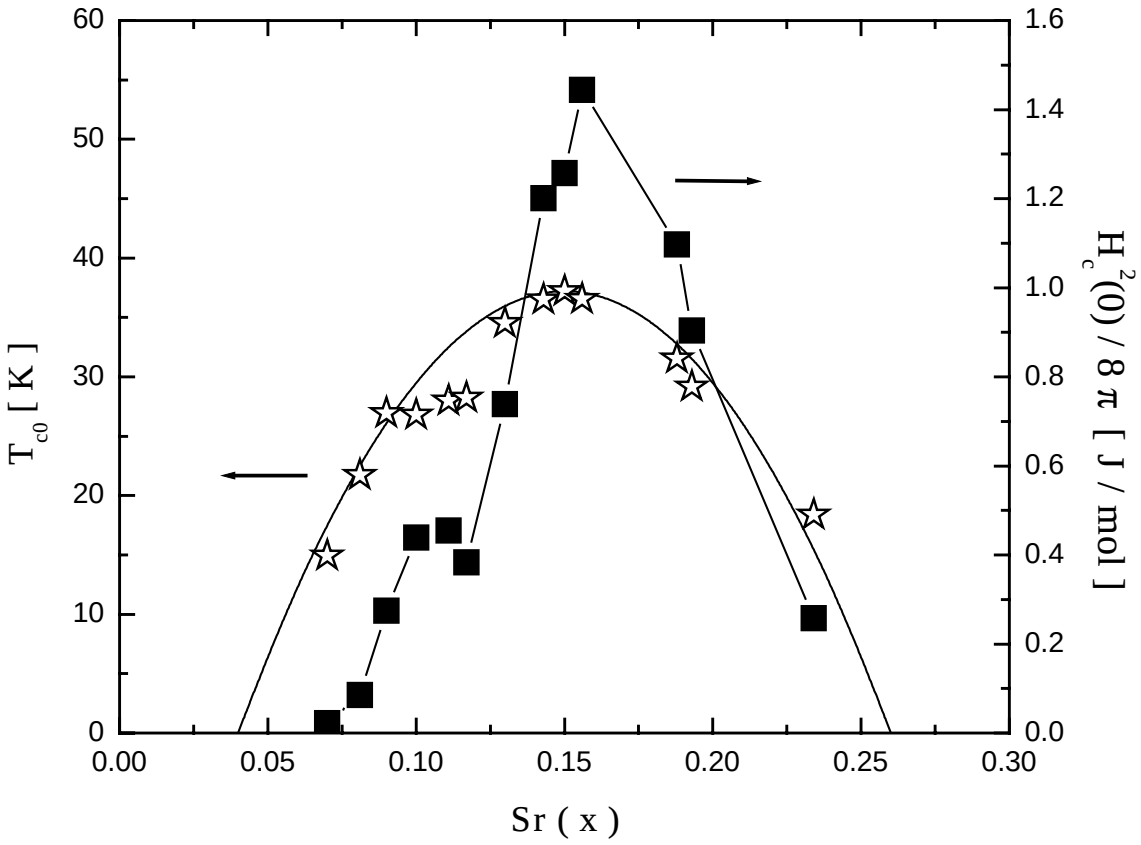

Figure 5.14 The free energy change, $H_c^2(0)/8\pi$, of $La_{2-x}Sr_xCuO_4$.

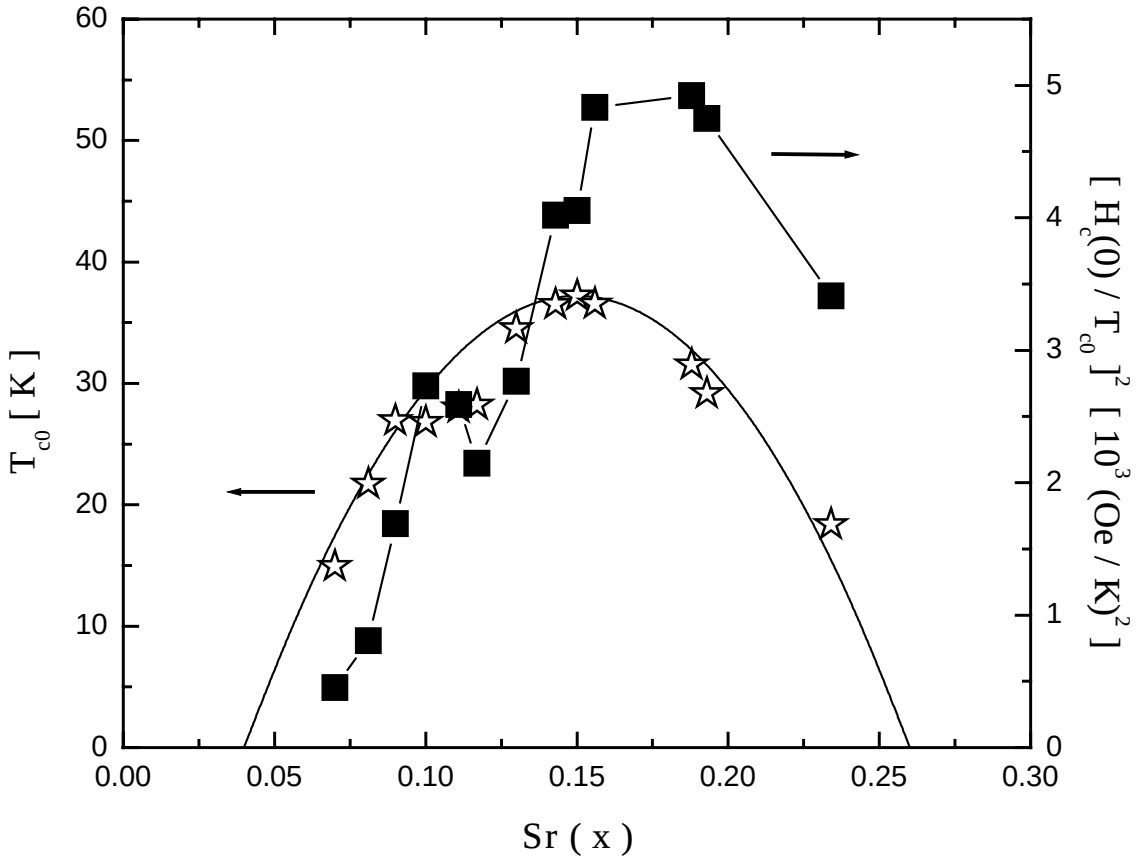

Figure 5.15 The plot of $[H_c(0)/T_{c0}]^2$ vs. x of $La_{2-x}Sr_xCuO_4$. The density of states, $N(0)$, is proportional to $[H_c(0)/T_{c0}]^2$.

Table 5.4 Thermodynamic parameters from the Two-Fluid Model.

Sr (x)	T_{c0} [K]	$H_c(0)$ [Oe]	$H_c(0)/T_{c0}$ [Oe/K]	U_0 [J/mol]	κ_c
0.06 SC	N/A	N/A	N/A	N/A	N/A
0.070	14.94	318.477	21.317	0.023	127
0.081	21.72	617.340	28.423	0.085	115
0.090	26.94	1107.964	41.127	0.275	140
0.10 SC	26.80	1400.359	52.252	0.439	175
0.111	27.99	1424.463	50.892	0.455	210
0.117	28.24	1308.698	46.342	0.384	170
0.13 SC	34.52	1815.814	52.602	0.739	60
0.143	36.52	2315.627	63.407	1.201	97
0.150	37.21	2369.089	63.668	1.257	72
0.156	36.53	2539.324	69.513	1.444	91
0.188	31.54	2212.630	70.153	1.097	83
0.193	29.15	2009.230	68.923	0.904	92
0.234	18.38	1073.742	58.406	0.258	115

numerical values. In Figure 5.12, the values of T_c obtained from dc-magnetization measurements at 10 Oe are also plotted in open circles and compared with those of derived from Two-Fluid model of the Hao-Clem results, shown in closed stars. The parabolic solid line is a guide for the eye. Data in open and closed squares are deduced from the current work and two open squares indicate that they are single crystal samples. Shown along as open triangles are the results of Li and co-workers [14], worked on single crystals of $La_{2-x}Sr_xCuO_4$, and they are in good agreement with current results.

The value of $H_c(0)$ (therefore the change of free energy, *i.e.* condensation energy which is plotted in Figure 5.14) peaks near optimum doping x = 0.156 in a manner of similar dependence of transition temperature on Sr contents. The ratio $H_c(0)/T_{c0}$ (Figure 5.13) as a function of carrier concentration also peaks at x = 0.188. The ratio is relatively slowly varying near the optimum doping level, while both T_{c0} and $H_c(0)$ vary much abruptly. Within the BCS theory [8], one would expect $H_c(0)/T_{c0}$ to vary as the square root of the electronic density of states $N(0)$. So $N(0)$ of La-214 system (Figure 5.15) increases rapidly in the underdoped regime and forms a plateau near the optimum doped regime and varies slowly towards the overdoped regime.

C. BCS Thermodynamics

It is now generally accepted that high temperature cuprate superconductors have different properties from conventional isotropic superconductors [for review refer to Ref. 15]. Among them, the two most striking properties might be firstly the existence of the pseudogap, opening of density of states at temperature much higher than transition temperature [16], and secondly the angular dependence of the superconducting gap parameter, Δ [17]. These two properties make it difficult to apply isotropic BCS thermodynamics directly to the high temperature cuprate superconductors. However, there have been attempts to apply the BCS theory to cuprate systems with the standard d-wave pairing interaction [18]. So it is still worthwhile to study the isotropic s-wave BCS thermodynamics to have a rough idea on the cuprate superconductors. The complete temperature dependence of H_c has been represented in well-developed explicit functions derived from the BCS theory by Muhlschlegel [19]. Thermodynamic critical fields, $H_c(T)$, are fitted to Eq. (29) of Ref. 19. We allow both gap ratio, $\Delta(0)/k_B T_{c0}$, and electronic specific heat coefficient, γ, to be two unknown parameters. The temperature variation of the BCS energy gap $\Delta(T)/\Delta(0)$ is given as [20]

$$\begin{aligned}
\Delta(T)/\Delta(0) &= (1 - t^{2.75})^{1/2}\,(0.9847 + 0.1577t - 0.0953t^2) && ;\ 1 > t > 0.7 \\
&= (1 - t^{3.3})^{1/2}\,(0.971 + 0.1786t - 0.2035t^2) && ;\ 0.7 > t > 0.36 \\
&= 1 - 1.89t^{1/2}\exp(-1.76/t) && ;\ 0.36 > t, \qquad (2)
\end{aligned}$$

where t is the reduced temperature.

The results of fitting $H_c(T)$ to the BCS thermodynamics are shown in Figure 5.16 as a function of reduced temperature. In Figure 5.17, closed circles are $H_c(0)$ derived from the BCS theoretical curves. For comparison, the results from the Two-Fluid model are also plotted as open squares. Open stars are transition temperatures. The deduced values of $\Delta(0)/k_B T_{c0}$ and γ are plotted in Figure 5.18 and Figure 5.19, respectively. Numerical values of T_{c0}, $H_c(0)$, $\Delta(0)/k_B T_{c0}$, and γ are listed in Table 5.5. The BCS theory predicts gap ratio to be 1.76 [8], which is drawn as a solid line in Figure 5.18, and those of some elements [21] are inserted. The average value of $\Delta(0)/k_B T_{c0}$ is about 2.01 for the entire La-214 system and this is comparable value to the strongly coupled (the large coupling constant $N(0)V$) superconductors such as lead (~ 2.19) and mercury (~ 2.30). Recently it is reported that the gap ratio for optimum doped La-214 system (T_c = 38 K) is around 2.6 from ultrahigh-resolution photoemission spectroscopy [22].

With increasing Sr content, γ increases rapidly and becomes saturated near optimum doped regime and tends to stay nearly constant in the overdoped regime even though transition temperature drops rather quickly. Note that there is a substantial dip near 0.117 and a broad maximum is seen near 0.188. This result is quite comparable with published systematic $N(0)$ studies in the La-214 system by several other groups such as the angle-integrated photoemission spectroscopy (AIPES) for DOS, $\rho(\mu)$ [23], the electronic specific heat coefficient, γ [24], and the Pauli-paramagnetic component χ_s^c of the spin susceptibility [7]. They showed the similar results of the variation of $N(0)$ as a

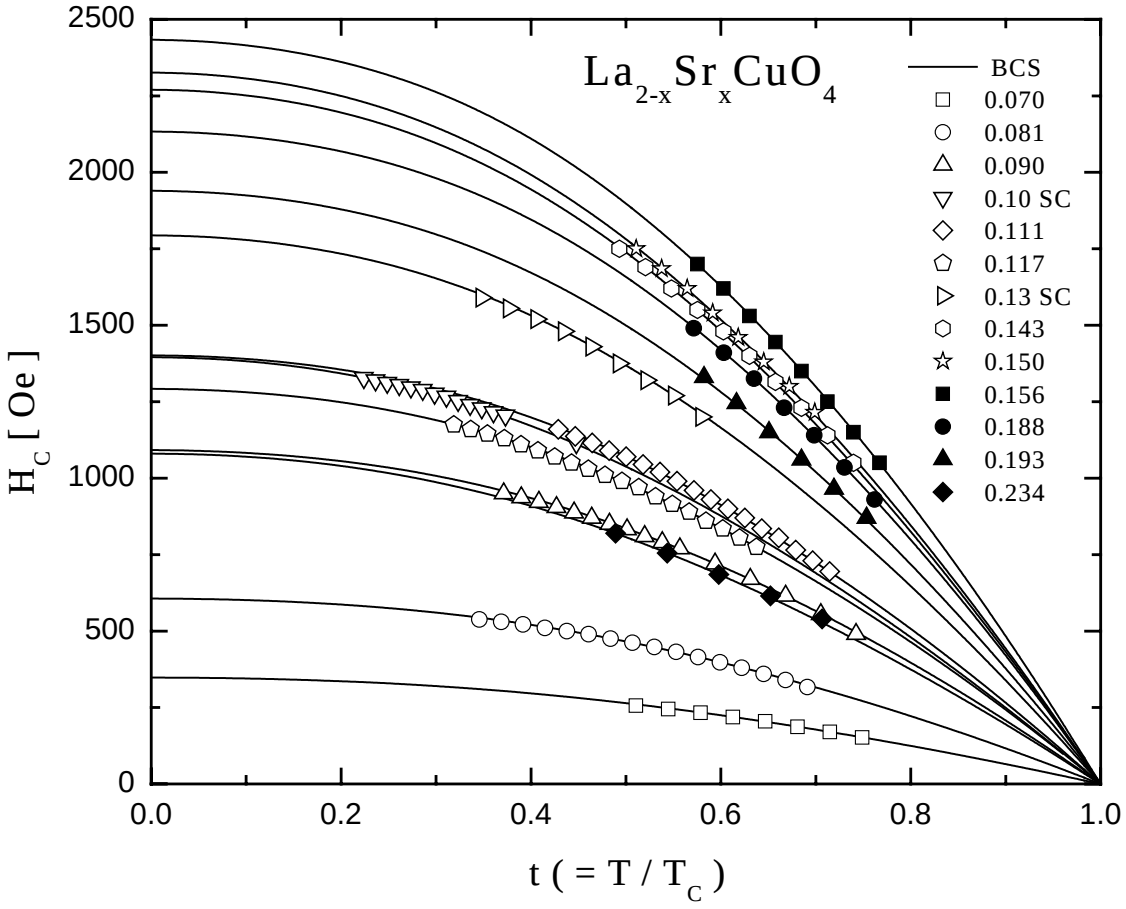

Figure 5.16 The H_c(T) and the BCS thermodynamics curves (solid lines) for $La_{2-x}Sr_xCuO_4$.

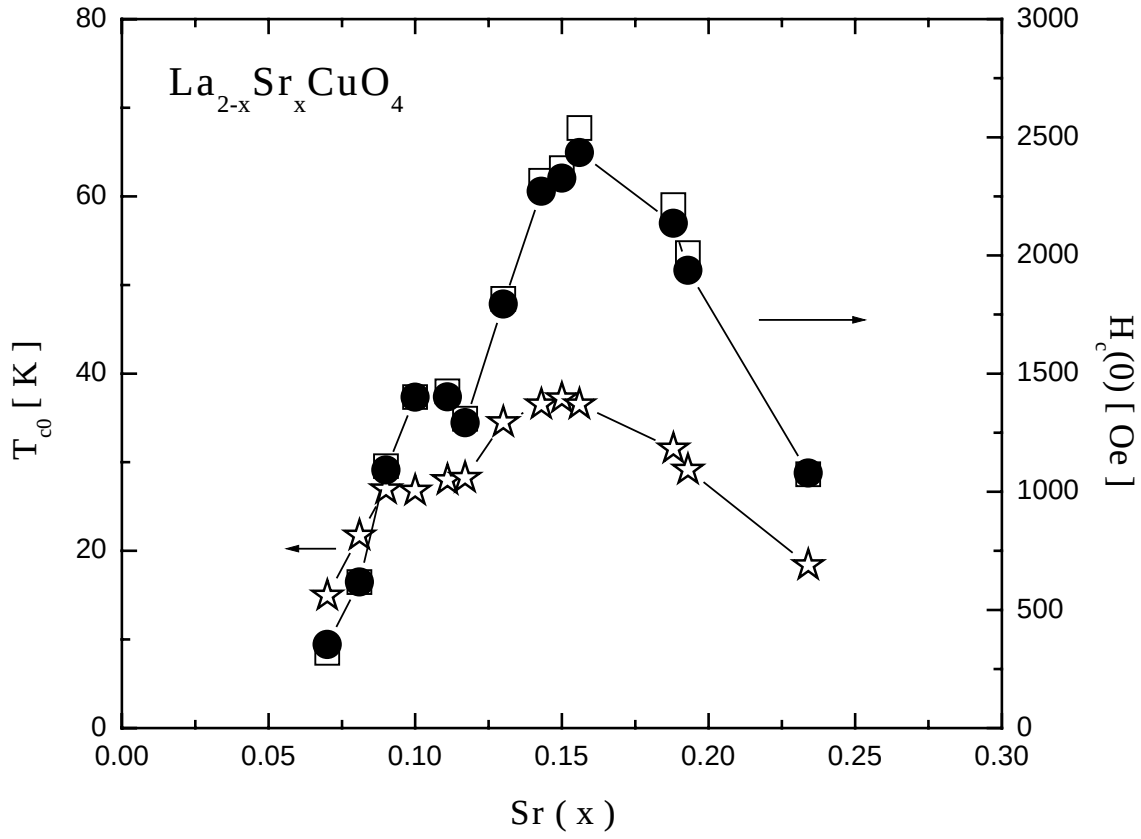

Figure 5.17 The $H_c(0)$ from the BCS thermodynamics (closed circles) and from the Two-Fluid model (open squares) together with T_{c0} (stars) of $La_{2-x}Sr_xCuO_4$.

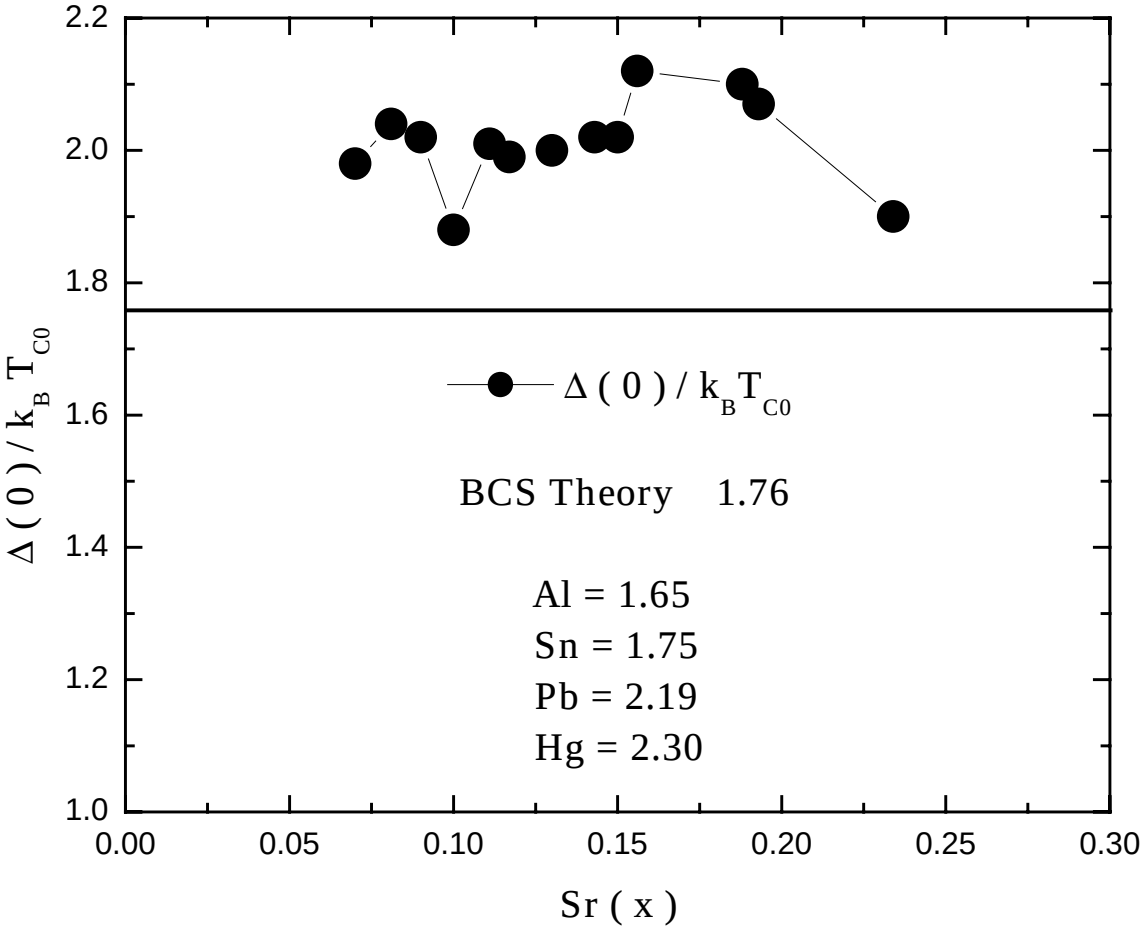

Figure 5.18 The gap ratio $\Delta(0)/k_B T_{c0}$ (closed circles) derived from the BCS thermodynamics for $La_{2-x}Sr_xCuO_4$. In the figure are shown empirically determined values of some elemental superconductors.

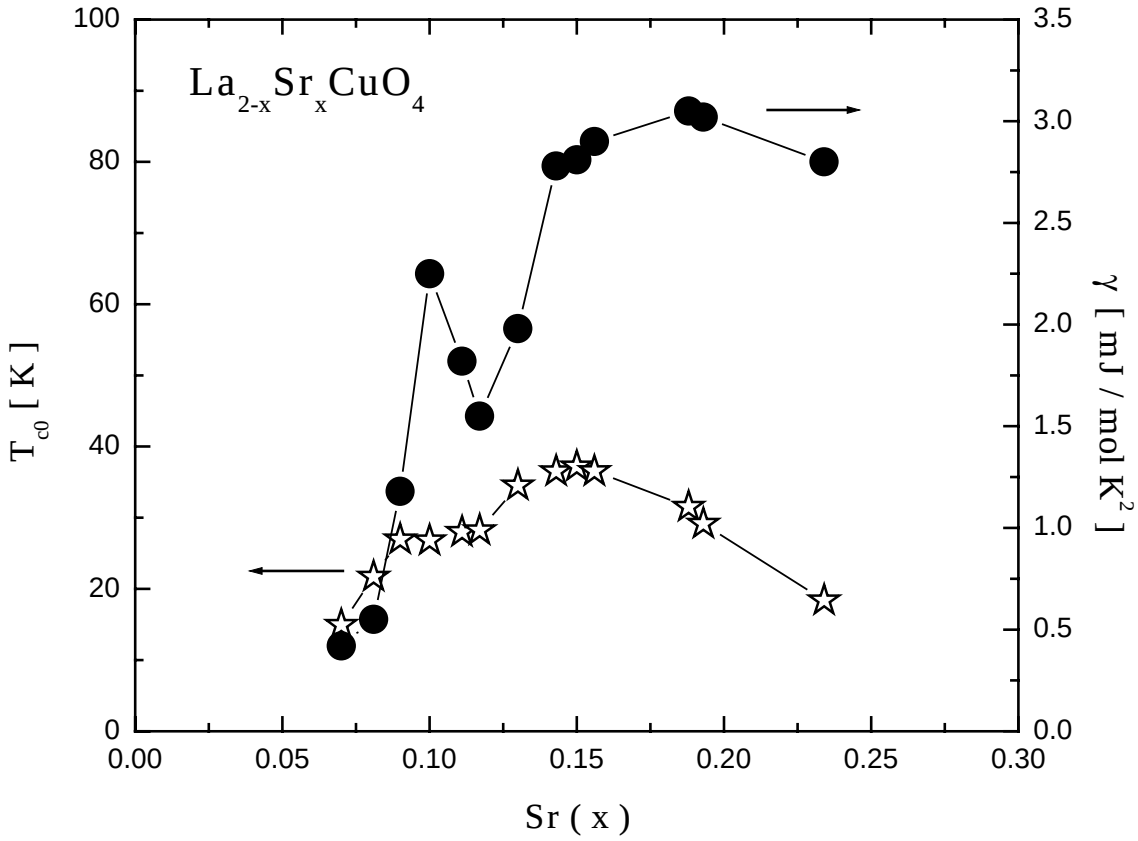

Figure 5.19 The specific heat coefficient γ derived from the isotropic BCS fit for $La_{2-x}Sr_xCuO_4$.

Table 5.5 Thermodynamic parameters from the BCS theory.

Sr (x)	T_{c0} [K]	$H_c(0)$ [Oe]	$\Delta / k_B T_{c0}$	γ[mJ/mol K^2]
0.06 SC	N/A	N/A	N/A	N/A
0.070	14.94	354.033	1.98	0.42
0.081	21.72	617.977	2.04	0.55
0.090	26.94	1091.690	2.02	1.18
0.10 SC	26.80	1400.407	1.88	2.25
0.111	27.99	1401.655	2.01	1.82
0.117	28.24	1292.093	1.99	1.55
0.13 SC	34.52	1794.073	2.00	1.98
0.143	36.52	2271.507	2.02	2.78
0.150	37.21	2326.853	2.02	2.81
0.156	36.53	2435.528	2.12	2.90
0.188	31.54	2136.173	2.10	3.05
0.193	29.15	1936.626	2.07	3.02
0.234	18.38	1079.398	1.90	2.80

function of doping concentration. All three quantities increase slowly or remain nearly constant with decreasing x from 0.3, taking a broad maximum around x = 0.2, below which they decrease rather rapidly towards zero. Our conclusion on γ supports the same dependence of $N(0)$ on Sr concentration.

The BCS theory has been proven to be rather successful in explaining thermodynamics of the conventional superconductors. One way to appreciate the consequence of the BCS thermodynamics is to plot $H_c(0)/T_{c0}$ as a function of square root of empirically measured specific heat coefficients. Conventional superconductors show nice agreements with the BCS prediction. However, for cuprate systems it is very difficult to measure γ directly with specific heat measurement due to the extremely high upper critical field that makes superconducting phase be normal state and the closed gap parameter in certain directions even at zero temperature. The usual way to overcome this problem is to use the parent insulating material as a reference material [25] to obtain electronic contribution of specific heat by subtracting the insulating contribution from the total specific heat. There is yet no accepted γ value available for cuprate systems from direct specific heat measurements.

In Figure 5.20, we plot $H_c(0)/T_{c0}$ vs. square root of empirically measured γ for conventional superconductors [numerical values are from Ref. 26] and our deduced values of γ by fitting H_c to the BCS theory for La-214 system. Niobium, Vanadium, and Tantalum form a d-band metal group and lead, mercury, Aluminum, tin, and Indium are of an s-p band metal group. The values of La-214

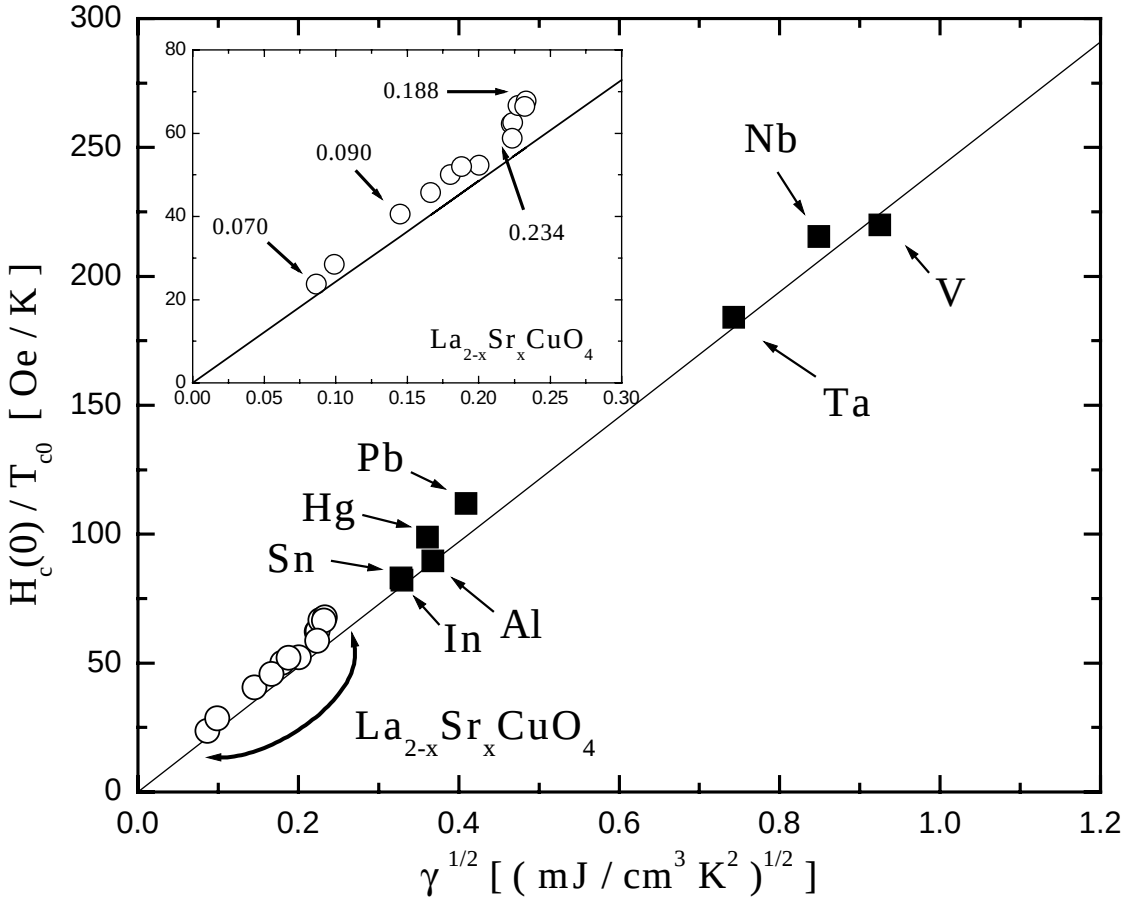

Figure 5.20 The plot of $H_c(0)/T_{c0}$ vs. measured γ for conventional superconductors [numerical values are from Ref. 26] and our derived values of γ of $La_{2-x}Sr_xCuO_4$.

system in Figure 5.20, which are deduced from the two-parameter fit of $H_c(T)$ to the isotropic s-wave BCS theory, scale well both with the s-p band and with the d-band superconductors.

IV. Conclusion

A series of grain aligned and single crystal samples has been shown to have wide ranges of thermodynamic reversibility in the *H-T* plane so that systematic free energy study of $La_{2-x}Sr_xCuO_{4-\delta}$, La-214, family becomes possible with reversible superconducting magnetization. Normal state magnetization behaves rather well so that background signals are subtracted to obtain superconducting magnetization in consistent manner throughout the entire superconductive range from strongly underdoped to strongly overdoped regimes.

At temperatures away from the transition temperatures, the M_{sc} vs. H curves can be analyzed by following the Hao-Clem model and thermodynamic critical fields are derived. At any given temperature H_c takes a maximum for x = 0.156. The zero temperature thermodynamic critical field, $H_c(0)$, rises and falls in a quite similar manner to the variation of doping concentration dependence of transition temperature, being maximum at optimum doped and approaches zero towards both 0.05 and 0.25 ends. $H_c(0)$ depends strongly on the transition temperature of the system and varies roughly linearly to each other. The Meissner shielding fraction at 10 Oe does not seem to be correlated with the

value $H_c(0)$ that is obtained. The ratio of $H_c(0)$ to T_{c0} also peaks in the region of somewhat larger than optimum doping at x = 0.188. It rises steeply from underdoped regime and saturates near optimum doped and changes slowly even though both $H_c(0)$ and T_{c0} drop to zero abruptly. By applying the isotropic BCS thermodynamics, the gap ratio, $\Delta(0)/k_BT_{c0}$, is determined to be 2.01±0.11 indicating La-214 is strongly coupled superconductor and γ shows the tendency to remain nearly constant over the wide range of optimum and overdoped regimes taking a broad maximum around x = 0.188 and then drops quickly towards zero in the underdoped regime.

Acknowledgement

We thank Dr. Q. Li at Brookhaven National Laboratory for providing the 0.13 single crystal sample for our work. This research was supported by the U.S. Department of Energy, Basic Energy Sciences, Office of Science, through the Ames Laboratory under Contract No. W-7405-ENG-82.

Appendix: Calculation of $\Delta(0)/k_BT_c$ and γ

The BCS theory relates thermodynamic critical field and normal electronic specific heat coefficient γ to the energy gap Δ/k_BT_c by the equation

$$H_c(0)/T_c = (6/\pi)^{1/2}(\Delta(0)/k_BT_c)\,\gamma^{1/2}, \qquad \text{(A1)}$$

at zero temperature. The complete temperature variation of thermodynamic quantities such as superconducting electronic entropy S_{es} and critical field H_c is well developed by Muhlschlegel [19] in explicit forms derived from the BCS theory:

$$S_{es}/\gamma T_c = t\,[1+3(xa' - a) - 3x/2], \tag{A2}$$

$$(H_c(T)/T_c)^2 = 12\,\pi\,\gamma\,t^2\,(xa' - a), \tag{A3}$$

where

$$x = \left(\frac{\Delta(T)}{\Delta(0)} \times \frac{\alpha}{\pi t}\right)^2, \tag{A4}$$

$$a(x) = -\frac{2}{\pi}\int_{-\infty}^{\infty} \ln\left[1+\exp\left(-\pi\sqrt{u^2+x}\right)\right]du + x\left[\ln\left(1.78107\sqrt{x}\right) - \frac{1}{2}\right] + \frac{1}{3}, \tag{A5}$$

and a' is a derivative of a with respect to x. The gap ratio $\Delta(0)/k_B T_c$ is replaced by α and the BCS theory predicts α to be 1.76.

In the early study to deduce gap ratio in tin, indium, and mercury, Finnemore and Mapother [27] employed the Eq. (A2) to scale superconducting electronic entropy with empirically determined value of γ. They found $\Delta(0)/k_B T_c$ to be 1.81, 1.84, and 2.40 for Sn, In, and Hg respectively and they are in good agreement with other experimental results. However, roughly speaking, it is not necessary to know γ beforehand to deduce $\Delta(0)/k_B T_c$ if we take logarithm on both sides of Eq. (A3)

$$ln\{[H_c(T)/T_c]^2\} = \epsilon + ln(\gamma) + ln[f(t)], \tag{A6}$$

where ϵ is a constant and $f(t)$ is a function dependent on t. Therefore γ translates the whole shape of the curve vertically in the plot of $ln\{[H_c(T)/T_c]^2\}$

vs. t (this is not strictly true since ϵ varies slightly as t changes but this gives rise to negligible effects). The energy gap $\Delta(0)/k_BT_c$ is only connected with the term $ln[f(t)]$ which determines the slope of curve in $ln\{[H_c(T)/T_c]^2\}$ vs. t plot. The physics behind this interpretation is that $H_c(T)/H_c(0)$ is determined uniquely by $\Delta(0)/k_BT_c$ and then $H_c(0)/T_c$ depends only on the $N(0)$ of the system within the BCS theory. Two variables $\Delta(0)/k_BT_c$ and γ can be deduced simultaneously and nearly independently by fitting the shape of thermodynamic critical fields to the plot of $ln\{[H_c(T)/T_c]^2\}$ vs. t. The only assumption is that the energy gap $\Delta(T)/\Delta(0)$ follows the temperature variation as given in Eq. (2) in text and plotted in Figure 5.A1, which is derived from the BCS theory. It is shown by Finnemore and Mapother that Sn, In, and Hg indeed have the same temperature dependence of $\Delta(T)/\Delta(0)$ although they have different $\Delta(0)/k_BT_c$ values [27].

We deduced both $\Delta(0)/k_BT_c$ and γ by fitting $H_c(T)$ data given in Ref. 27 of Sn, In, and Hg to Eq. (A3) to check the validity of the fit using both $\Delta(0)/k_BT_c$ and γ as two unknown adjustable parameters. The results are plotted in Figure 5.A2, 5.A3, and 5.A4 for Sn, In, and Hg, respectively. The numerical values are listed in Table A1. The deduced values are compared with corresponding values from Ref. 27. They are in quite good agreement except Hg which shows differences about 0.3 and 0.05, for $\Delta(0)/k_BT_c$ and γ respectively. The $\Delta(0)/k_BT_c$ of Hg was confirmed to be 2.30 later by electron tunneling experiment by Bermon and Ginsberg [28]. We take these differences as error-ranges arising from dealing with H_c. We also conducted the scaling in the limited temperature range to get a measure of the errors that might be introduced by taking a limited data

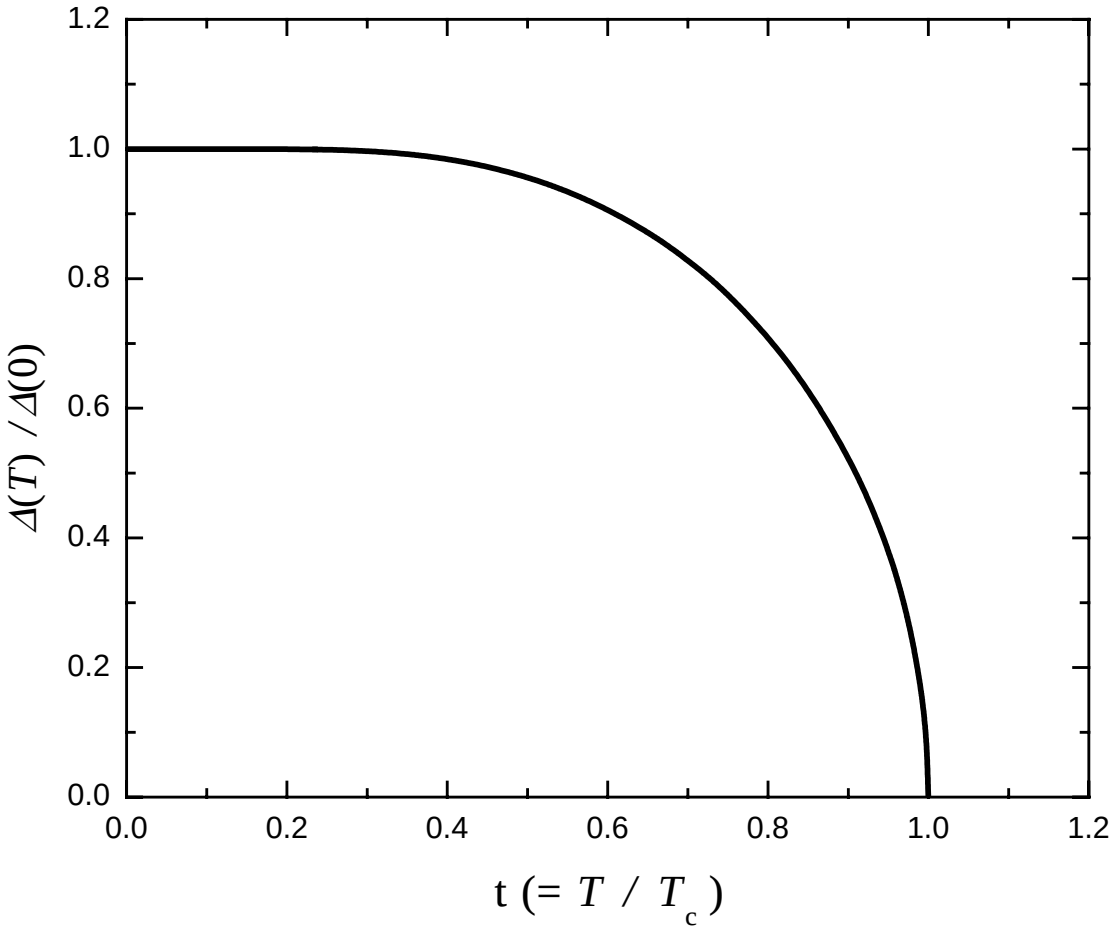

Figure 5.A1 The temperature variation of the energy gap $\Delta(T)/\Delta(0)$.

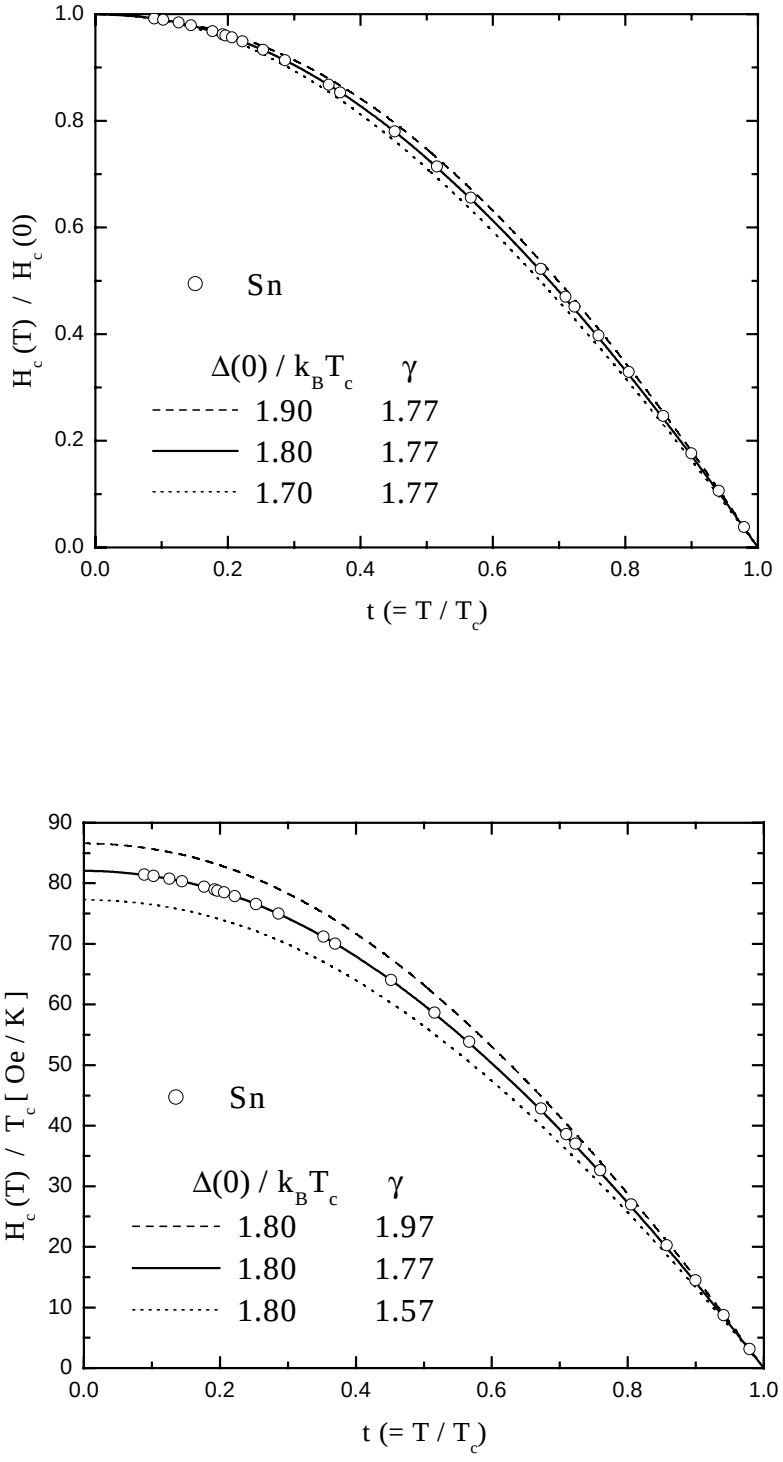

Figure 5.A2 The BCS theory fit gives $\Delta(0)/k_B T_c$ =1.80 and γ = 1.77 for Sn.

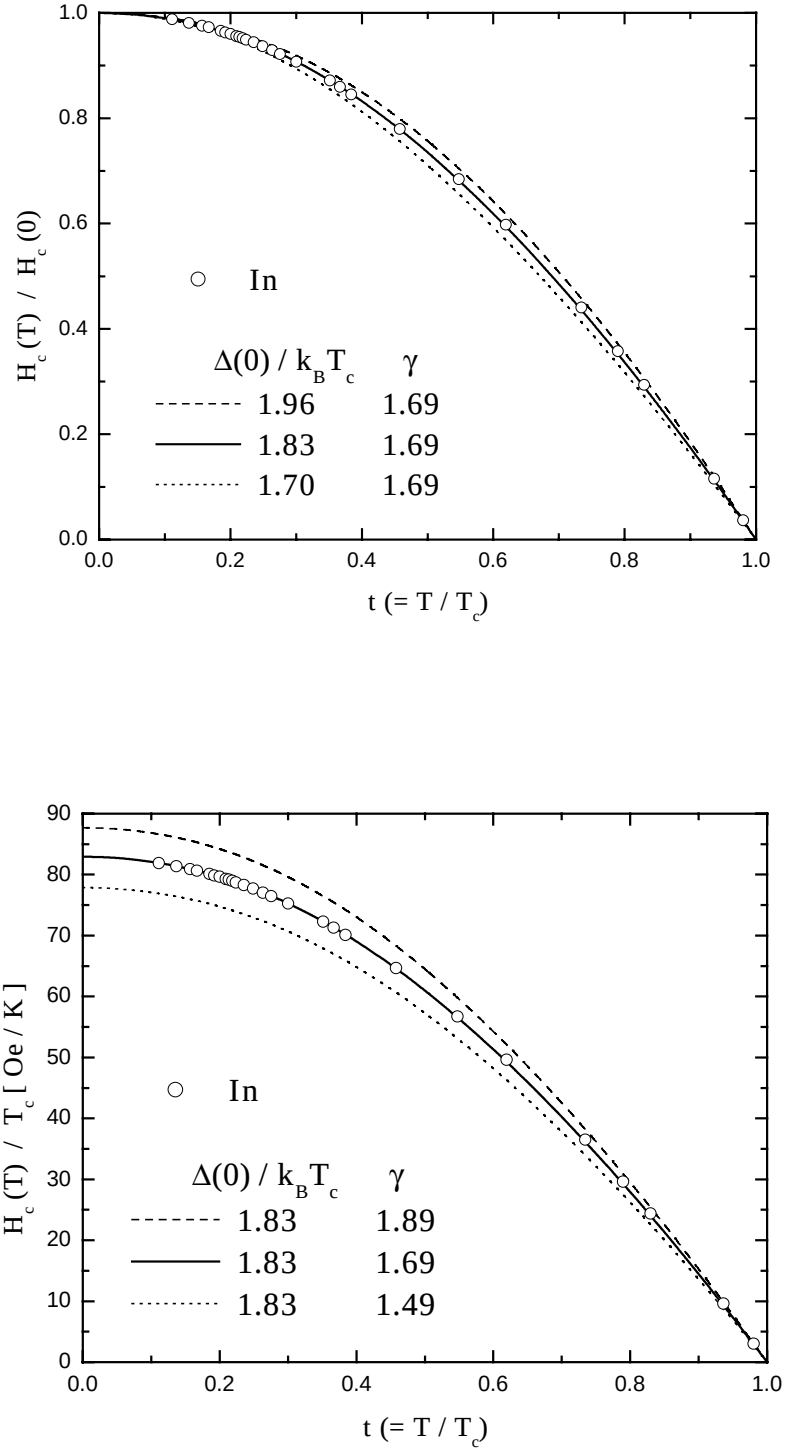

Figure 5.A3 The BCS theory fit gives $\Delta(0)/k_B T_c$ =1.83 and γ = 1.69 for In.

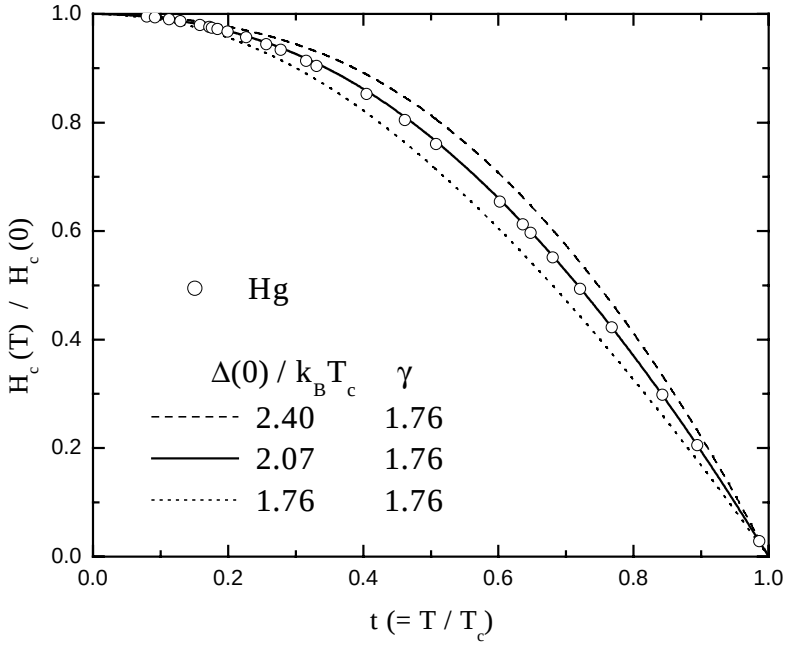

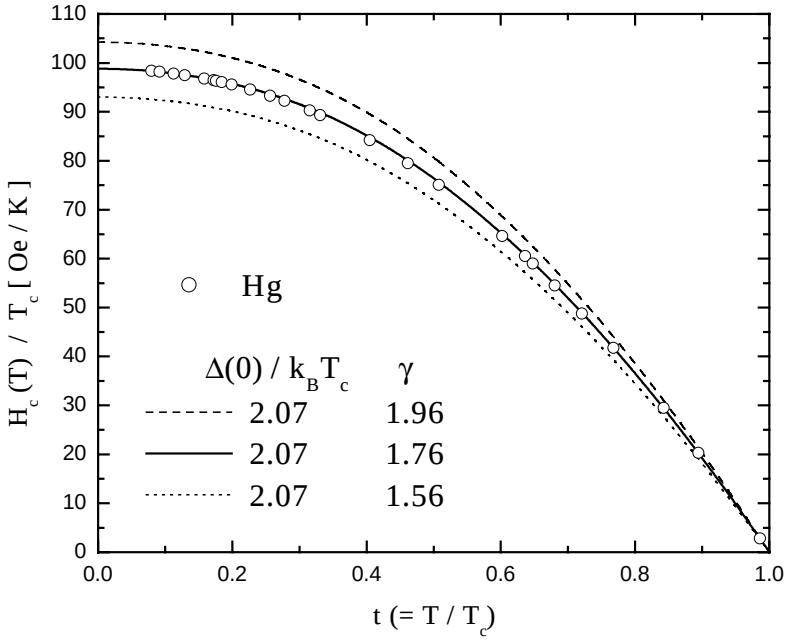

Figure 5.A4 The BCS theory fit gives $\Delta(0)/k_B T_c$ =2.07 and γ = 1.76 for Hg.

set. In the range of *t* between 0.36 and 0.7 (this is deliberately chosen since most of our $H_c(T)$ data in $La_{2-x}Sr_xCuO_4$ falls in this range), the resolution in selecting the values of $\Delta(0)/k_BT_c$ and γ are within ±0.02 and ±0.03, respectively. In Figure 5.A5 and 5.A6 are the fitting results of the $La_{1.857}Sr_{0.143}CuO_4$ and $La_{1.970}Sr_{0.130}CuO_4$, respectively. The values of both Δ/k_BT_c and γ for each sample are inserted.

Table 5.A1 The values of Δ/k_BT_c and γ from this work. They are compared with the results of Ref. 27.

		$\Delta(0)/k_BT_c$	γ [mJ/mol K^2]
Sn	This work	1.80	1.77
	Ref. 27	1.81	1.74
In	This work	1.83	1.69
	Ref. 27	1.84	1.66
Hg	This work	2.07	1.76
	Ref. 27	2.40	1.81

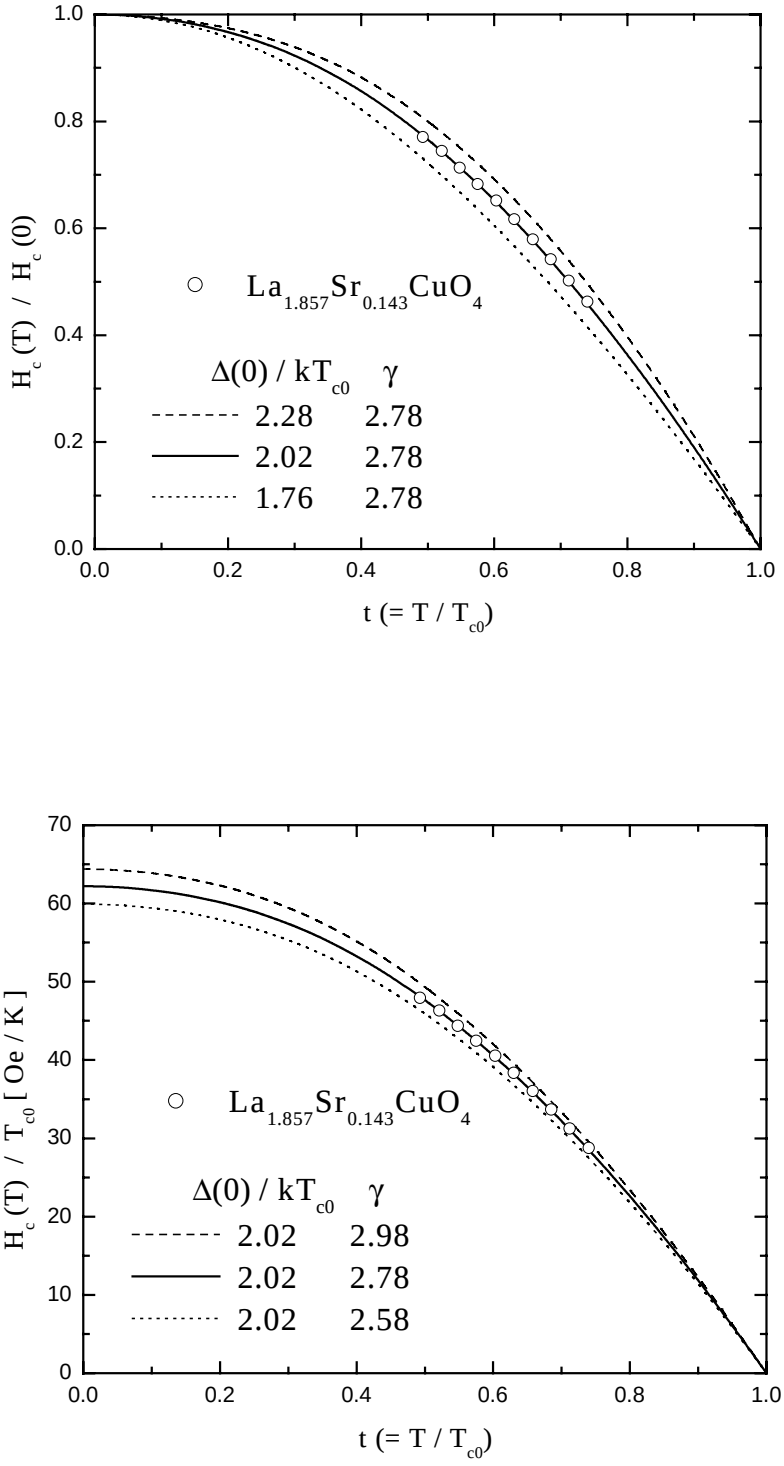

Figure 5.A5 The BCS theory fit gives $\Delta(0)/k_BT_c$ =2.02 and γ = 2.78 for x = 0.143.

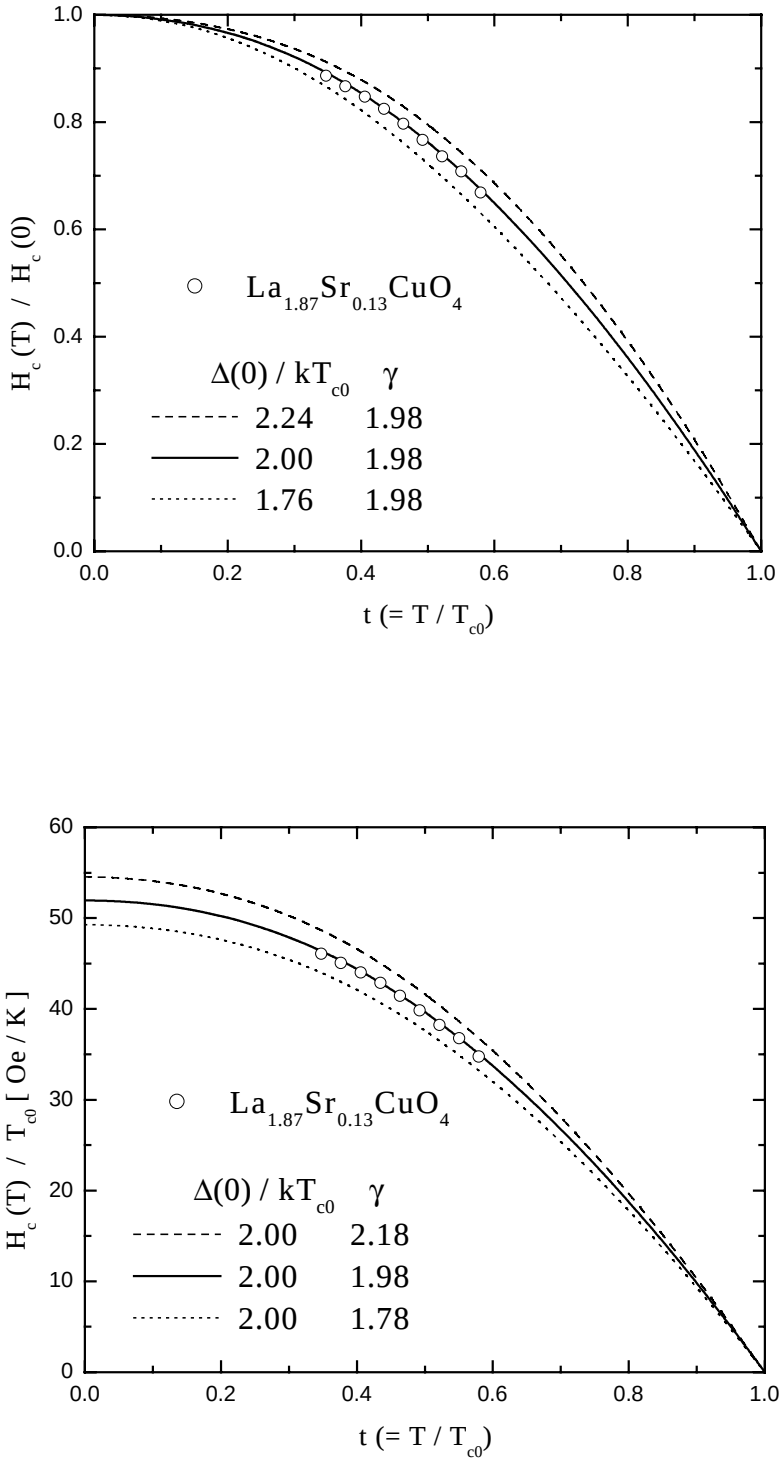

Figure 5.A6 The BCS theory fit gives $\Delta(0)/k_B T_c$ =2.00 and γ = 1.98 for x = 0.13.

References

1. Yung M. Huh, J. E. Ostenson, F. Borsa, V. G. Kogan, D. K. Finnemore, A. Vietkin, A Revcolevschi and M.-H. Julien, Phys. Rev. B **63**, 064512 (2001).
2. Z. Hao and J. R. Clem, Phys. Rev. B **43**, 2844 (1991); Phys. Rev. Lett. **67**, 2371 (1991).
3. P. H. Kes, C. J. van der Beek, M. P. Maley, M. E. McHenry, D. A. Huse, M. J. Menken, and A. A. Minovsky, Phys. Rev. Lett. **67**, 2383 (1991).
4. Z. Tesanovic, L. Xing, L. N. Bulaevskii, Q. Li, and M. Suenaga, Phys. Rev. Lett. **69**, 3563 (1992)
5. V. G. Kogan, M. Ledvij, A. Yu. Simonov, J. H. Cho, and D. C. Johnston, Phys. Rev. Lett. **70**, 1870 (1993).
6. D. E. Farrell, B. S. Chandrasekhar, M. R. DeGuire, M. M. Fang, V. G. Kogan, J. R. Clem, and D. K. Finnemore, Phys. Rev. B **39**, 222 (1989); J. Gohng and D. K. Finnemore, Phys. Rev. B **46**, 398 (1992).
7. T. Nakano, M. Oda, C. Manabe, N. Momono, Y.Miura, and M. Ido, Phys. Rev. B **49**, 16 000 (1994).
8. J. Bardeen, L. N. Cooper, and J. R. Schrieffer, Phys. Rev. **108**, 1175 (1957).

9. P. G. Radaelli, D. G. Hinks and A. W. Mitchell, B. A. Hunter and J. L. Wagner, B. Dabrowski, K. G. Vandervoort, H. K. Viswanathan, and J. D. Jorgensen, Phys. Rev. B **49**, 4163–4175 (1994); J. B. Torrance, A. Bezinge, A. I. Nazzal, T. C. Huang, S. S. Parkin, D. T. Keane, S. J. LaPlaca, P. M. Horn and G. A. Held, Phys. Rev. B **40**, 8872 (1989); J. B. Torrance, Y. Tokura, A. I. Nazzal, A. Bezinge, T. C. Huang and S. S. Parkin, Phys. Rev. Lett. **61**, 1127 (1988); H. Takagi, R. J. Cava, M. Marezio, B. Battlog, J. J. Krajewski and W. F. Peck, Jr., Phys. Rev. Lett. **68**, 3777 (1992); T. Nagano, Y. Tomioka, Y. Nakayama, K. Kishio and K. Kitazawa, Phys. Rev. B **48**, 9689 (1993).

10. C. T. Lin, E. Schönherr and K. Peters, Physica C (Amsterdam) **282C–287C**, 491 (1997).

11. This sample is provided by Dr. Q. Li at Brookhaven National Laboratory.

12. L. J. de Jongh, Magnetism and Magnetic Materials, edited by C. D. Graham and J. Rhyne, AIP Conf. Proc. No. 10 (AIP, New York, 1973), p. 561.

13. This is the same sample worked in NMR study. M.-H. Julien, F. Borsa, P. Carretta, M. Horvatić, C. Berthier, and C. T. Lin, Phys. Rev. Lett. **83**, 604 (1999).

14. Q. Li, M. Suenaga, T. Kimura, and K. Kishio, Phys. Rev. B **47**, 11384-11390 (1993).

15. B. Batlogg and C. Varma, *The underdoped phase of cuprate superconductors*, Vol. 13 Issue 2, Physics World, February (2000), p. 33.

16. T Timusk and B Statt, *The pseudogap in high-temperature superconductors: an experimental overview*, Rep. Pro. Phys. **62**, pp. 61-122 (1999).

17. C. C. Tsuei and J. R. Kirtley, Phys. Rev. Lett. **85**, 182 (2000).

18. K. Maki and H. Won, J. Phys. France **6**, 2317 (1996): J.R.Copper, cond-mat/0008270 18 Aug (2000)

19. B. Muhlschlegel, Zeitschrift fur Physik **155**, 313-327 (1959).

20. *Formulae for superconductors*, Tristan Technologies, Inc

21. T. van Duzer and C. W. Turner, *Principles of superconductive devices and circuits*, Prentice-Hall, New Jersey, Second Ed, (1999).

22. T. Sato, T. Yokoya, Y. Naitoh, T. Takahashi, K. Yamada, and Y. Endoh, Phys. Rev. Lett. **83**, 2254 (1999).

23. A. Ino, T. Mizokawa, K. Kobayashi, A. Fujimori, T. Sasagawa, T. Kimura, K. Kishio, K. Tamasaku, H. Eisaki, and S. Uchida, Phys. Rev. Lett. **81**, 2124 (1998).

24. N. Momono, M. Ido, T. Nakano, M. Oda, Y. Okajima, and K. Yamaya, Physica C (Amsterdam) **233C**, 395 (1994).

25. J. W. Loram, K. A. Mirza, W. Y. Liang, and J. Osborne, Physica C **162-164**, 498 (1989).

26. M. W. Zemansky, *Heat and Thermodynamics*, McGraw-Hill, Fourth Ed. York, PA (1957).

27. D. K. Finnemore and D. E. Mapother, Phy. Rev. **140**, A 507 (1965).

28. S. Bermon and D. M. Ginsberg, Phy. Rev. **135**, A 306 (1964).

CHAPTER 6. SUPERCONDUCTING FLUCTUATION OF VORTICES FOR $La_{2-x}Sr_xCuO_4$

A paper to be published in Phys. Rev. B.

Yung M. Huh and D. K. Finnemore
Ames Laboratory, U.S. Department of Energy and
Department of Physics and Astronomy, Iowa State University, Ames, Iowa 50011

Abstract

The $La_{2-x}Sr_xCuO_4$ (La-214) system displays a full range of fluctuating vortex behavior with the characteristics of two-dimensional (2D) fluctuation in some regions and of three-dimensional (3D) fluctuation in other regions as indicated by clearly identifiable crossing points in magnetization vs. temperature curves. Close to the superconducting transition temperature there are crossing points where the magnetization is independent of magnetic field as expected for fluctuating vortices in the quasi-two-dimensional materials such as layered high temperature cuprate superconductors. A detailed study shows that the dimensional character of the fluctuations depends on both magnetic field and the density of charge carriers. For a sample having Sr content of 0.081, the low fields, from 0.3 to 1.0 T, data show a crossing point at 19.6 K in M_{sc} vs. T curves that displays 2D fluctuations. For this same sample at higher fields, from 5.0 to 7.0 T, the crossing point slides out to 22.7 K and the vortex fluctuations show the

characteristic of 3D behavior. At lower *x*-value, the series of samples with Sr contents ranging from 0.070 to 0.156 show the aspects of this general behavior of multiple crossing points. For strongly underdoped samples with Sr contents of 0.070 and 0.081, crossover in dimensionality of the vortex fluctuations is observed when magnetic field becomes strong enough near upper critical field. Presumably, the *c*-axis coherence distance ξ_c is less than the spacing between adjacent CuO_2 layers *s* at low field and then two-dimensional or pancake-like vortex fluctuation is observed. However, at sufficiently high fields near the upper critical field, then the ξ_c becomes comparable to *s* and a transition from 2D to 3D fluctuation occurs. Magnetic field induced 2D to 3D crossover is not seen for the samples at higher *x*-values.

I. Introduction

Superconducting fluctuation of vortices in the presence of magnetic field plays an important role in the high temperature cuprate superconductors associated with high transition temperature and anisotropic layered structure, and small coherence length along *c*-direction. Although the value of ξ_c in high temperature cuprate superconductors is usually less than the unit-cell lattice parameter *c* and is often less than the spacing between adjacent CuO_2 layers *s*, having nearly constant value far below transition temperature, it becomes much larger than *s* as temperature approaches to T_c. Therefore the ratio of the *c*-axis

coherence distance to the CuO_2 plane spacing ξ_c/s is an important variable that determines whether the vortex fluctuations have a 2D or a 3D character. Literature values for cuprate superconductors have ξ_c/s less than 1 for a zero magnetic field at low temperature.

The fluctuating quantity in the low field near $T_c(H)$ is considered as the phase of order parameter (or the position of the vortex core) [1], while in high fields near upper critical field $H_{c2}(T)$, it is largely caused by the amplitude of order parameter [2]. These fluctuations display unique crossing point in magnetization vs. temperature curves, M_{sc} vs. T, where the magnetization is independent of magnetic field. Many groups have observed this behavior in the anisotropic layered material, e.g. $YBa_2Cu_3O_{7-\delta}$ (Y-123) [3], $Bi_2Sr_2CaCu_2O_{8+\delta}$ (Bi-2212) [4, 5, 6], $Bi_2Sr_2Ca_2Cu_3O_{10+\delta}$ (Bi-2223) [7], $Tl_2Ba_2CuO_{6+\delta}$ (Tl-2201) [8], $YBa_2Cu_4O_{8+\delta}$, (Y-124) [9], and organic superconductor [10] so that these crossing point may be understood as a generic property of a two-dimensional system with fluctuations.

Soon after, theoretical frameworks were provided by Bulaevskii and co-workers [1] and Tesanovic and co-workers [2, 11]. Bulaevskii, Ledvij and Kogan [1] included an additional entropy term of thermally fluctuating pancake vortices to the free energy. By taking account of thermally generated entropy contribution to the free energy, they showed the existence of characteristic temperature T^* at which magnetization has no dependence on magnetic field resulting in crossing point in magnetization at $-k_B T^*/\phi_0 s$ within constant order

of 1, where ϕ_0 is a flux quantum. Tesanovic and co-workers [11] proposed a theory that the critical fluctuations in the thermodynamics of high temperature superconductors near the upper critical field line, $H_{c2}(T)$ can be studied in terms of the Ginzburg-Landau (GL) field theory on a degenerate manifold spanned by the lowest Landau level (LLL) for Cooper pairs [11, 12, 13] and it also predicts a crossing point at a temperature such that $M^*(T^*) = -k_B T^*/\phi_0 s$.

One of the special properties among layered compounds is that it may be possible to observe *dimensional crossover* between two-dimensional (2D) and three-dimensional (3D) behavior of the vortex fluctuations. This is to be contrasted with conventional bulk superconductors where only three-dimensional (3D) rigid vortex lattices are normally formed. The issue of dimensional crossover was discussed by Klemm and co-workers [14] for layered compounds with weak Josephson coupling between the layers. A transition from bulk-like (3D) to two-dimensional-like (2D) behavior is expected upon lowering the temperature below transition temperature, where the coherence length perpendicular to the layers becomes comparable with the layer distance. Farrell and co-workers [15] observed systematic departure from the 3D result in $YBa_2Cu_3O_{7-\delta}$ with high-resolution torque-magnetometry data. For the sample of T_c = 90.5 K, the data are fit extremely well to the accepted three-dimensional phenomenological theory at T = 80 K and above, but below this temperature there was strong evidence of a crossover to two-dimensional superconducting behavior. Crossover from 2D (T<77 K) to anisotropic 3D (T>77 K) behavior in the

Bi-2212 was reported by Fastampa and co-workers [16]. Bauhofer and co-workers [17] showed that for $YBa_2Cu_3O_{7-\delta}$, the oxygen deficient sample with $\delta \sim 0.4$ has more pronounced 2D character than the sample with $\delta \sim 0.1$.

The importance of thermal fluctuations to dimensional transition of the layered structure in the presence of magnetic fields was emphasized by Glazman and co-workers [18] by showing that thermal fluctuations cause the melting of the three-dimensional Abrikosov vortex lattice at temperatures well below the superconducting transition temperature. When magnetic field is applied perpendicular to the planes, each vortex line can be thought of as a stack of 2D pancake vortices connected by Josephson strings. The crossover from vortex lines in 3D to vortex points in 2D occurs when the restoring forces exerted on a given pancake vortex in the same plane overcome the forces from pancake vortices in different layers by both magnetic and Josephson coupling. In the weak field region, fluctuations of a vortex lattice are of three-dimensional (3D) nature. For fields larger than the crossover value B_{cr}, both fluctuations and melting of the vortex lattice become two-dimensional. Experimental results were demonstrated by Bernard and co-workers [19] in $Bi_2Sr_2CaCu_2O_{8+\delta}$, Bi-2212. The crossover value, B_{cr}, from the 3D to the 2D regime is reported to be 8 mT for the underdoped (T_c = 77 K), 60 mT for the slightly overdoped(T_c = 84 K), and 150 mT for the strongly overdoped (T_c = 64 K) sample, respectively. By equating to $\phi_0/(\gamma_{\text{ani}}\, s)^2$, these values of B_{cr} correspond to anisotropy parameter $\gamma_{\text{ani}} = \lambda_c/\lambda_{ab}$, of 350, 150, and 70, respectively.

The expression of scaling behavior of the temperature and magnetic field dependence of physical quantities given by Ullah and Dorsey [12] is useful to study the dimensionality of fluctuations in high fields near $H_{c2}(T)$. Subsequently, Welp and co-workers [3] found that the superconducting contribution to the magnetization, electric conductivity, Ettinghausen effect, and specific heat of the Y-123 single crystal displays a three-dimensional (3D) scaling behavior in the variable of $[T - T_c(H)]/(TH)^{2/3}$ near the upper critical field line. Soon after, Li and co-workers [7] observed that the high-field magnetization data of both a *c*-axis oriented superconducting Bi-2223 single crystal and a thin tape near the $H_{c2}(T)$ line show a 2D scaling behavior in the variable of $[T - T_c(H)]/(TH)^{1/2}$.

More recently, Poddar and co-workers [20] first reported that a single sample of underdoped $YBa_2Cu_3O_{6.5}$ would show vortex fluctuation behavior of both two-dimensional and three-dimensional character as the magnetic field changed. They found that between 0.2 T and 0.75 T, M vs. T data had a crossing at 43.4 K with three-dimensional scaling. They also found that between 1.5 T and 3.5 T the data had a crossing at 42.8 K with two-dimensional scaling behavior. For fields between 0.75 T and 1.5 T, the crossing point moved with fields. In a more detailed paper by Rosenstein and co-workers [21], the authors provided a theoretical picture for the dimensional crossover with these data [20].

The purpose of this work is to study the crossover in dimensionality of vortex fluctuations with increasing magnetic field as Sr content is decreased systematically in the $La_{2-x}Sr_xCuO_4$, La-214, system. Since the dimensional

crossover of the vortex fluctuations is strongly related to the anisotropy of the system [22], La-214 is the convenient system to investigate vortex fluctuation. In this system, the anisotropic parameter γ_{ani} increases with decreasing doping level [23]. In addition, its γ_{ani} value is intermediate between Y-123 (γ_{ani} ~ 7) [15] and Bi-2223 (γ_{ani} ~ 200) [24] so that the anisotropy could be continuously changed without any alteration of the basic structure. We reported in the previous work the two-dimensional fluctuation behavior in an x = 0.10 single crystal having T_c = 26.8 K and T^* = 22.0 K [25]. For this sample, there is a single crossing point on the M_{sc} vs. T plot for all fields up to 7.0 T and the data scale as two-dimensional fluctuations.

Here we report data for samples of 0.070, 0.081, 0.100, 0.117, 0.130, 0.143, and 0.156 of Sr contents. For these samples, it is expected that the *c*-axis coherence distance ξ_c, longitudinal to H, will grow and become comparable with the CuO_2 plane spacing s, as the applied magnetic fields approach towards the upper critical magnetic field [26]. Then the vortices will show three-dimensional behavior. For the samples with x less than 0.10, both T_c and H_{c2} are falling rapidly, so it becomes possible to explore the crossover from two-dimensional to three-dimensional behavior in experimentally accessible magnetic fields up to 7.0 T.

II. Experiment

Grain aligned powder samples of $La_{2-x}Sr_xCuO_4$ were prepared by solid reaction. Appropriate amounts of lanthanum oxide (La_2O_3), strontium carbonate ($SrCO_3$), and copper oxide (CuO) were mixed and reacted initially at 750 °C. Pellets then were pressed and fired in an oxygen flowing tube. After repeated grinding and firing at successively higher temperatures, the final pellet was ground to a particle size of about 20 μm. This powder was mixed and suspended in a low viscosity and low magnetic susceptibility liquid epoxy, Epotek 301, oriented in a magnetic field of 8.0 T, and then the epoxy was allowed to harden in the field. All metal elements were analyzed by employing an inductively coupled plasma (ICP) technique from which Sr contents were determined.

Magnetization measurements were made with magnetic fields applied in the *c*-direction up to 7.0 T in a Quantum Design SQUID magnetometer over the temperature range from 2.0 to 300 K. Corrections for the background and normal state magnetization of the Cu spins were made in the consistent manner described previously [25, 27]. Reversible magnetization data are obtained by averaging zero-field-cooled and field-cooled data above irreversible temperature for each field within one percent of differences. A linear extrapolation of susceptibility measurements at 10 Oe to the zero magnetization line defines transition temperature T_c.

III. Results and Discussion

A. Strongly Underdoped Regime: x = 0.070 and 0.081.

Figure 6.1 illustrates the reversible M_{sc} vs. T crossing points for the sample of Sr content of 0.081. Constant magnetic field data were taken every 100 mT from 0.1 to 1.0 T and every 500 mT from 1.0 to 7.0 T. The crossing point temperature T^* is defined at the intersection of two successive curves for close magnetic fields (this is little bit different from the originally suggested definition of T^* which is rather defined as the temperature at which magnetization has no dependence on magnetic field. Therefore T^* is a characteristic temperature in the entire field range).

The inset in Figure 6.1 shows a plot of the crossing temperature vs. magnetic field indicating that the crossing temperature initially drops from 20.9 K at 0.1 T to 19.6 K at 0.3 T where it remains constant up to 1.0 T. Above 1.0 T, the crossing-point slides out to 22.7 K when field reaches 5.0 T and then the second plateau is formed up to 7.0 T. Two plateaus of crossing points are pointed with arrows in M_{sc} vs. T plot.

We investigated dimensionality of the vortex fluctuations for these two field ranges, where plateaus of crossing points are formed, by employing scaling function of 2D and 3D in the variable of $[T - T_c(H)]/(TH)^n$, where n is 1/2 for a 2D system and 2/3 for a 3D system [12]. Figure 6.2 shows plots of $M/(HT)^{1/2}$ vs.

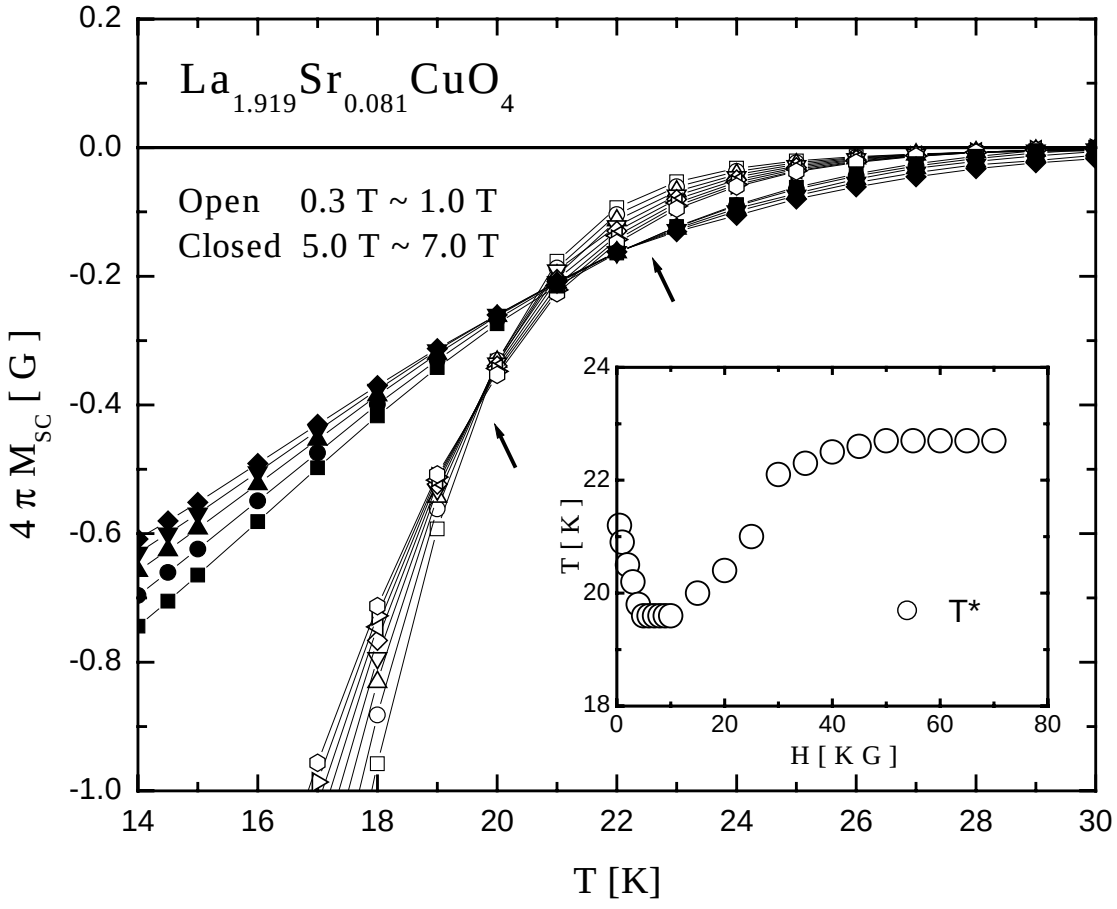

Figure 6.1 Two distinctive crossing points are indicated by arrows. The inset shows field dependence of T^* of $La_{1.919}Sr_{0.081}CuO_4$.

$[T - T_c(H)]/(TH)^{1/2}$ for 2D scaling and $M/(HT)^{2/3}$ vs. $[T - T_c(H)]/(TH)^{2/3}$ for 3D scaling for both low fields and high fields data. The magnetization data from 0.3 to 1.0 T as shown in Figure 6.1 by the open symbols are fit very well into 2D scaling and are plotted at the top in Figure 6.2 (a). Attempts to fit to 3D scaling gave rather poor fits and the result is also shown in Figure 6.2 (a) at the bottom plot. Surprisingly, high fields data from 5.0 to 7.0 T (closed data in Figure 6.1) obey 3D scaling very well and again gave poor fits to 2D scaling as seen at the top (2D scaling) and bottom (3D scaling) plots in Figure 6.2 (b).

To summarize, this strongly underdoped $La_{1.919}Sr_{0.081}CuO_4$ grain aligned powder sample shows a crossover from two-dimensional to three-dimensional fluctuation behavior as the magnetic field increases. From 0.3 to 1.0 T, the crossing points of the M_{sc} vs. T data remain constant at 19.6 K and the data obey two-dimensional (2D) scaling. Above 1.0 T, the crossing point slides out and forms the second plateau at 22.7 K from 5.0 T up to 7.0 T. Three-dimensional (3D) scaling is observed from 5.0 to 7.0 T.

Table 6.1 shows parameters used in fitting to the scaling function. Taking account of strong fluctuations near transition temperature, both T_{c0} and $T_c(H)$ were derived from a full fitting of the magnetization data to the Hao-Clem model [28] which works for the outside region of fluctuation as previously described [25, 27]. The discrepancy between transition temperatures obtained from a linear extrapolation of zero-field-cooled data taken at 1.0 mT to the zero magnetization line and those from the Hao-Clem thermodynamics is typically

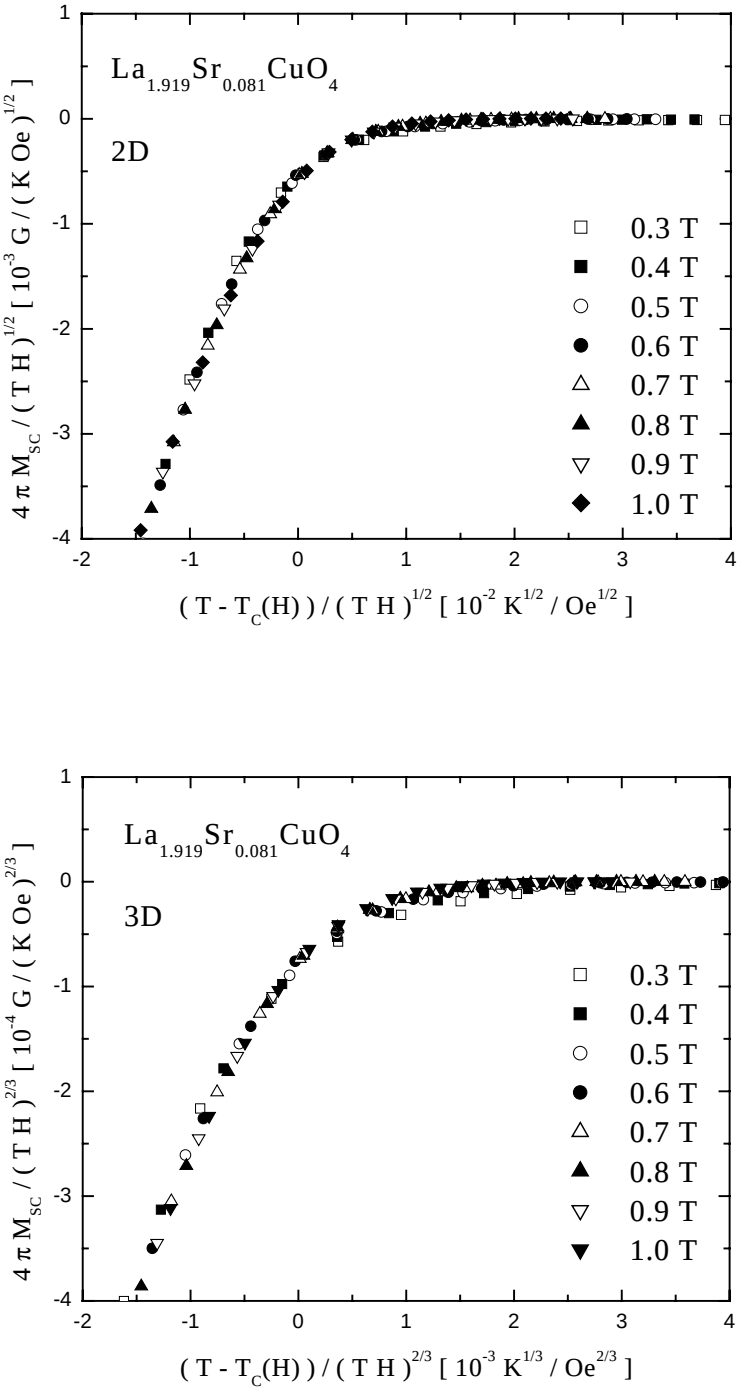

Figure 6.2 (a) Low field scaling, from 0.3 to 1.0 T, indicates better fit to 2D for $La_{1.919}Sr_{0.081}CuO_4$.

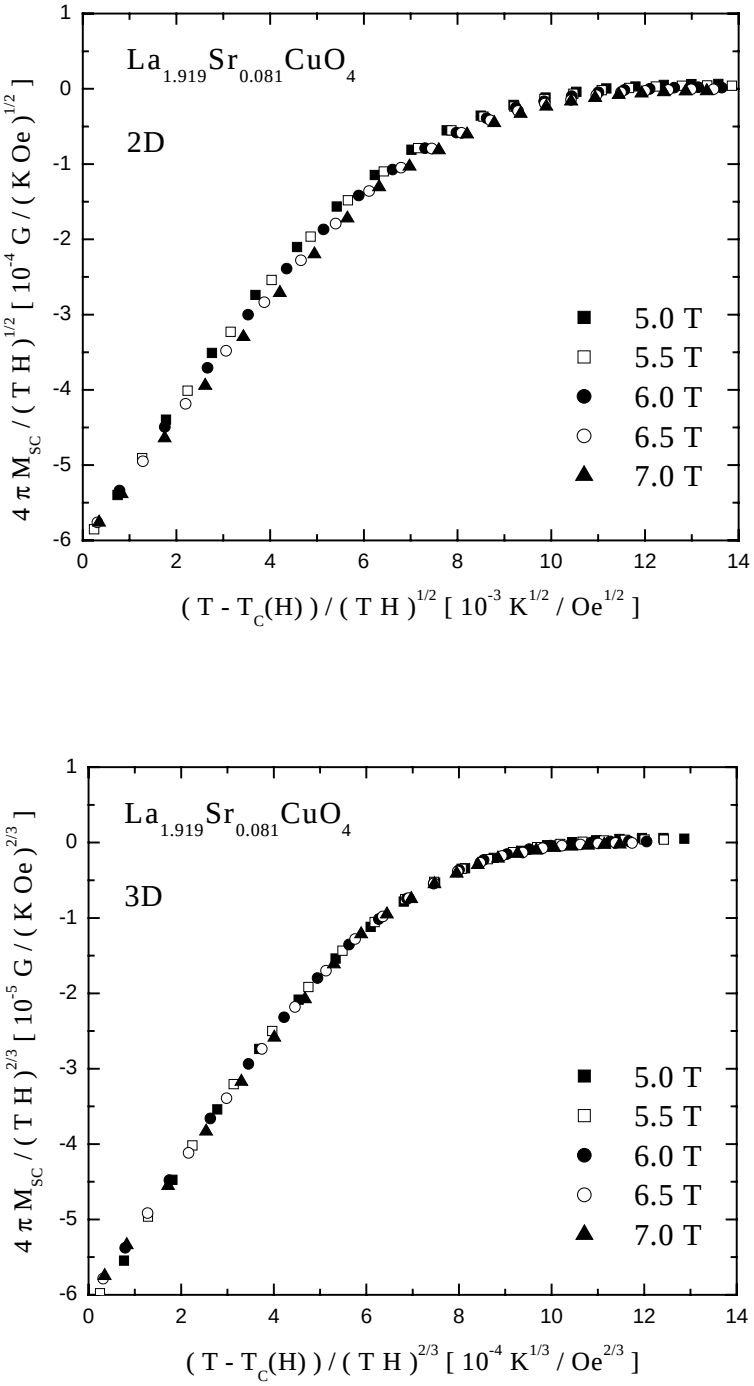

Figure 6.2 (b) High field scaling, from 5.0 to 7.0 T, indicates better fit to 3D for $La_{1.919}Sr_{0.081}CuO_4$.

Table 6.1 Thermodynamic parameters used to fit the scaling function.

Sr(x)	T_c [K]	T_{c0} [K]	H'_{c2} at T_{c0} [T/K]	$H_{c2}(0)$ [T]
0.070	14.5	14.94	-0.77	8
0.081	20.5	21.72	-0.93	14
0.100	26.7	26.80	-2.59	48
0.117	28.2	28.24	-2.23	44
0.143	36.4	36.52	-1.74	44
0.156	36.7	36.53	-1.79	45

within ±0.5 K. Thermodynamic critical fields for the family of $La_{2-x}Sr_xCuO_4$ in the range of Sr content between 0.070 and 0.234 are reported elsewhere [27]. With the $H_c(T)$ from the Hao-Clem model, and using $H_{c2}(T) = \sqrt{2}\ \kappa\ H_c(T)$, we can obtain $T_c(H)$ by equating $T_c(H) = T_{c0} - H/H'_{c2}$, where H'_{c2} is the temperature derivative of the upper critical field at the transition temperature. The values $H_{c2}(0)$ included in Table 6.1 come from $-0.69\ T_{c0}\ H'_{c2}$.

Data from sample of Sr content 0.070 are qualitatively similar to 0.081. For the sample of 0.070, the crossing point is 14.2 K in the field region from 1.0 to 2.0 T measured every 200 mT and the two-dimensional scaling fits better than 3D as seen in Figure 6.3 (a). The crossing point then slides up to 15.2 K and magnetization data measured every 500 mT from 3.5 to 7.0 T collapse into single curve of three-dimensional scaling plot as shown at the bottom in Figure 6.3 (b). In fact, the randomly scattered iso-field lines above 3.5 T of 0.070 sample clearly indicate that 2D behavior is very unlikely to be realized in the strong magnetic field region. It is assumed that as doping concentration decreases towards the underdoped region three-dimensional fluctuations are strongly favored when magnetic fields approach close to the upper critical field and crossover in dimensionality from 2D to 3D can be observed as long as high enough magnetic field is experimentally accessible.

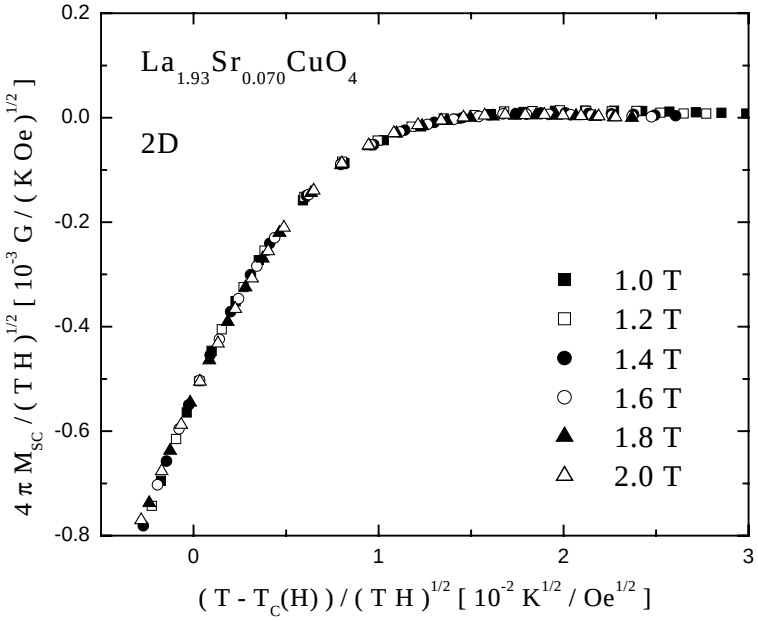

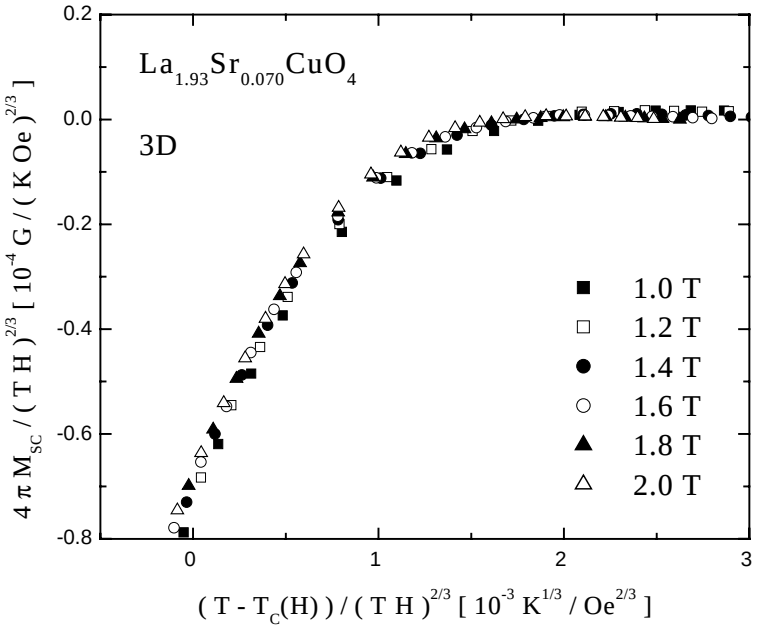

Figure 6.3 (a) Low field scaling, from 1.0 to 2.0 T, indicates better fit to 2D for $La_{1.930}Sr_{0.070}CuO_4$.

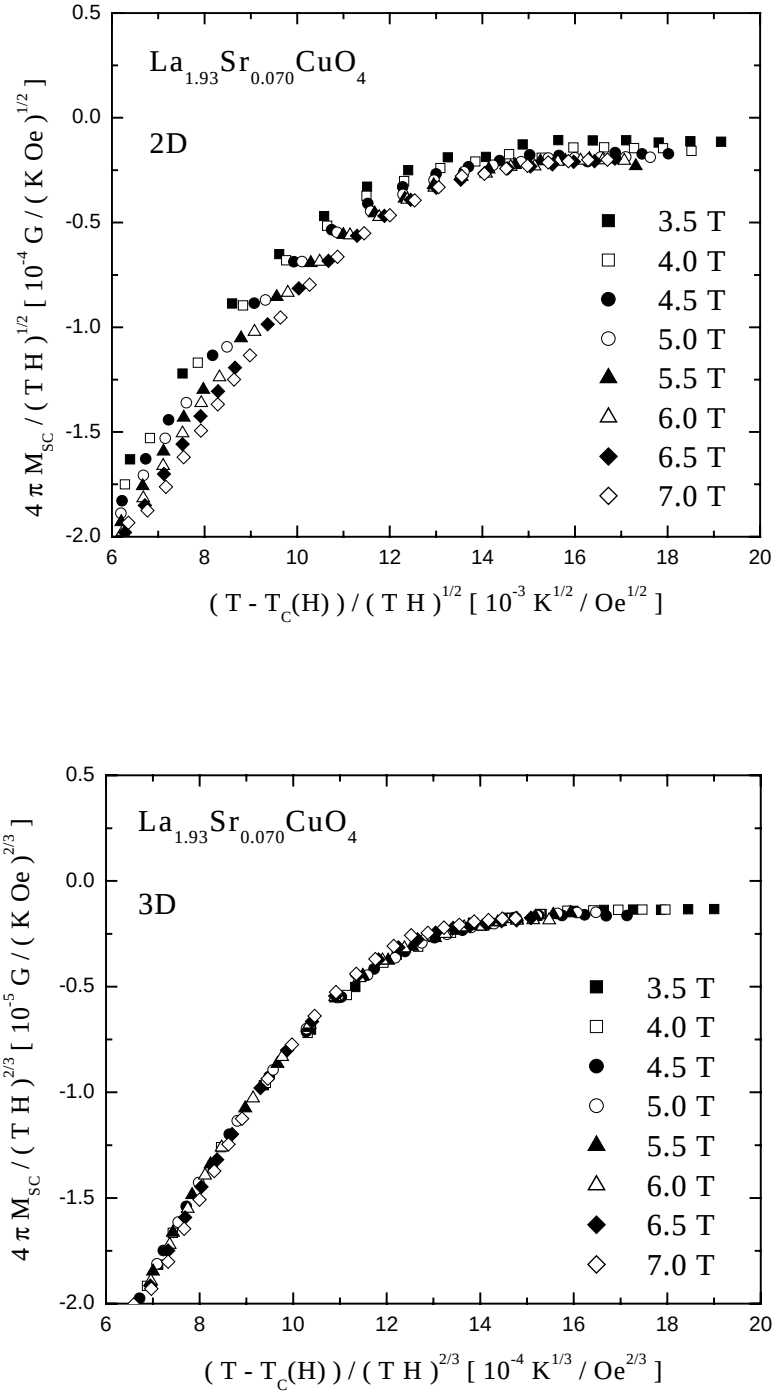

Figure 6.3 (b) High field scaling, from 3.5 to 7.0 T, indicates better fit to 3D for $La_{1.930}Sr_{0.070}CuO_4$.

B. Slightly Underdoped Regime: x = 0.100 and 0.117.

Samples in the slightly underdoped regime have transition temperatures of about 30 K. Even though distinctive plateaus of crossing points in more than one field region are also seen in this doping regime, each plateau corresponds only to the 2D scaling behavior and no dimensional crossover was observed up to the accessible magnetic field of 7.0 T. It seems that the upper critical fields are much higher than those of strongly underdoped samples and this is probably the reason why no dimensional crossover was observed in this doping regime.

In the previous work [25], we employed two different approaches to obtain H'_{c2} in attempt to study dimensional scaling behavior of slightly underdoped $La_{1.90}Sr_{0.10}CuO_4$. One is the Hao-Clem model [28] and the other is the explicit closed form of magnetization proposed by Tesanovic and co-workers [2]. In conclusion, we reported that both derived parameters and 2D scaling behavior are in good agreement with each model. We found only a single crossing point in the wide magnetic field region, ranging from 1.0 to 7.0 T, and presented 2D scaling result including theoretical fitting of closed form of the magnetization. Plotted in Figure 6.4 (a) is the 2D scaling fit from 3.0 to 7.0 T using parameters taken from the Hao-Clem model [28] while Figure 6.4 (b) shows again the 2D scaling plot with H'_{c2} obtained from Eq. (13) of Tesanovic *et al*. [2] and less number of temperatures are plotted for clarity. Both fit results clearly demonstrate 2D nature of 0.10 sample.

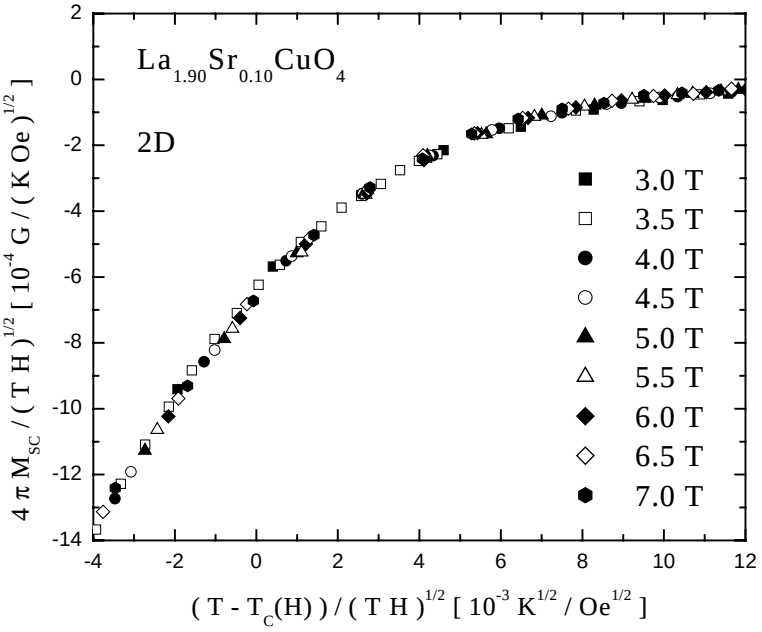

Figure 6.4 (a) 2D scaling with H'_{c2} from the Hao-Clem fit for $La_{1.90}Sr_{0.10}CuO_4$.

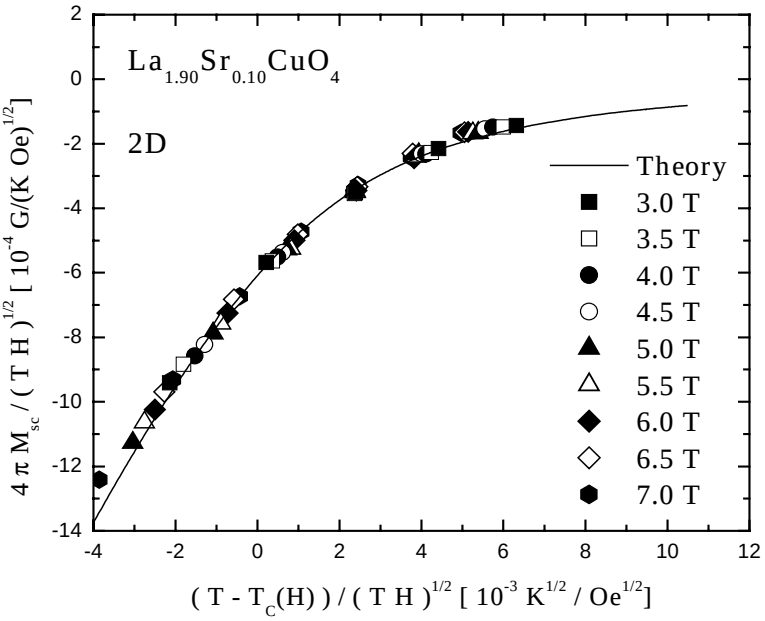

Figure 6.4 (b) 2D scaling with H'_{c2} from the Tesanovic fit for $La_{1.90}Sr_{0.10}CuO_4$.

The evolution of crossing points with applied fields for all samples studied here - strongly underdoped, slightly underdoped, and near optimum doped regimes - is plotted in Figure 6.5. The crossing points are again plotted in Figure 6.6 in the corresponding fields vs. reduced temperature scale where it specifies dimensionality of the corresponding field ranges for the plateaus of T^*. The closed and the open data denote 3D and 2D scaling behavior, respectively, in the corresponding field ranges.

The sample of 0.117, as shown in Figure 6.5, does display more than one plateau of crossing points in T^* vs. H plot. It does not show, however, dramatic change in the crossing points with increasing magnetic field as in the case of strongly underdoped samples. Two plateaus of crossing points are found to exist in the regions of field from 0.5 to 1.0 T and from 2.0 to 7.0 T. The crossing temperature T^* moves from 27.0 K down to 26.3 K as magnetic fields increase. It is interesting to note that samples of Sr content 0.10 and above show decreasing crossing points in temperature scale as magnetic field becomes stronger, while for the strongly underdoped samples, both 0.070 and 0.081, T^* increases even beyond transition temperature T_{c0} after the initial small drop with increasing fields. There is no dimensional crossover observed in the slightly underdoped regime. The 0.10 sample has only a single 2D crossing point. The 0.117 sample has two plateaus of T^* and both magnetization data fit nicely to 2D scaling in each range of low and high fields. Figure 6.7 (a) and (b) show the 2D scaling results and the insets are poor 3D scaling attempts for each field range.

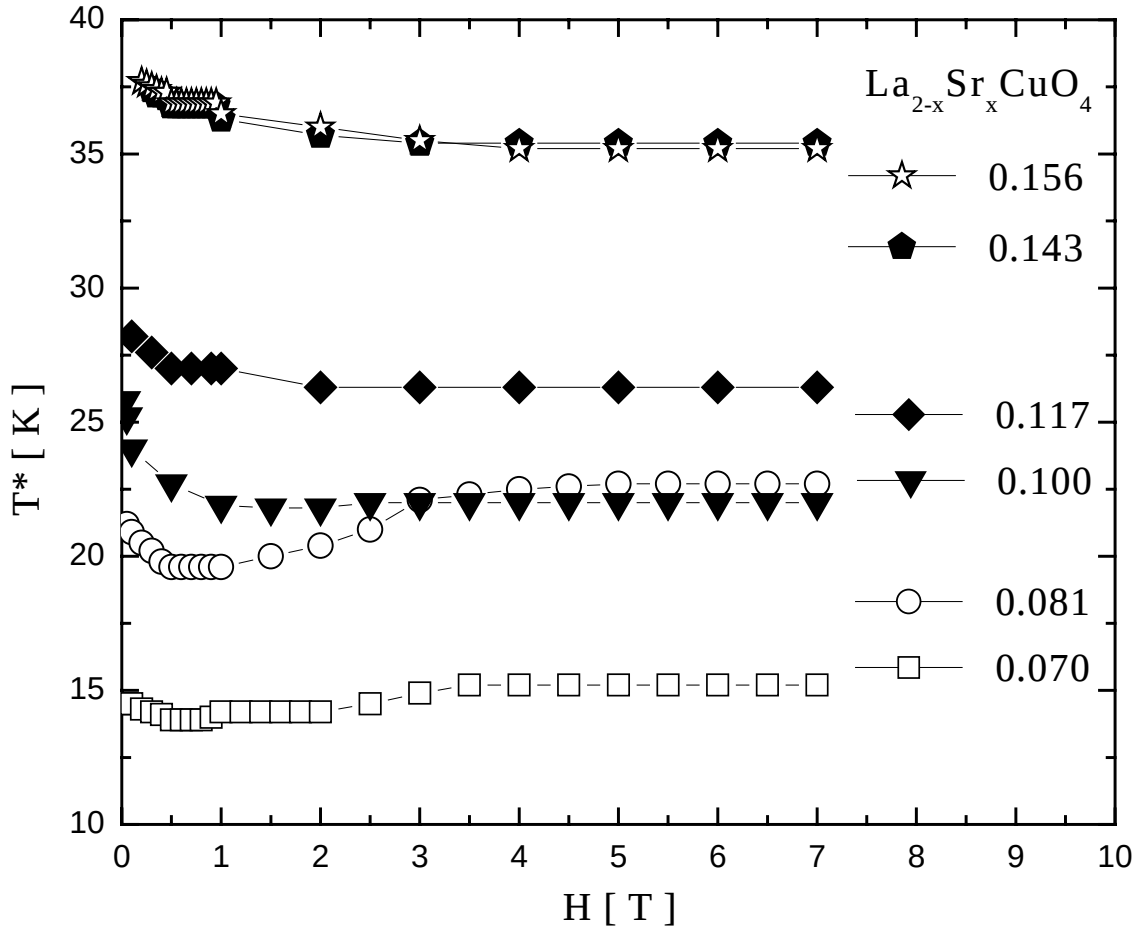

Figure 6.5 The field dependence of crossing points T^*. The distinctive plateaus of T^* are then scaled to study the dimensional character of fluctuating vortices in the underdoped and optimum doped regimes of $La_{2-x}Sr_xCuO_4$

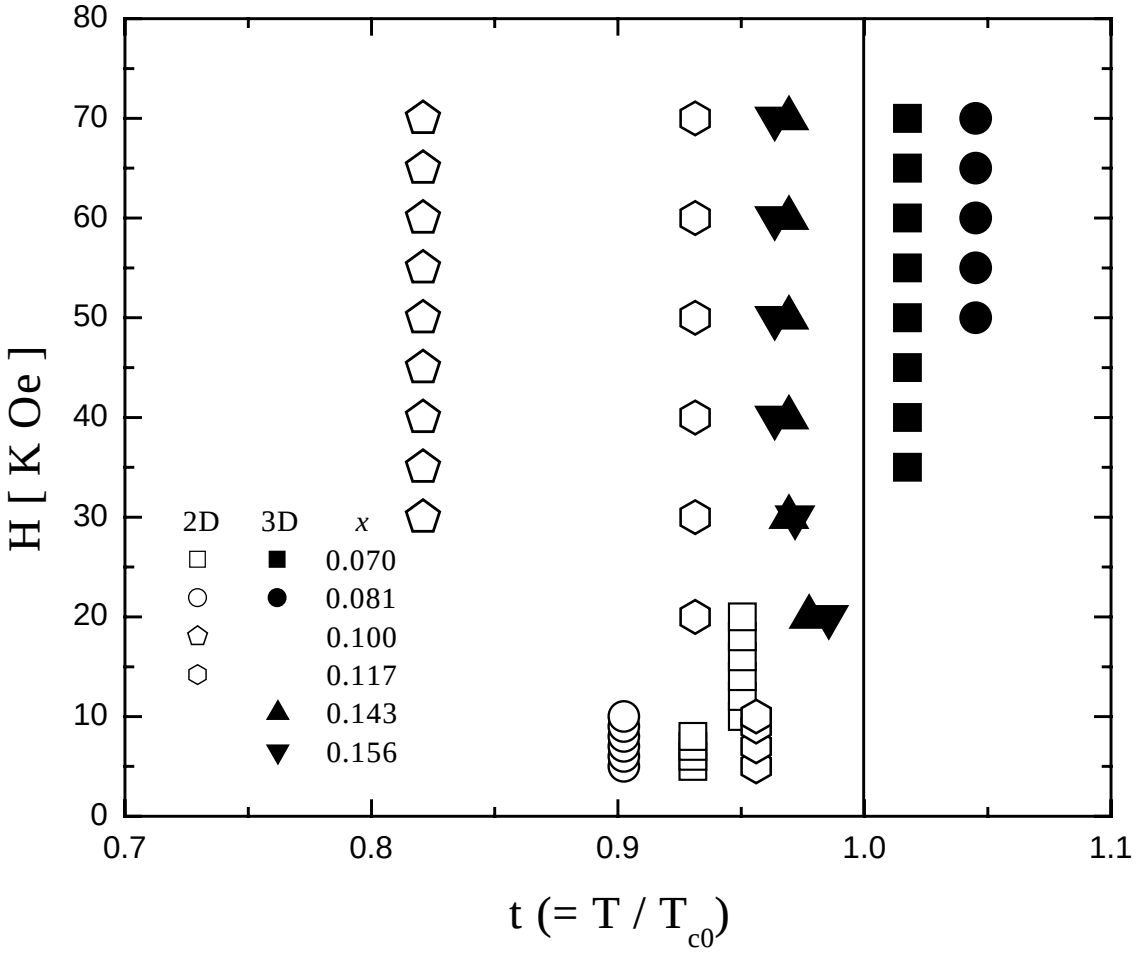

Figure 6.6 The crossing points are plotted in the corresponding fields vs. reduced temperature scale. Open data are for 2D regime and closed data for 3D regime.

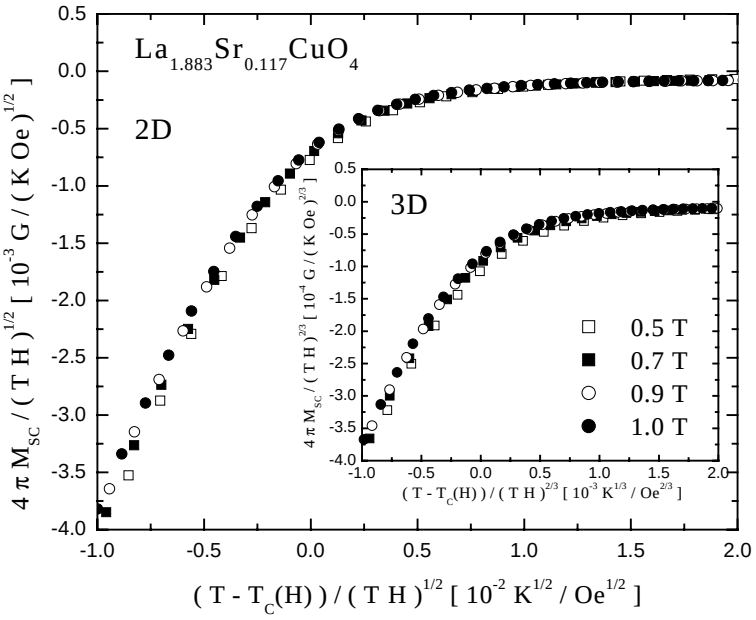

Figure 6.7 (a) Low field scaling (2D), from 0.5 to 1.0 T, for $La_{1.883}Sr_{0.117}CuO_4$.

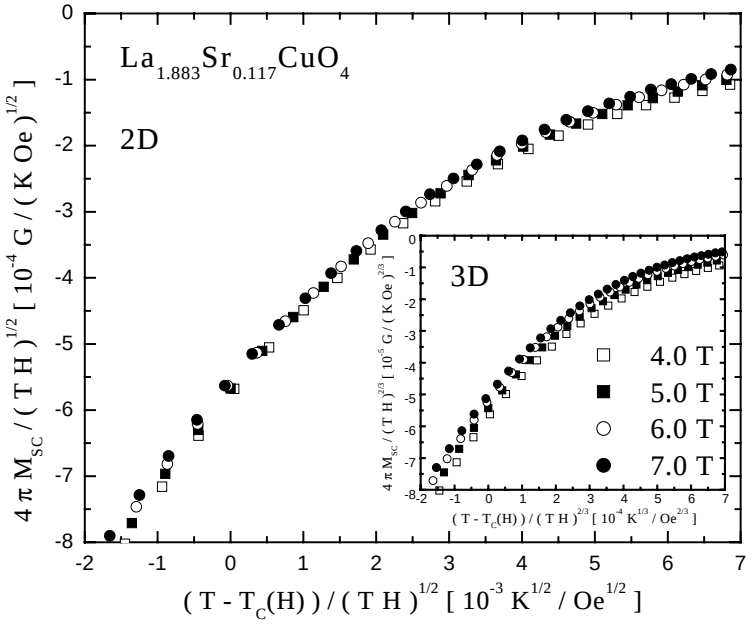

Figure 6.7 (b) High field scaling (2D), from 4.0 to 7.0 T, for $La_{1.883}Sr_{0.117}CuO_4$.

C. Near Optimum Doped Regime: x = 0.143 and 0.156.

The optimum doped La-214 is generally considered to show three-dimensional fluctuations due to its small value of anisotropy ratio γ_{ani} [23]. Iwasaki and co-workers [29] reported that a single crystal $La_{1.86}Sr_{0.14}CuO_4$ has a crossing point in the region of magnetic fields between 1.0 T and 7.0 T with essentially the same magnitude of magnetization as our result of 0.143 sample and showed 3D scaling behavior.

Our work with grain aligned samples of 0.143 and 0.156, however, displays the existence of the second plateau in crossing points of the successive iso-field magnetization curves in the field region from 0.50 to 0.95 T at the temperature of 36.8 K and 36. 9 K for the samples of Sr content of 0.143 and 0.156, respectively. Then each crossing point makes transition towards lower temperatures and stays there independently of field, all the way up to 7.0 T. Two crossing points are seen in Figure 6.8 (a) and (b) for 0.143 and 0.156 samples respectively. Interestingly the first plateau forms at the temperature about 0.3 K higher than transition temperature as indicated in Figure 6.6 and it moves down below T_{c0} with increasing fields.

As expected, magnetization data above 2.0 T fit very well to 3D scaling behavior and the fit results are plotted in Figure 6.9 (a) for 0.143 and in Figure 6.9 (b) for 0.156 sample. However, for low fields data below 0.95 down to 0.50 T, the scaling fit does not show clear-cut dimensionality as seen in Figure 6.10 (a)

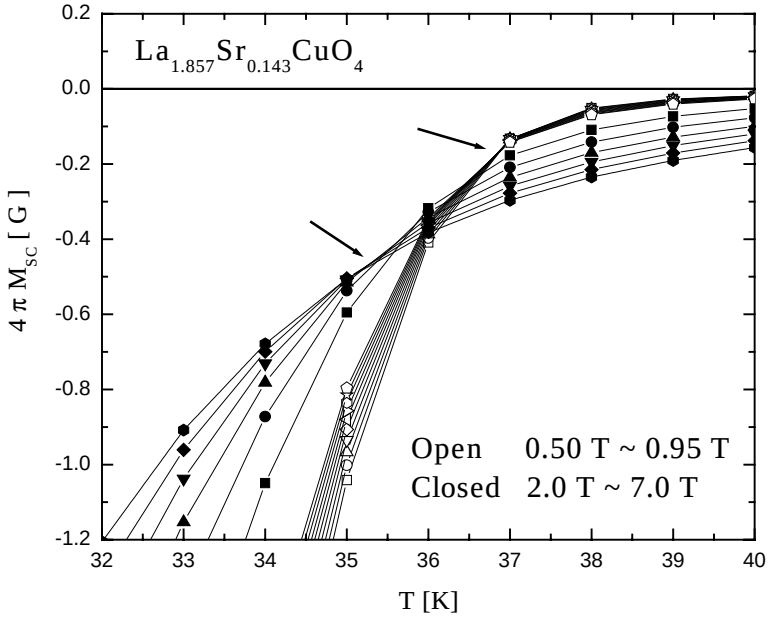

Figure 6.8 (a) Two crossing points for $La_{1.857}Sr_{0.143}CuO_4$.

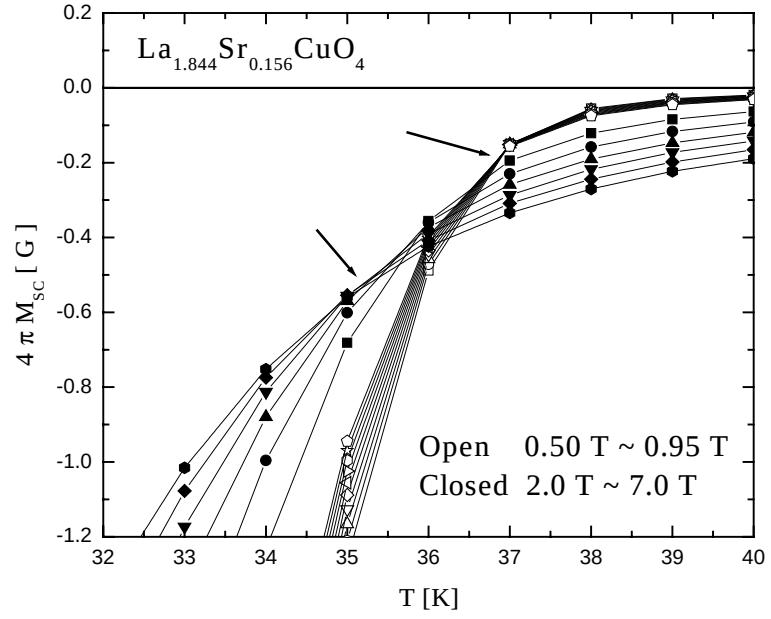

Figure 6.8 (b) Two crossing points for $La_{1.844}Sr_{0.156}CuO_4$.

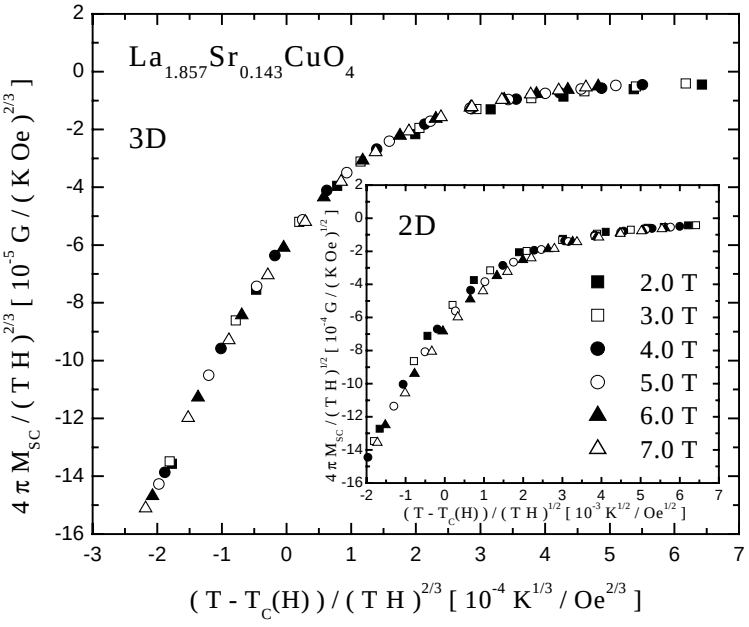

Figure 6.9 (a) High field scaling (3D), from 2.0 to 7.0 T, for $La_{1.857}Sr_{0.143}CuO_4$.

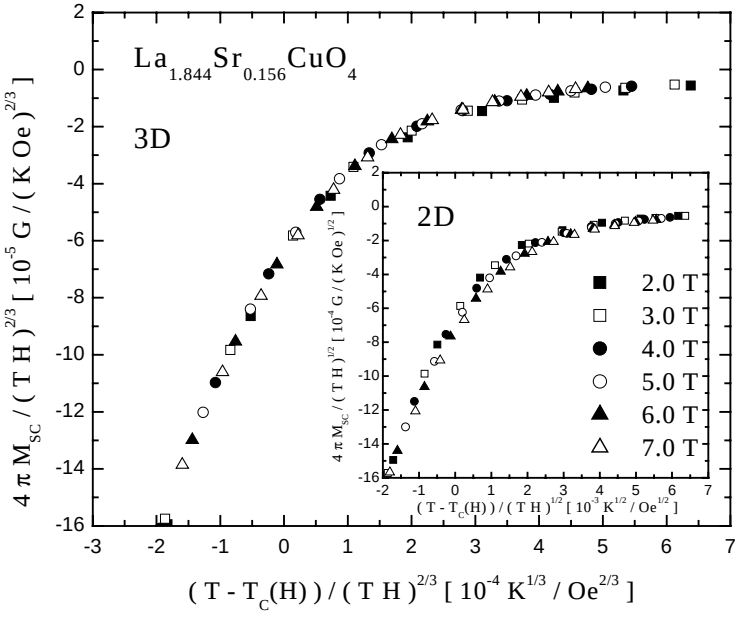

Figure 6.9 (b) High field scaling (3D), from 2.0 to 7.0 T, for $La_{1.844}Sr_{0.156}CuO_4$.

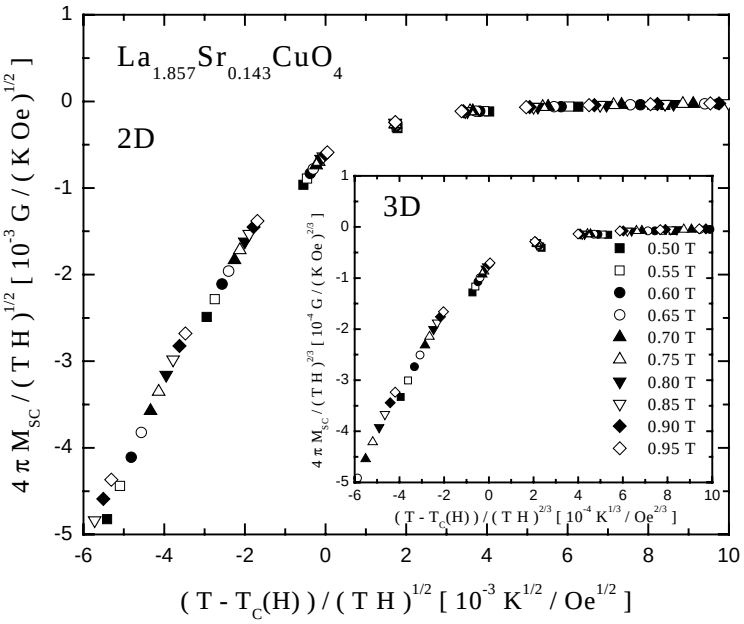

Figure 6.10 (a) Low field scaling, from 0.50 to 0.95 T, for $La_{1.857}Sr_{0.143}CuO_4$.

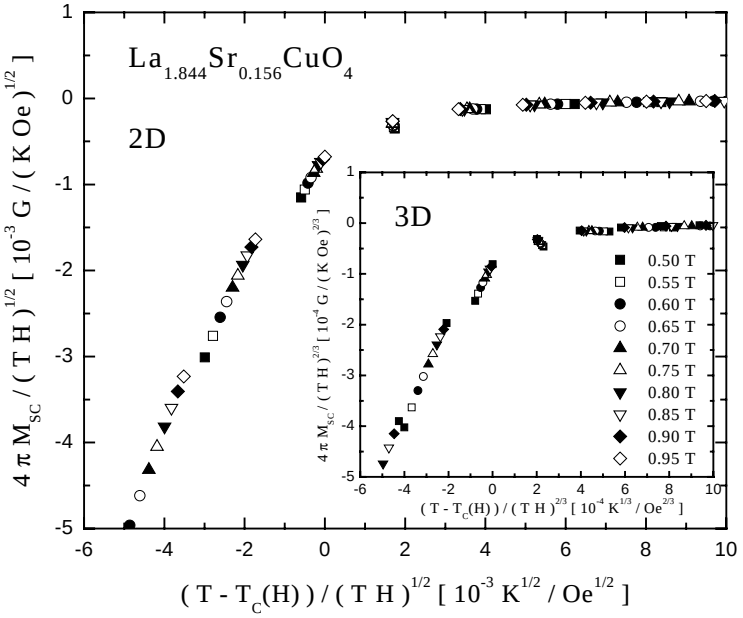

Figure 6.10 (b) Low field scaling, from 0.50 to 0.95 T, for $La_{1.844}Sr_{0.156}CuO_4$.

for 0.143 and in Figure 6.10 (b) for 0.156.

The analysis of intermediate doping level of x = 0.13 (T_{c0} = 34.52 K) single crystal sample shows that there also exist two distinctive crossing points. They are indicated with arrows in Figure 6.11. The crossing point temperature moves in a direction of lowering temperature with increasing magnetic field. However they do not fit to either 2D or 3D scaling function. The scaling function is only applicable to the limiting cases of 2D or 3D, and does not hold between these limits. It seems that this sample cannot be describable within the theory of scaling function of magnetization.

The main result of this work is summarized in the Table 6.2. Listed are values of crossing temperatures, which form plateaus in a region of both low fields and high fields, and their corresponding field ranges with dimensionality determined by fitting magnetization data to the scaling function.

The generic evolution of dimensionality in fluctuation of vortices depends on the value of anisotropy parameter γ_{ani}. In the anisotropic layered material, there are two interactions playing the important role in determining the dimensionality of fluctuation of vortices. The first is the interaction of pancake vortices in adjacent layers. The second one is the interaction of pancake vortices in the same planes. They are competing each other in a sense that the former is in favor of 3D and the latter is for 2D behavior of vortices. Any anisotropic superconductor establishes rigid 3D vortex lattice in a very weak field region since the distance between pancake vortices in the same layer is far away and

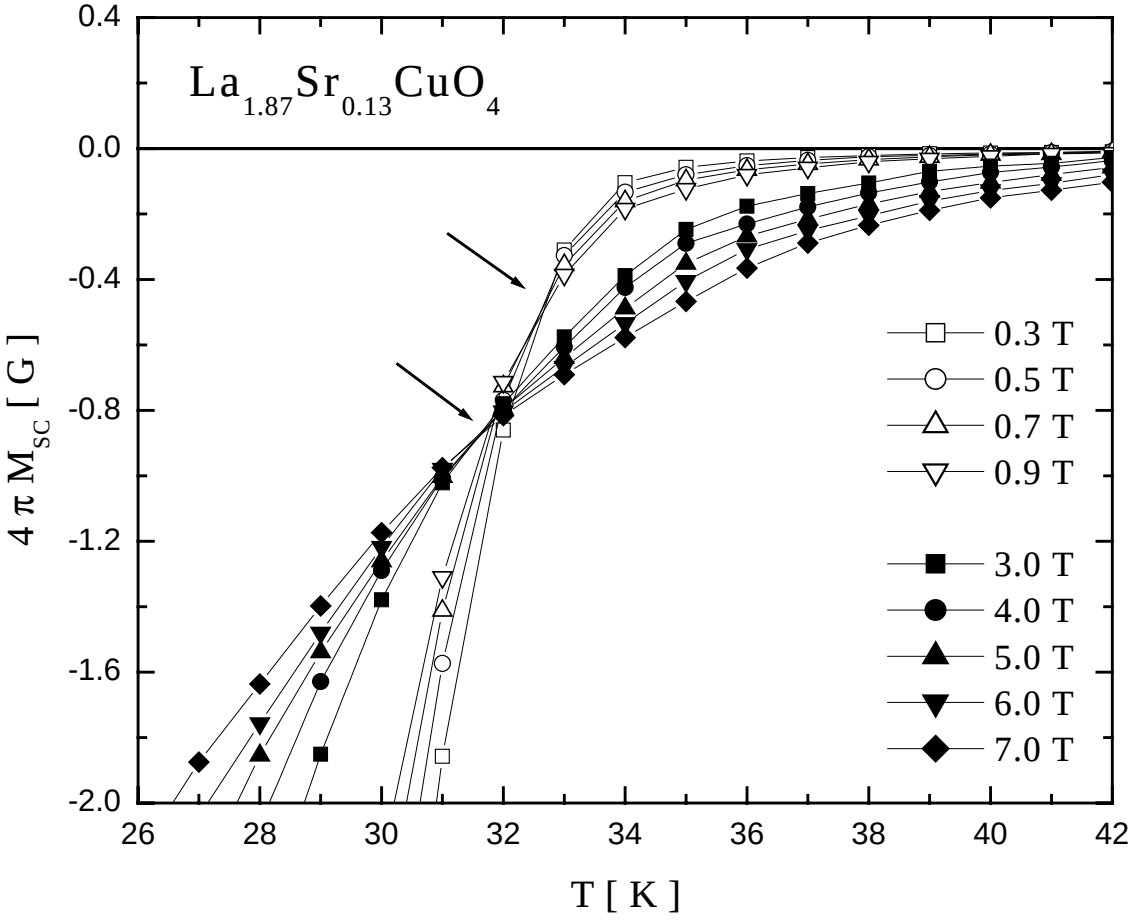

Figure 6.11 Two distinctive crossing points are indicated by arrows for a single crystal $La_{1.87}Sr_{0.13}CuO_4$.

Table 6.2 Crossing temperatures and dimensions in the corresponding field ranges for the strongly underdoped, slightly underdoped and optimum doped regimes. The scaling of low field data for x = 0.143 and 0.156 does not show clear-cut dimensionality.

Sr(x)	T^* Low Field [K]	T^* High Field [K]	Dimension Low Field Range	Dimension High Field Range
0.070	14.2	15.2	1.0 T< H^{2D} <2.0 T	3.5 T< H^{3D} <7.0 T
0.081	19.6	22.7	0.3 T< H^{2D} <1.0 T	5.0 T< H^{3D} <7.0 T
0.100	N/A	22.0	N/A	1.0 T< H^{2D} <7.0 T
0.117	27.0	26.3	0.5 T< H^{2D} <1.0 T	2.0 T< H^{2D} <7.0 T
0.143	36.8	35.4	0.5 T< H <1.0 T	2.0 T< H^{3D} <7.0 T
0.156	36.9	35.2	0.5 T< H <1.0 T	2.0 T< H^{3D} <7.0 T

their interactions are very weak compared with the interactions between adjacent layers. A crossover from 3D to 2D occurs as the distance between vortices in each plane become closer when external field increases. This crossover field, B_{cr} ($\sim 1/\gamma_{ani}^{2}$) [18], seems to be very small (it can be as small as 8 mT for underdoped and 150 mT for overdoped Bi-2212 [19]) so that it might not be always possible to observe from the reversible magnetization study suffering from the emergence of irreversibility. This might be the reason why our reversible magnetization measurements could not see the crossover from 3D to 2D in the weak field region. The 2D behavior persists until applied fields approach close to the upper critical field where the vortices interact three-dimensionally. This is the crossover from 2D to 3D observed in the strongly underdoped La-214 samples. So the overall crossover for the material with large anisotropy ratio is to be 3D → 2D → 3D. The schematic sketch of the dimensional crossover in La-214 system is illustrated in Figure 6.12. In the experimentally accessible reversible field range, the crossover from 2D to 3D can be observed in the strongly underdoped regime (A in Figure 6.12). It is likely to see only 3D behavior in the optimum doped regime (C in Figure 6.12), while only 2D behavior is observed in the slightly underdoped regime (B in Figure 6.12) in the reversible fields up to 7.0 T.

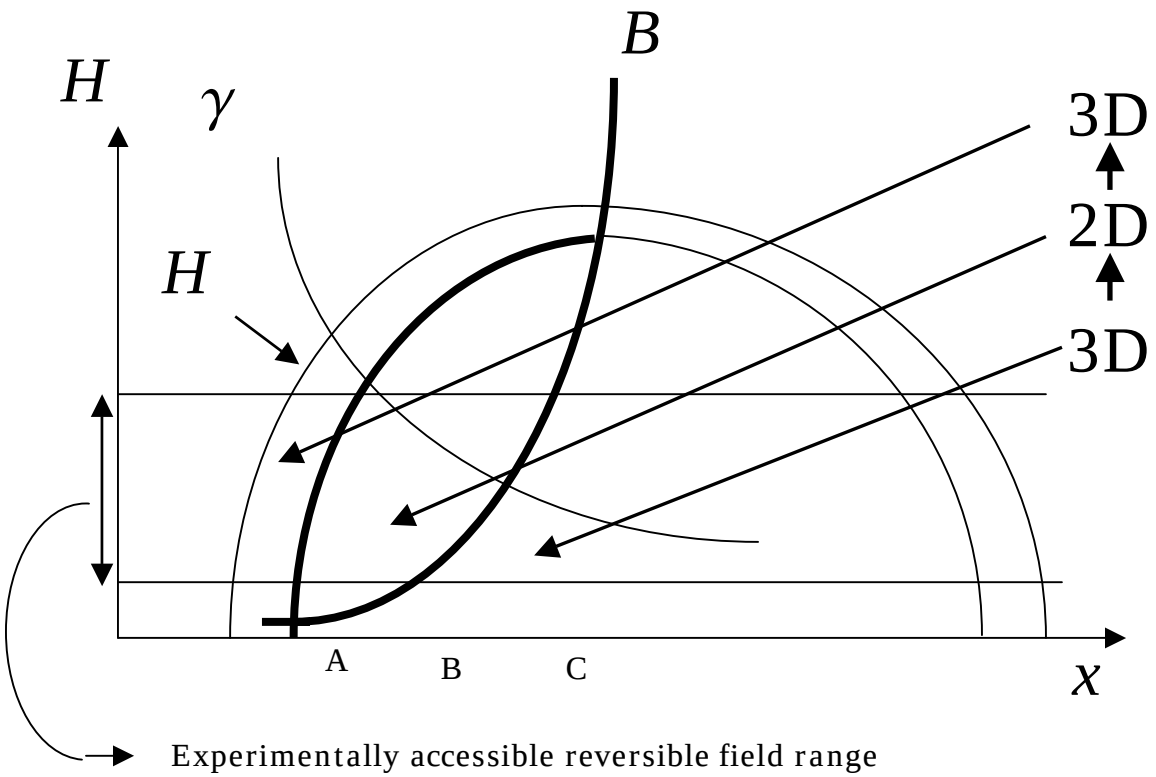

Figure 6.12 Sketch of the dimensional crossover in $La_{2-x}Sr_xCuO_4$. The low field crossover field B_{cr} is proportional to $1/\gamma_{ani}^2$. There is a 3D region close to the H_{c2}. The A, B, and C denote, respectively, the strongly underdoped, slightly underdoped, and optimum doped regimes.

IV. Conclusion

Large portions of reversible data are obtained from the single crystals and grain aligned samples, which make it possible to observe dimensional crossover by following drifting crossing points. The ratio of the *c*-axis coherence distance to the spacing between CuO_2 plane ξ_c/s as well as strong doping dependence of anisotropic ratio $\gamma_{\text{ani}} = \lambda_c/\lambda_{ab}$ is the important variable that determines whether fluctuations of vortices have a two-dimensional (2D) or three-dimensional (3D) character. The dimensional crossover of superconducting fluctuations of vortices from 2D to 3D is demonstrated as the magnetic field increases close to the upper critical field in the strongly underdoped $La_{2-x}Sr_xCuO_4$ samples.

For strongly underdoped samples with T_{c0} of about 20 K, x = 0.070 and 0.081, crossovers in dimensionality from 2D to 3D are observed and the onset of 3D behavior is about 3.5 T and 5.0 T, respectively. The slightly underdoped samples with T_{c0} of about 30 K, x = 0.10 and 0.117, show 2D behavior. The optimum doped samples, x = 0.043 and 0.156, with T_{c0} of about 40 K show 3D behavior in the wide range of magnetic field from 2.0 to 7.0 T. No dimensional crossover is observed up to the accessible field of 7.0 T in the slightly underdoped and optimum doped regimes.

Acknowledgement

We thank Dr. V. G. Kogan and Dr. J. R. Clem for useful discussions, their interest and encouragement and Dr. Q. Li at Brookhaven National Laboratory for providing the 0.13 single crystal sample for our work. Ames Laboratory is operated for the U.S. Department of Energy by Iowa State University under Contract No. W-7405-ENG-82 and supported by the DOE, the Office of Basic Energy Sciences.

References

1. L. N. Bulaevskii, M. Ledvij and V. G. Kogan, Phys. Rev. Lett. **68**, 3773 (1992).
2. Z. Tesanovic, L. Xing, L. Bulaevskii, Qiang Li, and M. Suenaga, Phys. Rev. Lett. **69**, 3563 (1992).
3. U. Welp, W. K. Kwok, R. A. Klemm, V. M. Vinokur, J. Downey, and G. W. Crabtree, Physica C **185-189**, 1785 (1991); U. Welp, S. Fleshler, W. K. Kwok, R. A. Kemm, V. M. Vinokur, J. Downey, B. Veal, and G. W. Crabtree, Phys. Rev. Lett. **67**, 3180 (1991).
4. P. H. Kes, C. J. van der Beek, M. P. Maley, M. E. McHenry, D. A. Huse, M. J. Menken, and A. A. Minovsky, Phys. Rev. Lett. **67**, 2383 (1991).

5. W. Kritscha, F. M. Sauerzopf, H. W. Weber, G. W. Crabtree, Y. C. Chang, and P. Z. Jiang, Physica C **179**, 59 (1991).

6. Q. Li, K. Shibutani, M. Suenaga, I. Shigaki and R. Ogawa, Phys. Rev. B **48**, 9877 (1993).

7. Qiang Li, M. Suenaga, T. Hikata and K. Sato, Phys. Rev. B **46**, 5857 (1992); Qiang Li, M. Suenaga, J. Gohng, D. K. Finnemore, T. Hikata and K. Sato, Phys. Rev. B **46**, 3195 (1992); Qiang Li, M. Suenaga, L. N. Bulaevskii, T. Hikata and K. Sato, Phys. Rev. B **48**, 13865–13870 (1993).

8. F. Zuo, D. Vacaru, H. M. Duan and A. M. Herman, Phys. Rev. B **47**, 8327 (1993).

9. Junghyun Sok, Ming Xu, Wei Chen, B. J. Suh, J. Gohng, D. K. Finnemore, M. J. Kramer, L. A. Schwartzkopf, and B. Dabrowski, Phys. Rev. B **51**, 6035 (1995).

10. M. Lang, F. Steglich, N. Toyota, and T. Sasaki, Phys. Rev. B **49**, 15227 (1994).

11. Z. Tesanovic and A. V. Andreev, Phys. Rev. B **49**, 4064 (1994).

12. S. Ullah and A. T. Dorsey, Phys. Rev. Lett. **65**, 2066 (1990); Phys. Rev. B **44**, 262 (1991).

13. R. Ikeda, T. Ohmi, and T. Tsuneto, Phys. Rev. Lett. **67**, 3874 (1991); J. Phys. Soc. Jpn. **60**, 1051 (1991).

14. R. A. Klemm, A. Luther, and M. R. Beasley, Phys. Rev. B **12**, 877 (1975); and reference therein.

15. D.E. Farrell, J.P. Rice, D.M. Ginsberg and J.Z. Liu, Phys. Rev. Lett. **64**, 1573 (1990).

16. R. Fastampa, M. Giura, R. Marcon, and E. Silva, Phys. Rev. Lett. **67**, 1795–1798 (1991).

17. W. Bauhofer, W. Biberacher, B. Gegenheimer, W. Joss, R. K. Kremer, Hj. Mattausch, A. Müller, and A. Simon, Phys. Rev. Lett. **63**, 2520 (1989).

18. L. I. Glazman, A. E. Koshelev, Phys. Rev. B, **43**, 2835 (1991).

19. C. Bernhard, C. Wenger, Ch. Niedermayer, D. M. Pooke, J. L. Tallon, Y. Kotaka, J. Shimoyama, K. Kishio, D. R. Noakes, C. E. Stronach, T. Sembiring, and E. J. Ansaldo, Phys. Rev. B, **52**, R7050 (1995); S. L. Lee, P. Zimmermann, H. Keller, M. Warden, I. M. Savic, R. Schauwecker, D. Zech, R. Cubitt, E. M. Forgan, P. H. Kes, T. W. Li, A. A. Menovsky, and Z. Tarnawski, Phys. Rev. Lett. **71**, 3862 (1993)

20. A. Poddar, R. Prozorov, Y. Wolfus, M. Ghinovker, B. Ya. Shapiro, A. Shaulov, and Y. Yeshurun, Physica C **282-287**, 1299 (1997).

21. B. Rosenstein, B. Ya. Shapiro, R. Prozorov, A. Shaulov, and Y. Yeshurun, Phys. Rev. B, 63, 134501.

22. V. G. Kogan, M. Ledvij, A. Yu. Simonov, J. H. Cho, and D. C. Johnston, Phys. Rev. Lett. **70**, 1870 (1993).

23. T. Kimura, K. Kishio, T. Kobayashi, Y. Nakayama, N. Motohira, K. Kitazawa and K. Yamafuji, Physica C **192**, 247 (1992); T. Shibauchi, H. Kitano, K. Uchinokura, A. Maeda, T. Kimura and K. Kishio, Phys. Rev. Lett. **72**, 2263 (1994); C. Panagopoulos,J. R. Cooper, T. Xiang, Y. S. Wang and C. W. Chu, Phys. Rev. B **61**, R3808 (2000).

24. J. C. Martínez, S. H. Brongersma, A. Koshelev, B. Ivlev, P. H. Kes, R. P. Griessen, D. G. de Groot, Z. Tarnavski, and A. A. Menovsky, Phys. Rev. Lett. **69**, 2276–2279 (1992).

25. Yung M. Huh, J. E. Ostenson, F. Borsa, V. G. Kogan, D. K. Finnemore, A. Vietkin, A. Revcolevschi, and M.-H. Julien, Phys. Rev. B **63**, 064512 (2001).

26. G. P. Mikitik, Zh. Ekesp. Teor. Fiz. **101**, 1042 (1992) [Sov. Phys. JEPT **74**, 558 (1992)].

27. Yung M. Huh and D. K. Finnemore (to be published); Yung M. Huh, Ph.D. thesis, Iowa State University, 2001 (unpublished).

28. Z. Hao and J. R. Clem, Phys. Rev. Lett. **67**, 2371 (1991).

29. H. Iwasaki, F. Matsuoka, and K. Tanigawa, Phys. Rev. B **59**, 14624 (1999).

CHAPTER 7. GENERAL CONCLUSION

The high temperature cuprate superconductor $La_{2-x}Sr_xCuO_{4-\delta}$ - La-214 family has been investigated to study the generic dependence of the thermodynamics on the doping concentration. Both single crystals and magnetically aligned powder samples at 8.0 T were studied. A total of eighteen samples was carefully selected in order to have the accepted transition temperatures and the largest Meissner shielding fractions. Magnetization measurements have been conducted from the 2.0 K to 300 K in the accessible magnetic field up to 7.0 T.

The normal-state magnetizations were well behaved and obey a universal equation $M_n = CH + M_s \tanh(\beta H)$. The superconducting state magnetizations are obtained by $M_{sc} = M_t - M_n$ throughout the entire superconductive region from the strongly underdoped (x = 0.060) to the strongly overdoped (x = 0.234) regimes. Below the transition temperature T_{c0}, the irreversibility line is the highest for the optimum doped sample and flux pinning decreases as the x-value decreases. For the overdoped regime, the irreversibility lines tend to stay the same in a reduced temperature scale plot regardless of the amount of doped Sr concentration.

With the varying Sr contents from x = 0.060 to 0.234, the thermodynamic

critical field (therefore, the free energy change) changes in a similar manner as the dependence of T_{c0} on x-value, taking a prominent maximum at the optimum doped regime and decreasing monotonically on both sides towards the underdoped and overdoped regimes. The thermodynamic critical field at zero temperature $H_c(0)$ shows a strong correlation with the transition temperature of the system, varying roughly linearly with T_c, while there is a rather small dependence on the Meissner shielding fraction measured at 10 Oe. The ratio $H_c(0)/T_c(0)$ also peaks in the region of somewhat larger than optimum doping, at x = 0.188. It rises steeply from the underdoped regime and saturates near the optimum doped, and then changes slowly even though both $H_c(0)$ and T_{c0} drop to zero abruptly.

By applying isotropic BCS thermodynamics, the gap ratio $\Delta/k_B T_{c0}$ was determined to be 2.01±0.11, indicating that La-214 is a strongly coupled superconductor, and the specific heat coefficient γ showed the similar behavior as found from an plot of $[H_c(0)/T_{c0}]^2$ vs. x. The density of states $N(0)$ remained nearly constant over the wide range of optimum and overdoped regimes, taking a broad maximum around x = 0.188, and then dropped quickly towards zero in the underdoped regime.

As the doping level was reduced below the optimum regime, the M_{sc} vs. T curves showed a clear crossing temperature T^* where the magnetization is independent of magnetic field, which is expected for fluctuating vortices in a two-dimensional layered material. Moreover, as higher fields were applied, the

crossing point moved to a different temperature.

The ratio of the *c*-axis coherence distance to the spacing between CuO_2 plane ξ_c/s as well as the strong doping dependence of the anisotropic ratio $\gamma_{ani} = \lambda_c/\lambda_{ab}$ is a important variable that determines whether fluctuations have a two-dimensional (2D) or three-dimensional (3D) character. The ξ_c is less than the spacing between adjacent CuO_2 layers at low field, resulting in two-dimensional or pancake-like vortex fluctuations. However, at sufficiently high fields near the upper critical field H_{c2}, the ξ_c becomes comparable to *s*, and a transition from 2D to 3D fluctuation occurs. In the strongly underdoped regime, for the samples of $x = 0.070$ and 0.081, the dimensional crossover from 2D to 3D was observed.

ACKNOWLEDGEMENTS

The author wishes to express deep appreciation to Dr. D. K. Finnemore for his invaluable guidance, continuing encouragement and support throughout the course of this research.

The author also wishes to appreciate Mr. J. E. Ostenson and committee professors: Dr. J. R. Clem, Dr. D. C. Johnston, and Dr. D. W. Lynch at Department of Physics and Astronomy, and Dr. V. L. Dalal at Department of Electrical and Computer Engineering. This work could not have been completed without their vigilance and criticism.

The priceless debt is to Dr. V. G. Kogan, Dr. S. L. Budko, Dr. L. L. Miller, Dr. I. R. Fisher, Dr. P. C. Canfield, Dr. F. Borsa, Dr. R. Modler, and Dr. J. Schmalian for their countless treasured advice, inspiring discussions and interests towards my work, and the author is very grateful.

This work was performed at Ames Laboratory under Contract No. W-7405-Eng-82 with the U.S. Department of Energy. The United States government has assigned the DOE Report number IS-T 2073 to this thesis.

BIOGRAPHICAL SKETCH

Yung Moo Huh was born November 8, 1970 in the city of Young-Ju, Korea. He received the Bachelor of Science in Physics from Myong Ji University in 1997. He has studied in Pittsburg State University from 1996 to 1997 as an exchange student who was officially selected and academically sponsored by both the state of Kansas and the Myong Ji University Foundation. He was awarded the *Academic Excellence Graduate Award* from Pittsburg State University in 1997, the *Outstanding First-Year Teaching Award* from Iowa State University in 1998, and the *Graduate College Teaching Excellence Award* from Iowa State University in 2000. He ranked the top scored in the Ph.D. Qualifying Exam in the Department of Physics and Astronomy at Iowa State University in 1998. He has served as a *Teaching Assistant* from 1997 to 2000 and as a *Research Assistant* from 1998 to 2001 in Ames Laboratory, U.S. Department of Energy and Department of Physics and Astronomy at Iowa State University in Ames, Iowa.